UNIVERSITY OF CALIFORNIA

Los Angeles

COMPUTATION OF TURBULENT RECIRCULATING FLOW IN CHANNELS, AND FOR IMPINGEMENT COOLING

A dissertation submitted in partial satisfaction of the

requirements for the degree doctor of philosophy

in Mechanical Engineering

by

Byong Hoon Chang

1992.

The dissertation of Byong Hoon Chang is approved.

David T. Allen

Christopher R. Anderson

Chih-Ming Ho

Adrienne G. Lavine

Anthony F. Mills, Committee Chair

University of California, Los Angeles

1992.

CONTENTS

NOMENCLATURE

b	rib width
c_μ, $c_{\varepsilon 1}$, $c_{\varepsilon 2}$	turbulence model constants
c_l	coefficient in source term of dissipation rate equation
c_p	constant pressure specific heat
d	upstream tube diameter, or jet outlet diameter
D	downstream tube diameter
D_k	diffusion of k
D_{ij}	diffusion of stress $\overline{u_i u_j}$
d_1	inner diameter
d_2	outer diameter
d_e	$d_2 - d_1$
d_j	jet diameter
E	empirical constant in the law of the wall
e	roughness height
f	friction factor
f_μ, f_ε	empirical functions in turbulence model
h	enthalpy, height of step, $\frac{D-d}{2}$
H	height of channel, distance from jet inlet to wall
e^+	roughness Reynolds number, $\frac{eu^*}{\nu}$
k	turbulence kinetic energy, $k = \frac{1}{2}\overline{u_i' u_i'}$
L	rib pitch

l	turbulence length scale
$\dot{m}$	mass flow rate
Nu	Nusselt number based on downstream diameter
Nu_{db}	$0.023 Re^{0.8} Pr^{0.4}$
n_i	unit vector
p	pressure
P	generation rate of turbulent energy, or function in Eq.(59)
P_{ij}	stress generation rate
Pr	molecular Prandtl number
Pr_t	turbulent Prandtl number
Q	volumetric flow rate
q_w	heat flux at wall
r	radial coordinate
r_1	inner radius of the annulus
r_2	outer radius of the annulus
R	radius of pipe
Re_D	Reynolds number, $\frac{4\dot{m}}{\pi\mu D}$
Re_d	$\frac{4\dot{m}}{\pi\mu d}$
Re_w	$\frac{\rho u D}{\mu_w}\frac{\rho_w}{\rho_b}$
S_i	source term for ϕ_i
St	Stanton number
T	local temperature
T^+	dimensionless temperature, $\rho u^* c_p (T_w - T) / q_w$
u	velocity in axial direction

u^*	friction velocity, $\sqrt{\frac{\tau_w}{\rho}}$
u^+	dimensionless velocity, $\frac{u}{u^*}$
$\overline{u_i u_j}$	Reynolds stress
y^+	dimensionless distance from wall, $\frac{yu^*}{v}$
w	rib width

Greek symbols

α, β	constants for algebraic model
ε	turbulence dissipation rate
$\tilde{\varepsilon}$	modified dissipation variable
Γ	thermal conductivity
μ	dynamic viscosity
μ_t	turbulent viscosity
v	kinematic viscosity
v_t	turbulent kinematic viscosity
σ_ϕ	turbulent Prandtl number for ϕ, $\phi = k, \varepsilon, h$
ρ	density
ϕ_{ij}	pressure strain tensor
$\forall$	volume
ψ	level of turbulence intensity

Subscripts

av	average
b	bulk

c	constant property
in	inlet
P	grid node at center of control volume
t	turbulent
v	viscous sublayer
w	wall
e,w,n,s	control volume faces
E,W,N,S	grid nodes at east, west, north, and south of control volume

ACKNOWLEDGMENTS

I would like to express my gratitude to Professor Mills for his excellent guidance, technical support, and kind encouragement towards the completion of this thesis, and to professors D. Allen, C. Anderson, C. Ho, and A. Lavine for their review of this work.

I also would like to thank Mr. Aeint de Boer, a consultant at the Office of Academic Computing, for his excellent assistance with installation of the PHOENICS code and numereous help in many areas of computing. Thanks are also extended to Dr. Virginia Hetrick for her kind assistance in installation of the post-processor of a graphics program. Her contribution has been very valuable not only to the current research work, but also to other students using the PHOENICS code. The financial support of the NASA Ames Dryden Flight Research Center is acknowledged. The contract monitor was Mr. Robert Quinn, and funding was facilitated by Dr. Kenneth Iliff.

ABSTRACT OF THE DISSERTATION

COMPUTATION OF TURBULENT RECIRCULATING FLOW IN CHANNELS, AND FOR IMPINGEMENT COOLING

by

Byong Hoon Chang

doctor of philosophy in Mechanical Engineering

University of California, Los Angeles, 1992.

Professor Anthony F. Mills, Chair

Fully elliptic forms of the transport equations have been solved numerically for two flow configurations. The first is turbulent flow in a channel with transverse rectangular ribs, and the second is impingement cooling of a plane surface. Both flows are relevant to proposed designs for active cooling of hypersonic vehicles using supercritical hydrogen as the coolant. Flow downstream of an abrupt pipe expansion and of a backward-facing step were also solved with various near-wall turbulence models as benchmark problems. A simple form of periodicity boundary condition was used for the channel flow with transverse rectangular ribs. The effects of various parameters on heat transfer in channel flow with transverse ribs and in impingement cooling were investigated using the Yap modified Jones and Launder low Reynolds number $k-\varepsilon$ turbulence model. For the channel flow, predictions were in adequate

agreement with experiment for constant property flow, with the results for friction superior to those for heat transfer. For impingement cooling, the agreement with experiment was generally good, but the results suggest that improved modelling of the dissipation rate of turbulence kinetic energy is required in order to obtain improved heat transfer prediction, especially near the stagnation point. The $k-\varepsilon$ turbulence model was used to predict the mean flow and heat transfer for constant and variable property flows. The effect of variable properties for channel flow was investigated using the same turbulence model, but comparison with experiment yielded no clear conclusions. Also, the wall function method was modified for use in the variable properties flow with a non-adiabatic surface, and an empirical model is suggested to correctly account for the behavior of the viscous sublayer with heating.

Chapter I

INTRODUCTION

1.1 BACKGROUND

Current interest in hypersonic flight has led to renewed activity related to high temperature structures. A critical problem is to ensure the survivability of components subjected to intense aerodynamic heating, such as the nose, wing leading edges, and the engine inlet. Hydrogen-fueled scramjet engines are under development, and a cooling system which shows considerable promise is based on the use of the hydrogen fuel as a coolant before it is injected into the combustor. Engine inlets require panels in which the hydrogen flows through channels beneath the skin. The use of enhanced surfaces to increase heat transfer coefficients inside the channels is an attractive option to improve performance. For the nose, or wing leading edges, impingement cooling is a possible approach. A jet of hydrogen impinges on the backface of the skin at the stagnation point or line, and flows rearwards.

Experimental data will certainly be required in order to develop systems described above. But test work using supercritical hydrogen is both expensive and hazardous: thus the use of modern computational fluid dynamics(CFD) methods are an attractive partial alternative. If successful computer models can be developed, the scope of the experimental program can be reduced accordingly. The CFD model then becomes a tool for interpolation in, and modest extrapolation of, the experimental data.

1.2 OBJECTIVES OF THE PRESENT STUDY

There are numerous problems relevant to active cooling, and suitable for CFD modeling. Two problems have been chosen for the present study. These are :

1. The development of roughness functions for transverse ribs used to augment heat transfer in channel flow. These functions will facilitate the engineering calculation of pressure drop and heat transfer in cooling panels.
2. Prediction of the flow field and heat transfer rates for two- dimensional impingement cooling. The results will facilitate the design of the impingement system as a heat exchanger.

These problems have three important features in common. Firstly, both involve recirculating flows with flow separations and reattachments. Thus the elliptic form of the transport equations must be solved. Secondly, both flows are turbulent, and due to the critical importance of heat transfer near flow re-attachment points, simple turbulence models, such as the mixing length model, are inadequate. Thirdly, fluid property variations are large adjacent to the wall of primary interest. It is therefore necessary to solve the conservation equations in the near wall region: so called conventional wall functions should not be used to bridge the region. Hence an essential requirement of this study is a suitable turbulence model which can be used for recirculating flows with large property variations.

A mixing-length turbulence model is not suitable for these flows because the turbulent viscosity and thermal conductivity vanish where the mean velocity

gradient is zero; also, the influence of convection and diffusion on the turbulence kinetic energy are not accounted for. Two-equation models of turbulence are more suitable for these flows, and many variations have been used by prior workers. The conventional wall function approach replaces the near wall region with formulas based on the logarithmic velocity and temperature profiles in order to avoid using a fine grid near the wall. However, unless special wall functions are developed, which properly account for variable property effects, a fine grid is required near the wall.

Since experimental data for the problems of interest is sparse, related problems, namely heat transfer downstream of a sudden pipe expansion and of a backward-facing step, will be used as benchmarks to initially test the turbulence model, and the computational technique. These flows have been the subject of many experimental and numerical studies: there is both a good data base, and a well documented history of turbulence model development.

1.3 LITERATURE SURVEY

1.3.1 *Flow downstream of a sudden pipe expansion*

The flow over a backward-facing step or the flow downstream of a sudden pipe expansion is very complex. It involves recirculating flow, shear layer reattachment, a counterrotating secondary vortex in the corner, and boundary layer redevelopment. According to Eaton and Johnston [1], the length of the separation region behind the step fluctuates so that the impingement point of

the separated shear layer is not stationary. The measured maximum backward velocity in the recirculating flow region is reported to be usually over 20 % of the freestream velocity. The $k-\varepsilon$ two-equation model that determines the turbulent viscosity from the solution of two transport equations, namely the turbulent kinetic energy, k, equation and its dissipation rate, ε, equation, has been used by various workers to solve this recirculating flow. The standard model is applicable only to regions of high Reynolds number, and its use with wall function approach to bridge the viscous sublayer has been popular in order to reduce computing costs. But, a conventional wall function based on the friction velocity, $u^*=\sqrt{\frac{\tau_w}{\rho}}$, is not appropriate for this flow since the predicted heat transfer is zero at separation and reattachment points. This deficiency in the wall function can be removed by adopting the turbulence kinetic energy as a velocity scale, as proposed by Launder and Spalding [2]. A wall function approach based on constant non-dimensional viscous sublayer thickness was attempted by Chieng and Launder [3]. A coding error of Chieng and Launder was detected by Johnson and Launder [4], and a subsequent recalculation showed underprediction of Nusselt number for the experimental heat transfer data of Zemanick and Dougall [5]. Johnson and Launder [4] obtained good results by making the nondimensional viscous sublayer thickness a linear function of the ratio of the rate of turbulence energy diffusion to the rate of turbulence energy dissipation in the sublayer. Amano [6] extended this two-layer model to a three-layer model by introducing a buffer layer between the viscous and turbulent regions. The prediction by the three-layer model compared favorably with the experimental data of Amano et al. [7].

Launder [8] has made a critical evaluation of the wall function approach, and concluded that a more appropriate form of the turbulence energy dissipation rate equation needs to be established before further refinement of wall functions. Also, the use of wall functions failed to predict the secondary corner vortex. Baughn et al. [9] have made extensive experimental measurements of the local heat transfer coefficients to an air flow downstream of an axisymmetric abrupt expansion in a circular pipe with a constant wall heat flux. The runs were made with the expansion ratio from 0.267 to 0.8 and over the Reynolds number range of 5300 to 87000. The maximum Nusselt number was almost eleven times larger than that for fully developed pipe flow, as given by the Dittus-Boelter relation, for an expansion ratio of 0.266 based on pipe diameters, and a downstream Reynolds number of 8,112. Launder [10] presented a review on the various methods for computing heat transfer coefficients in complex turbulent flows. A significant improvement in the calculation of heat transfer rates by Yap [11] was the addition of a source term to the dissipation rate equation to reduce the excessive turbulence near-wall length scale. A comparison with Baughn's experimental data showed that the method of adopting a low Reynolds number $k-\varepsilon$ model across the sublayer and an algebraic stress model beyond gave the best heat transfer prediction with a good Reynolds number dependence. However, the prediction by a low Reynolds number $k-\varepsilon$ model with the Yap's correction was fairly good. With the low Reynolds number $k-\varepsilon$ model, computations are performed all the way to the wall, and the algebraic stress model employs a simplified form of the Reynolds stress transport equations.

1.3.2 *Flow downstream of a backward-facing step*

Aeronautical researchers have long been interested in the flow over a backward-facing step because of the practical importance of predicting base pressure of bluff bodies moving with high speed(such as bullets and coasting missiles) [12]. More work has been done in supersonic flow, but the low speed flow over a backward-facing step is also used as a building block flow for workers developing turbulence models [1]. Some of more relevant work in literature to the present study are listed here.

Eaton and Johnston [1] were among the first to make measurements in the highly unsteady and reversing flow behind a backward-facing step using a pulsed-wire anemometer, thermal tuft, and pulsed-wall probe. Turbulence quantities and the skin friction were measured, and it was found that the turbulence intensity decreases rapidly downstream of reattachment in the redeveloping boundary layer with the turbulence actually beginning to decay upstream of reattachment some one or two step heights. Durst and Tropea [13] used a water channel to study a backward-facing step flow, acquiring the data with a laser-doppler anemometer. In their study, they varied the expansion ratio and found a strong dependence of the reattachment length on this quantity. Driver and Seegmiller [14] acquired wind-tunnel fluid dynamic data for the backward-facing step using a laser-doppler anemometer. They obtained many of the important turbulence quantities, such as production and dissipation rates in the flow. In their comparison with various numerical methods, they found that a modified algebraic stress model predicts the flow more accurately than does the $k - \varepsilon$ model or the unmodified algebraic model.

The modified algebraic stress model was found to be more sensitive to streamline curvature effects on the turbulence.

Seban [15] measured velocity and temperature distribution downstream of a backward facing step using a constant heat flux surface. For a one-inch step and a free-stream velocity of 150 *ft/* sec, he found that the mean reattachment point was about six step heights downstream of the step. The typical law of the wall was not found in either the separation or reattachment regions. Filetti and Kays [16] measured the local heat transfer coefficient on a constant-temperature surface behind a symmetric sudden expansion. The expansion ration of 2:1 was used, and the peak heat transfer rate occured at the reattachment point, which was approximately four step heights downstream of the step. Significant augmentation of heat transfer rate downstream of reattachment, up to six times the flat-plate value, was found. However the measurements were taken from the step edge to 14 step heights downstream and the Nusselt number profile did not approach the typical flat-plate value. The peak heat transfer rate based on Nusselt number was found to vary as $Re^{0.6}$ over the range $70{,}000 < Re < 205{,}000$. Seki et al. [17], [18] obtained temperature and velocity measurements in the flow over the constant heat flux surface of a double-sided, backward-facing step. The velocity and temperature measurements were correlated to measure $\overline{v'T'}$, the turbulent transport of energy in the direction normal to the wall. The $\overline{v'T'}$ profiles indicated that the turbulent transport of heat in the direction normal to the surface increases as $Re^{2/3}$ and is proportional to the heat flux rate from the wall. Vogel and Eaton [19] used a single sided sudden expansion with a constant heat flux surface to make

combined heat transfer and fluid dynamic measurements in a separated and reattaching boundary layer. Stanton number profiles were obtained for four different Reynolds numbers ranging from 13,000 to 42,000, and the bottom wall of the development section was porous to vary the boundary layer thickness at the test section entrance from 0.3 to 6 *cm*. The upstream boundary layer thickness had a significant effect of the heat transfer rate near reattachment but very little effect either up- or downstream of reattachment. The temperature profiles showed that the heat transfer resistance is dominated by the near-wall region.

Sindir [20] performed a numerical study of the effects of expansion ratio on two-dimensional separating and reattaching flow in plane backward-facing step with four models of turbulence. The $k-\varepsilon$ model, modified $k-\varepsilon$ model, algebraic stress model, and modified algebraic stress model were used, and the modified versions employed a production term in the dissipation equation that was made more sensitive to streamline curvature effects. The modified algebraic stress model produced the best predictions in the reverse flow region but performed more poorly than others in the redevelopment region. Heat transfer calculations were not performed. Gooray et al. [21] employed a two-pass procedure: the first pass with an improved $k-\varepsilon$ model with the standard wall function to find the reattachment point and the second pass with an improved low-Reynolds number model applied to downstream of the reattachment. Good prediction of the local Nusselt number was obtained downstream of the step, but comparasion was made with limited data. Scherer and Wittig [22] have used the $k-\varepsilon$ model with one-layer and two-layer wall function ap-

proach of Chieng and Launder [3]. The reattachment length was underpredicted by 10 to 20% for the Reynolds number from 40,000 to 85,000. The peak heat transfer was significantly underpredicted by the one-layer model, and the two-layer model gave good prediction of local Nusselt number downstream of the step. Ciofalo and Collins [23] have noted that the method of Johnson and Launder [4] involves the near-wall profile of the turbulence kinetic energy, and is sensitive to numerical errors. They have noted that slopes of the nondimensional velocity profiles in the reverse flow region and shortly downstream of reattachment point were not far from the equilibrium value, while the intersection with the linear region was greatly reduced. They modified the standard wall functions to relate the non-dimensional viscous sublayer thickness to the near-wall turbulence intensity. Comparison of the Nusselt number prediction with the experiment data on backward-facing step showed significant improvement over the standard wall functions. However, the prediction downstream of the reatttachment point converged to a value about 12% lower than that of the experimental data.

1.3.3 *Roughness functions for transverse ribs*

The pioneering work on roughness functions was done by Nikuradse [24] who performed extensive experimental measurements on circular pipes with sand of a definite grain size glued on the inside surface. He showed that the dimensionless velocity distribution is given by :

$$u^+ = 2.5 \ln \left(\frac{y}{e}\right) + R(e^+) \qquad (1)$$

where $R(e^+)$ is termed the roughness function.

A similar approach based on a modified Reynolds analogy was used by Dipprey and Sabersky [25] to correlate their heat transfer data for flow inside tubes with a sand grain indentation surface. The Stanton number was given as :

$$St = \frac{\frac{c_f}{2}}{1 + \sqrt{\frac{c_f}{2}}\,[H(e^+, Pr) - R(e^+)]} \tag{2}$$

where the heat transfer roughness function $H(e^+, Pr)$ was correlated as

$$H = 5.19\, k_s^{+\,0.22}\, Pr^{0.44} \tag{3}$$

Following Nikuradse, $R(e^+)$ was taken as 8.5 for fully rough flow.

Webb, Eckert, and Goldstein [26] used their experimental data to develop the roughness functions R and H for flow in a tube of repeated transverse rib roughness. For $0.01 < \frac{e}{D} < 0.04$, $10 < \frac{L}{e} < 40$, and $e^+ \geq 35$,

$$R = 0.95\,(\frac{L}{e})^{0.53} \tag{4}$$

$$H = 4.5\, e^{+\,0.28}\, Pr^{0.57} \tag{5}$$

Han et al. [27] performed experiments to study additional effects of rib shape and angle of attack of ribs to main flow in a channel with repeated transverse rib roughness. A 45° flow attack angle was found to give higher heat transfer for the same pressure drop, as compared to a 90° flow attack angle. Their roughness functions for 90° flow attack angle are

$$R = 0.97\,(\frac{L}{e})^{0.53} \quad \text{for} \quad L/e \geq 10,\ e^+ \geq 35$$
$$= 4.45\,(\frac{L}{e})^{-0.13} \quad \text{for} \quad L/e \leq 10,\ e^+ \leq 35 \tag{6}$$

$$H = 5.05\,e^{+0.28}\,Pr^{0.57} \quad \text{for} \quad e^+ \geq 35 \tag{7}$$

Han et al. based the heat transfer coefficient on the total area of the heat transfer surface including the rib area, for the ribs constituted an appreciable fraction of the total area for a small value of L/e. When the heat transfer coefficient is based on the projected area, the heat transfer roughness function becomes

$$H = 4.04\,e^{+0.28}\,Pr^{0.57} \quad \text{for} \quad e^+ \geq 35 \tag{8}$$

Dalle Donne and Meyer [28] performed experiments in an annulus with an inner surface of transverse rectangular ribs and a smooth outer surface. For, $e^+ \geq 30$, the roughness functions were correlated as

$$R = R(\infty) + 0.4\,ln(\frac{e}{0.01D/2}) \tag{9}$$

where

$$R(\infty) = 9.3\,(\frac{L-b}{e})^{-0.73} - [\,2 + \frac{7}{(L-b)/e}\,]\,\log_{10}(\frac{e}{b}) \tag{10}$$

$$\text{for} \quad 1 \leq \frac{L-b}{e} \leq 6.3$$

$$R(\infty) = 1.04\,(\frac{L-b}{e})^{0.46} - [\,2 + \frac{7}{(L-b)/e}\,]\,\log_{10}(\frac{e}{b}) \tag{11}$$

$$\text{for} \quad 6.3 \leq \frac{L-b}{e} \leq 160$$

$$H = (4.16\, e^{+0.282} + \frac{53}{e^{+1.6}})\, Pr^{0.44} (\frac{T_w}{T_b})^{0.5} [\frac{e}{0.01\,(r_2 - r_1)}]^{0.053} \quad (12)$$

The first attempt to analytically determine the roughness functions for flow over rectangular ribs was made by Lewis [29]. The flow was approximated by a series of attached and separated flow regions, and some empirical information from experiments over cavities and steps was required. The $k - \varepsilon$ turbulence model with the wall function boundary condition was used by Lee et al. [30] to predict roughness functions in an annulus with ring type rectangular roughness on the inner pipe. In a numerical study, fully developed flow in a single module was solved using the periodicity conditions, as proposed by Patankar et al. [31], in order to avoid the entrance region problem. A correction to the turbulent viscosity similar to that of Leschziner and Rodi [32] was used to account for extra strain rates due to streamline curvature. However, as shown by Launder [10] the use of a wall function gives rather poor prediction of Nusselt number for flow in an abrupt pipe expansion and flow around a 180° square-sectioned bend.

1.3.4 *Variable properties flow*

There have been numerous experimental studies on heat transfer in turbulent flow in smooth round tubes with large wall to bulk temperature ratio, and many correlation methods have been proposed. A good review is given by Petukhov [33]. For heat transfer, a recommended correlation is

$$Nu_b = C\, Re_b^{0.8}\, Pr_b^{0.4} \left(\frac{T_w}{T_b}\right)^n \tag{13}$$

where C and n are constants far from the entrance. Petukhov observes that different investigators obtained different values for n depending on the range of T_w/T_b. For variable property gases, he suggests

$$n = -(a \log \left(\frac{T_w}{T_b}\right) + 0.36) \tag{14}$$

$a = 0$ for cooling, and $a = 0.3$ for heating was recommended.

For the friction factor, the recommended correlation is

$$\frac{f_b}{f_c} = \left(\frac{T_w}{T_b}\right)^m \tag{15}$$

where

$$m = -0.6 + 5.6\, Re_w^{-0.38} \tag{16}$$

Petukhov used the Reichardt eddy diffusivity profile to obtain analytical results.

Sleicher and Rouse [34] found a better fit to large amount of heating data when n was modified to

$$n = -\log \left(\frac{T_w}{T_b}\right)^{1/4} + 0.3, \quad 1 < T_w/T_b < 5,\ x/D > 40 \tag{17}$$

Many correlations are of similar form and three that are among the many reviewed by Petukhov are summarized below. McEligot et al. [35] have per-

formed experiments with air, nitrogen, and helium in a tube with entering Re from 15,000 to 233,000. The following forms were recommended

$$Nu_b = 0.021\, Re_b^{0.8}\, Pr_b^{0.4} \left(\frac{T_w}{T_b}\right)^{-0.5} \left[1 + \left(\frac{x}{D}\right)^{-0.7}\right]$$
$$\frac{f_b}{f_c} = \left(\frac{T_w}{T_b}\right)^{-0.1} \qquad \text{for } 1 < T_w/T_b < 2.5 \tag{18}$$

Lelchuk and Dyadyakin [36] recommend the same correlation for the heat transfer without the entry length correction term, but for the friction factor the exponent on the temperature ratio, m, was recommended as -0.16 for $1.3 < \frac{T_w}{T_b} < 2.4$. Perkins and Worsoe-Schmidt [37] used precooled nitrogen to obtain local values of T_w/T_b from 1.24 to 7.54. Recommended correlations were

$$Nu_b = 0.024\, Re_b^{0.8}\, Pr_b^{0.4} \left(\frac{T_w}{T_b}\right)^{-0.7} \left[1 + \left(\frac{x}{D}\right)^{-0.7} \left(\frac{T_w}{T_b}\right)^{0.7}\right]$$
$$\frac{f_w}{f_c} = \left(\frac{T_w}{T_b}\right)^{-0.6} \tag{19}$$

Perkins found that when the correlation of friction factor was tried on the bulk Reynolds number, the exponent, n, had to increase from 0.1 to 0.3 over the temperature ratio range of the experiment. The above correlation for friction factor was based on the wall Reynolds number.

Experiments with repeated-rib roughness were performed by Vilemas and Simonis [38]. Air was used in annuli with a rough inner wall for $5 \times 10^3 < Re < 5 \times 10^5$, $1 < T_w/T_{in} < 2.8$, $0.0028 < e/d_e < 0.021$, and $8.3 < L/e < 13$. For rectangular roughness d_1/d_2 was 0.42, and for rounded trapezoidal roughness d_1/d_2 was 0.35. The outer wall was smooth, and only the

inner wall heated. It was found that, unlike smooth channels, the influence of T_w/T_b on the local heat transfer in rough annular channels depends heavily on Re. The effect of T_w/T_b decreased with increasing Re. The influence of Re on the exponent, n, was greater for larger e/d_e. For example, for a channel with $e/d_e = 0.021$, n changed from about -0.36 at $Re = 2.8 \times 10^4$ to -0.1 at $Re = 3.5 \times 10^5$. The exponent, n, was correlated within $\pm$ 10 % by

$$n = -(0.29 + 0.03\, e^{5/\sqrt{e/d_e}})\, Re^{24\, e/d_e}(1 - e^{-0.16\, x/d_e}) \qquad (20)$$

The friction factor for annular channels with rectangular roughness was correlated within $\pm$ 4 % by

$$f_b = (0.053 + 1.83\frac{e}{d_e})\, Re_b^{-0.07} \qquad (21)$$

In their experiment, an influence of variable properties on the friction was not observed in smooth channels for T_w/T_{in} up to 1.8. For the rough channel, the effect of variable properties decreased with an increasing Re and became negligible at Re of about 5×10^5.

Wassel and Mills [39] performed numerical calculations for variable properties turbulent flow with cooling for both smooth and rough walls. For flow in rough pipes, the Nikuradse mixing length expression was used with a roughness form drag coefficient and sub-layer Stanton number characterizing transport to the wall. The variable properties in the roughness functions were evaluated at the characteristic roughness height. Flow in a pipe with the sandgrain roughness size equal to $k_s/R = 15$ and 60, and rectangular rib roughness with $e/R = 0.02$ and $L/e = 10$ were investigated. The results

showed that f_b/f_c depends on the roughness pattern and size, and a slight effect of Reynolds number was observed. For the large sandgrain size, the Reynolds number effect on St_b/St_c was large. The following correlations were recommended for the ribs.

$$\frac{f_b}{f_c} = \left(\frac{h_w}{h_b}\right)^{-0.2}, \quad \frac{St_b}{St_c} = \left(\frac{h_w}{h_b}\right)^{-0.25} \tag{22}$$

1.3.5 *Jet impingement cooling*

There have been numerous experimental studies of both turbulent free jets and turbulent impinging jets in literature: some of the work relevant to the present study is described. Poreh, Tsuei, and Cermak [40] made measurements of mean velocities, turbulence intensities, Reynolds stresses, and the wall friction in a radial jet formed by an impinging circular jet on a smooth flat plate. The ranges of parameters were H/d = 8 - 24, and Re = 64,000 - 288,000, where H is the distance from jet outlet to the impingement surface and d is the jet outlet diameter. Beltaos and Rajaratnam [41] performed experiments on plane turbulent impinging jets over the range, H/d = 14.04 - 67.5 and Re = 5,270 - 9,400. Mean velocities, static pressure, and shear stresses over the impingement surface, and mean velocities and turbulent shear stresses over the free jet region have been reported. Beltaos and Rajaratnam [42] also made similar measurements for circular turbulent jet impingement over the range of H/d = 21.2 - 65.7 and Re = 35,200 - 80,400. Giralt et al. [43] made measurements for circular turbulent impinging jets over the range, H/d = 1.2

- 25 and Re = 30,000 - 80,000. Velocity and length scales of the impingement flow field were used to scale impinging jet centerline velocities and pressure distributions. Wygnanski and Fiedler [44] made measurements of mean velocities and turbulence quantities for an axisymmetric turbulent free jet. It was concluded that the jet was truly self-preserving some 70 diameters downstream of the nozzle. The Reynolds number was in the order of 100,000, and most of the measurements were made for the distance of 40 to 100 diameters downstream.

Gardon and Akfirat [45] were among the first workers to make thorough heat transfer measurements for two-dimensional turbulent impinging jets. Their results showed that stagnation heat transfer coefficients can be increased by artificially increasing the initial turbulence of the jet, with the effect being the largest for $H/d < 8$. A secondary peak in heat transfer coefficient for $H/d = 2$ gradually disappeared with increasing induced turbulence. With circular jets, they also observed the peak heat transfer coefficient at $r = 1/2\, d$ (rather than at the stagnation point) over a range of nozzle-to-plate spacings, up to about $H/d = 3$. Goldstein and Behbahani [46] performed experiments to study the effects of cross flow on a circular jet impinging on a flat plate. The maximum Nusselt number was found to decrease with increasing cross flow for jet-to-plate spacing, L/d_j , of 12, but for $L/d_j = 6$, the maximum Nusselt number increased with moderate cross flow when $(\rho_j u_j)/(\rho_\infty u_\infty) > 9$. Hrycak [47] made stagnation point heat transfer measurements for round jets impinging on a flat plate, and found a Nusselt number dependence on the 1/2 power of the Reynolds number over the range, H/d = 1 - 20 and Re = 14,000

- 67,000. More recently, Baughn and Shimizu [48] made a careful measurement of heat transfer coefficients of a single air jet impinging on a flat surface. For $H/d = 2$, a second maximum heat transfer occurred at r/d of approximately 2. The local Nusselt number decreased to 70% of the Nusselt number at the stagnation point at about $r/d = 1.5$, increased to 80% at about $r/d = 2$, and then decreased to 20% at $r/d = 9$. The experimental data for only one Reynolds number equal to 23,750 was reported, and the stagnation Nusselt number was 140 for $H/d = 2$. As with other investigators, the maximum stagnation point heat transfer occurred at a H/d of approximately 6. Unlike Gardon and Akfirat's measurements, the peak heat transfer rate occurred at the stagnation point, and not at $r = 1/2\ d$ for $H/d = 2$.

Wolfshtein [49] employed a one-equation turbulence model with wall function boundary condition for a jet normal to a flat plate. Only momentum equations were solved in the numerical study. Amano and Brandt [50] performed a numerical study of the flow characteristics of a turbulent jet with the high Reynolds number form of $k - \varepsilon$ model. Upper plate surface pressure, ground plane surface pressure, and velocity field for two-dimensional jet impingement were computed by Chuang [51] using the high Reynolds number $k - \varepsilon$ model. Similar computations were also performed by Hwang and Liu [52] with a fully developed jet velocity profiles along the inlet of computation domain. Agarwal and Bower [53] used the Jones and Launder's low-Reynolds number model to study the pressure distributions on the ground plane in the presence of upper surface in normal impingement of the compressible jet as in the case of VTOL aircraft. Good agreement was ob-

tained. Malin [54] has used variations of the standard $k-\varepsilon$ model and $k-W$ model of Spalding [55] to compute free jets and wall jets with the forward marching-integration procedure of PHOENICS. Inclusion of the irrotational strain terms in the production term of the turbulent kinetic energy generally gave improvements in the jet spreading rates. Predictions of the turbulent shear stress and the turbulent kinetic energy improved close to the center of the jet or the impingement wall, and somewhat deteriorated in the outside regions.

A plane turbulent jet impinging obliquely at 70° on a flat surface was solved by Hwang and Tsou [56] using a two- equation turbulence model with wall function boundary conditions. The distribution of the inlet profile was obtained from the solution of plane turbulent jet, and the Nusselt number predictions compared well with experimental data, except at the stagnation point where there seems to be about 32% overprediction. Rodi and Scheuerer [57] used Lam and Bremhorst's [58] low-Reynolds number version of the $k-\varepsilon$ model to predict the heat transfer coefficients around gas turbine blades. The stagnation point was avoided by prescribing inlet profiles of dependent variables. Predicted and measured heat transfer coefficients were in good agreement except in the transition region due to its short length predicted by the turbulence model. Computations of two-dimensional turbulent free jet and turbulent impinging jet were made by Looney and Walsh [59]. Generally good predictions of hydrodynamic and turbulence quantities were obtained with the standard $k-\varepsilon$ model, but the results of the heat transfer coefficients on the impingement surface were generally poor. The algebraic stress model

gave improvement in prediction of both mean and turbulence quantities for a developing plane free jet. Amano and Sugiyama [60] employed Chieng and Launder's wall functions to predict heat transfer coefficients for an axisymmetric jet impinging on a flat plate. A fairly good prediction for H/d = 4 and Re = 20,000 was obtained , but there was a 35% overprediction at the stagnation point, and about 27-33% underprediction over the range r/d = 3 - 15 occured when compared with data for H/d = 10. Polat et al. [61] studied the effect of various wall functions on prediction of heat transfer for a confined two- dimensional turbulent air jet impinging on a flat surface. Chieng and Launder's wall functions approach with the turbulent kinetic energy evaluated at the first node instead of at the edge of the viscous sublayer in the evaluation of wall shear stress gave the best prediction. Even though this method correctly predicted the secondary peak in heat transfer coefficient for H/d = 2.6, the prediction became poor downstream of the stagnation point, with about 37% overprediction at y/d = 16. For $H/d > 6$, the model continued to predict off-stagnation minima and maxima even though such features are not present in experiment, thus the prediction became poor in the vicinity of the stagnation point also. As with Amano and Sugiyama, the wall function approach seems to perform poorly in the redeveloping region. Polat et al. [62] made flow and heat transfer predictions for confined turbulent impinging slot jets, with and without through-flow. Chieng and Launder's wall functions and the modified shear stress expression to account for the effect of mass transfer at the impingement surface were used. Generally good predictions for heat transfer coefficients within 10% were obtained for small through-flow,

but substantial overprediction at the stagnation point and at higher through-flow rates occured. Yap [11] has made calculations for the impinging jet flow experiment of Goldstein and Behbahani [46], with both the algebraic stress model and the low Reynolds number $k-\varepsilon$ model. Comparisons of the two methods were made for predictions of centerline velocity decay and mean velocity and temperature profiles downstream of the stagnation point, and there was little difference. Local heat transfer predictions by both models were almost the same, and both overpredicted the stagnation point heat transfer by 15 %. Predictions were not in good agreement within about a nozzle diameter of the stagnation point, but improved further away. Only one value of the parameter H/d ($= 6$) and one value of Reynolds number was investigated.

Hrycak [63] reports that there are a substantial number of investigations of heat transfer from jets impinging on flat plates but only relatively few experimental results concerning heat transfer from jets impinging on concave surfaces. Some of the early experimental studies related to the concave inner surface of gas turbine airfoils cooled by impinging air jets were done by Metzger et al. [64], Chupp et al. [65], and Jusionis [66]. More relevant to the present study is the experimental work by Livingood and Gauntner [67] [68], [69]. Correlations of Nusselt number were presented in terms of the dimensionless quantities involving nozzle diameter, nozzle-to-target separation distance, target cylinder diameter, and nozzle center-to- center spacing for number of air jets more than one. The nozzle-to- target separation distance was found to have a greater effect on the normalized Nusselt number distribution than did the variation of Reynolds number. Hrycak [63] performed a

similar experiment with a much more careful study of the hydrodynamics of the impinging jet. His heat transfer correlation was based on Froessling's hydrodynamics solution [70] and Colburn's analogy.

Chapter II

MATHEMATICAL MODEL

2.1 MEAN TRANSPORT EQUATIONS

The set of elliptic partial differential equations governing a single- phase, compressible, variable property flow is as follows.

Continuity:

$$\frac{\partial \rho}{\partial t} + \frac{\partial}{\partial x_i}(\rho u_i) = 0 \tag{23}$$

Momentum:

$$\frac{\partial}{\partial t}(\rho u_i) + \frac{\partial}{\partial x_j}(\rho u_i u_j) = -\frac{\partial p}{\partial x_i} + F_i + \frac{\partial \tau_{ij}}{\partial x_j} \tag{24}$$

Energy:

$$\frac{\partial}{\partial t}(\rho h) + \frac{\partial}{\partial x_j}(\rho u_j h) = \frac{\partial}{\partial x_j}(\Gamma \frac{\partial T}{\partial x_j}) + \tau_{ij}\frac{\partial u_i}{\partial x_j} + \frac{\partial P}{\partial t} + u_j \frac{\partial P}{\partial x_j} \tag{25}$$

where the stress tensor, τ_{ij}, is given by

$$\tau_{ij} = \mu(\frac{\partial u_i}{\partial x_j} + \frac{\partial u_j}{\partial x_i}) - \frac{2}{3}\mu \frac{\partial u_k}{\partial x_k}\delta_{ij} \tag{26}$$

The instantaneous components in the above equations can be decomposed into sums of mean and fluctuating parts. For example, the streamwise velocity component, u, can be written as,

$$u = \overline{U} + u'$$

Ignoring fluctuations of physical properties except density, and time-averaging the decomposed equations yields the following.

Continuity:

$$\frac{\partial \overline{\rho}}{\partial t} + \frac{\partial}{\partial x_i}(\overline{\rho}\ \overline{U}_i + \overline{\rho' u'_i}) = 0 \tag{27}$$

Momentum:

$$\begin{aligned}\frac{\partial}{\partial t}(\overline{\rho}\ \overline{U}_i + \overline{\rho' u_i'}) + \frac{\partial}{\partial x_j}(\overline{\rho}\ \overline{U}_i\ \overline{U}_j) = &-\frac{\partial \overline{P}}{\partial x_i} - \frac{\partial}{\partial x_j}(\overline{\rho' u_i'}\ \overline{U}_j + \overline{\rho' u_j'}\ \overline{U}_i) \\ &+ \frac{\partial}{\partial x_j}\left[\mu\left(\frac{\partial \overline{U}_i}{\partial x_j} + \frac{\partial \overline{U}_j}{\partial x_i}\right)\right] - \frac{\partial}{\partial x_j}(\overline{\rho' u_i' u_j'}) - \frac{\partial}{\partial x_j}(\overline{\rho}\ \overline{u_i' u_j'}) + F_i\end{aligned} \tag{28}$$

Energy

$$\begin{aligned}\frac{\partial}{\partial t}(\overline{\rho}\overline{h} + \overline{\rho' h'}) + \frac{\partial}{\partial x_j}(\overline{\rho}\ \overline{U}_j\,\overline{h}) = &\frac{\partial}{\partial x_j}\left[\Gamma \frac{\partial}{\partial x_j}\left(\frac{\overline{h}}{c_p}\right)\right] \\ - \frac{\partial}{\partial x_j}(\overline{\rho}\ \overline{u_j' h'}) - \frac{\partial}{\partial x_j}(\overline{\rho' u_j' h'}) &- \frac{\partial}{\partial x_j}(\overline{\rho' h'}\ \overline{u}_j + \overline{\rho' u_j'}\ \overline{h}) \\ &+ \mu\left(\frac{\partial \overline{U}_i}{\partial x_j} + \frac{\partial \overline{U}_j}{\partial x_i}\right)\frac{\partial \overline{U}_i}{\partial x_j}\end{aligned} \tag{29}$$

The equations (27),(28), and (29) cannot be solved in their exact form. Modelling of certain terms in the equations such as $\overline{u_i' u_j'}$ are required to provide a closed set of equations.

2.2 TURBULENCE MODELS

For steady flow and neglecting turbulent correlations involving density fluctuations, the transport equations reduce to the following.

$$\frac{\partial}{\partial x_i}(\rho U_i) = 0 \tag{30}$$

$$\frac{\partial}{\partial x_j}(\rho U_i U_j) = -\frac{\partial P}{\partial x_j} + \frac{\partial}{\partial x_j}\left[\mu\left(\frac{\partial U_i}{\partial x_j} + \frac{\partial U_j}{\partial x_i}\right) - \rho\overline{u_i u_j}\right] \tag{31}$$

$$\begin{aligned}\frac{\partial}{\partial x_j}(\rho U_j h) = \frac{\partial}{\partial x_j}\left[\Gamma \frac{\partial}{\partial x_j}\left(\frac{h}{c_p}\right) - \rho\overline{u_j h'}\right] \\ + \mu\left(\frac{\partial U_i}{\partial x_j} + \frac{\partial U_j}{\partial x_i}\right)\frac{\partial U_i}{\partial x_j}\end{aligned} \tag{32}$$

where the overbar notation for mean values and the prime notation for the fluctuating component of velocities has been dropped. The time mean of the product of the fluctuating velocities are modelled using the modified Boussinesq concept

$$-\overline{u_i u_j} = \nu_t\left(\frac{\partial U_i}{\partial x_j} + \frac{\partial U_j}{\partial x_i}\right) - \frac{2}{3} k\,\delta_{ij} \tag{33}$$

The turbulent heat fluxes are approximated using the eddy diffusivity concept as

$$-\rho\overline{u_j h'} = \frac{\mu_t}{Pr_t}\frac{\partial h}{\partial x_j} \tag{34}$$

2.2.1 *The high-Reynolds number k-ε model*

For the $k-\varepsilon$ model, the turbulent viscosity, μ_t, is modelled as

$$\mu_t = c_\mu \rho \frac{k^2}{\varepsilon} \tag{35}$$

where c_μ is a constant for high Reynolds number flow.

The transport equation for turbulent kinetic energy k can be obtained from manipulation of the three normal stress equations [71].

$$\frac{\partial}{\partial x_j}(\rho U_j k) = -\frac{\partial}{\partial x_j}\overline{\left[u_i(p' + \rho k)\right]} - \rho\,\overline{u_i u_j}\frac{\partial U_i}{\partial x_j} + \mu\frac{\partial}{\partial x_j}\overline{u_i\left(\frac{\partial u_i}{\partial x_j}+\frac{\partial u_j}{\partial x_i}\right)} - \mu\overline{\frac{\partial u_i}{\partial x_j}\left(\frac{\partial u_i}{\partial x_j}+\frac{\partial u_j}{\partial x_i}\right)} \tag{36}$$

Following Jones and Launder [72], the diffusion term is modelled as

$$-\frac{\partial}{\partial x_j}\overline{\left[u_i(p' + \rho k)\right]} = \frac{\partial}{\partial x_j}\left(\frac{\mu_t}{\sigma_k}\frac{\partial k}{\partial x_j}\right) \tag{37}$$

Substitution of the above equation into Eq.(36) and rewriting the last two terms on the RHS results in the following form valid for high Reynolds number flow,

$$\frac{\partial}{\partial x_j}(\rho U_j k) = \frac{\partial}{\partial x_j}\left(\frac{\mu_t}{\sigma_k}\frac{\partial k}{\partial x_j}\right) + P - \rho\varepsilon \tag{38}$$

where ε is the dissipation rate of turbulent kinetic energy defined as

$$\varepsilon \equiv \nu \overline{\frac{\partial u_i}{\partial x_j}\frac{\partial u_i}{\partial x_j}} \tag{39}$$

and P denotes the generation rate of turbulence energy.

$$P \equiv -\rho\overline{u_i u_j}\frac{\partial U_i}{\partial x_j} \tag{40}$$

The transport equation for ε is obtained by taking the derivative of the instantaneous x_i direction momentum equation with respect to x_j, multiplying by $2\nu\,\partial u_i'/\partial x_j$ and then averaging.

$$\begin{aligned}\frac{\partial}{\partial x_j}(\rho U_j \varepsilon) = &-\frac{\partial}{\partial x_j}\left[-\mu\overline{u_j\left(\frac{\partial u_i}{\partial x_k}\right)^2} - 2\nu\overline{\frac{\partial p'}{\partial x_i}\frac{\partial u_j}{\partial x_i}} + \mu\frac{\partial \varepsilon}{\partial x_j}\right] \\ &- 2\mu\frac{\partial U_k}{\partial x_j}\left(\overline{\frac{\partial u_i}{\partial x_j}\frac{\partial u_i}{\partial x_k}} + \overline{\frac{\partial u_k}{\partial x_i}\frac{\partial u_j}{\partial x_i}}\right) - 2\mu\overline{u_k\frac{\partial U_i}{\partial x_j}}\frac{\partial^2 u_i}{\partial x_j \partial x_k} \\ &- 2\mu\overline{\frac{\partial u_i}{\partial x_k}\frac{\partial u_i}{\partial x_j}\frac{\partial u_k}{\partial x_j}} - 2\mu\overline{\left(\frac{\partial^2 u_i}{\partial x_j \partial x_k}\right)^2}\end{aligned} \tag{41}$$

Following Jones and Launder [72], the diffusion term is modelled as

$$\frac{\partial}{\partial x_j}\left[-\mu\overline{u_j\left(\frac{\partial u_i}{\partial x_k}\right)^2}\right] = \frac{\partial}{\partial x_j}\left(\frac{\mu_t}{\sigma_\varepsilon}\frac{\partial \varepsilon}{\partial x_j}\right) \tag{42}$$

The last two terms on the RHS of Equation (41) are approximated as

$$-2\mu\overline{\frac{\partial u_i}{\partial x_k}\frac{\partial u_i}{\partial x_j}\frac{\partial u_k}{\partial x_j}}-2\mu\overline{\left(\frac{\partial^2 u_i}{\partial x_j\partial x_k}\right)^2}=\frac{\varepsilon^2}{k}\left(c_{\varepsilon 1}\frac{P}{\varepsilon}-\rho\,c_{\varepsilon 2}\right)\quad(43)$$

Assuming the turbulent diffusion due to pressure fluctuations is small, Hanjalic [73] has found the following form may provide the basis for satisfactory predictions for high Reynolds number flows,

$$\frac{\partial}{\partial x_j}(\rho U_j\varepsilon)=\frac{\partial}{\partial x_j}\left(\frac{\mu_t}{\sigma_\varepsilon}\frac{\partial\varepsilon}{\partial x_j}\right)+c_{\varepsilon 1}\frac{\varepsilon}{k}P-c_{\varepsilon 2}\rho\frac{\varepsilon^2}{k}\quad(44)$$

The recommended empirical coefficients are

$$c_\mu=0.09,\ c_{\varepsilon 1}=1.44,\ c_{\varepsilon 2}=1.92,\ \sigma_\varepsilon=1.3,\ \sigma_k=1.0\quad(45)$$

This model is valid only in the turbulent flow regime where viscous effects are negligible. The wall function approach, that uses a form of the law of the wall to approximate the solution for the near wall region where viscous effects are not negligible can be used with the above model. This will be discussed in detail in section 2.2.3.

2.2.2 *The low-Reynolds number k-ε model*

Jones and Launder [72] extended the two equation turbulence model to predict the flow in the viscous sublayer. The model includes the viscous diffusion of k and ε and the coefficients in Eqs. (38) and (44) are assumed to be dependent on turbulent Reynolds number. The approximate transport equations of Jones and Launder's low Reynolds number turbulence model(JL) [72] with some constants modified by Launder and Sharma [74] are summarized below.

$$\frac{\partial}{\partial x_j}(\rho U_j k) = \frac{\partial}{\partial x_j}\left[\left(\frac{\mu_t}{\sigma_k} + \mu\right)\frac{\partial k}{\partial x_j}\right] + P - \rho\varepsilon - 2\mu\left(\frac{\partial k^{1/2}}{\partial x_k}\right)^2 \tag{46}$$

$$\begin{aligned}\frac{\partial}{\partial x_j}(\rho U_j \tilde{\varepsilon}) = &\frac{\partial}{\partial x_j}\left[\left(\frac{\mu_t}{\sigma_\varepsilon} + \mu\right)\frac{\partial \tilde{\varepsilon}}{\partial x_j}\right] + c_{\varepsilon 1}\frac{\tilde{\varepsilon}}{k}P - c_{\varepsilon 2} f_\varepsilon \rho \frac{\tilde{\varepsilon}^2}{k} \\ &+ \frac{2\mu\mu_t}{\rho}\left(\frac{\partial^2 U_i}{\partial x_k^2}\right)^2\end{aligned} \tag{47}$$

The turbulent viscosity, μ_t, is given by

$$\mu_t = c_\mu f_\mu \rho \frac{k^2}{\tilde{\varepsilon}} \tag{48}$$

where the dissipation rate, ε, is equal to $\tilde{\varepsilon} + 2\nu(\partial k^{1/2}/\partial x_k)^2$, and the function f_μ is introduced to produce the effect of molecular viscosity on the shear stress. The empirical coefficients adopted are

$$\begin{aligned} f_\mu &= \exp\left[\frac{-3.4}{(1 + Re_t/50)^2}\right] \\ f_\varepsilon &= 1.0 - 0.3\exp(-Re_t^2) \\ Re_t &= \frac{k^2}{\nu\tilde{\varepsilon}} \end{aligned} \tag{49}$$

The above equations with the appropriate boundary conditions for h, and $u_i = k = \tilde{\varepsilon} = 0$ at the wall comprise a complete model.

Chieng and Launder [3] applied this low Reynolds number model to the flow in a sudden pipe expansion, and the predicted heat transfer rates in the vicinity of the reattachment point were too high by up to a factor of 5 as a result of too large a length scale near the wall. Yap [11] added a source term S_ε to the right hand side of the transport equation for $\tilde{\varepsilon}$

$$S_\varepsilon = 0.83\left(\frac{\tilde{\varepsilon}^2}{k}\right)\left(\frac{k^{1.5}}{c_l y \tilde{\varepsilon}} - 1\right)\left(\frac{k^{1.5}}{c_l y \tilde{\varepsilon}}\right)^2 \tag{50}$$

where y is the distance from the wall, and $c_l = 2.5$. Yap found that inclusion of this source term gave Nusselt number predictions comparable with the experiment and improved the Reynolds number dependence. This term was also used in the present study.

2.2.3 *Wall functions*

For many turbulent wall boundary layers the inner portion of the flow has the logarithmic law of the wall behavior. With the wall function approach, the equations are solved on a relatively coarse grid, and the near wall region is replaced with formulas based on the logarithmic velocity and temperature profile. The logarithmic velocity profile is given as

$$u^+ = \frac{1}{\kappa} \ln (Ey) \tag{51}$$

where κ is the von Karman's constant($=0.41$), and E is equal to 9.0 for a smooth wall.

The skin friction coefficient is defined as

$$\frac{c_f}{2} = \frac{\tau}{\rho u^2} = \frac{1}{u^{+2}} \tag{52}$$

Substitution of Eq.(51) into the Equation (52) with the definition of local Reynolds number

$$Re = \frac{u\,y}{\nu} \tag{53}$$

yields a relation for momentum transfer to the wall.

$$\frac{c_f}{2} = \left[\frac{\kappa}{\ln\left(E\,Re\sqrt{\frac{c_f}{2}} \right)} \right]^2 \tag{54}$$

The logarithmic temperature profile is given as

$$T^+ = Pr_t(\,u^+ + P\,) \tag{55}$$

where P is an empirical function of the molecular Prandtl number. Substitution of the above equation into the definition of Stanton number

$$St = \frac{q_w}{\rho u c_p (T_w - T)} = \frac{1}{u^+\,T^+} \tag{56}$$

yields the relationship for the heat flux to the wall as

$$St = \frac{c_f/2}{Pr_t\left(1 + \sqrt{\frac{c_f}{2}}\;P \right)} \tag{57}$$

For a smooth wall, Launder and Spalding [2] proposed a simpler version of Jayatilleke's correlation [75] of the P-function,

$$P = 9.0\left(\frac{Pr}{Pr_t} - 1 \right)\left(\frac{Pr_t}{Pr} \right)^2 \tag{58}$$

Convection and diffusion of turbulence energy are found to be nearly always negligible in the vicinity of a wall [76]. The balance between the production

and dissipation terms in the turbulence kinetic energy equation yields the boundary values of k and ε as

$$k = \frac{\tau_w}{\rho\, c_\mu^{0.5}} \tag{59}$$

$$\varepsilon = \frac{k^{1.5}}{C_d y} \tag{60}$$

where C_d is a constant equal to 2.55.

The above wall functions have been tested for channel flow in the present study and satisfactory results were obtained for both momentum and heat transfer. They were used for flow in a sudden pipe expansion to supply fully developed conditions at the inlet.

Although the above wall functions correctly predict zero shear at reattachment points, they also predict zero values of heat flux and turbulence kinetic energy. However, experimental measurements show that these quantities have maximum values at reattachment points. This deficiency can be removed by choosing $k_p^{1/2}$ as the velocity scale, which was first proposed by Launder and Spalding [2]. This is discussed in the next section.

Wall functions have been derived above for smooth walls. For rough walls, only the empirical functions need be replaced. For example, Han's [27] roughness functions for transverse rectangular ribs reduce to

$$E = \frac{\exp[0.39\,(L/e)^{0.53}]}{e^+} \tag{61}$$

$$P = 5.05\, e^{+0.28} - 0.97\,(\frac{L}{e})^{0.53} \tag{62}$$

2.2.4 *Improvements in wall functions*

As pointed out earlier, the wall functions based on the velocity scale of $\sqrt{\tau_w/\rho}$ are not suitable for recirculating flows because of incorrect predictions of heat transfer rates and turbulent kinetic energy at reattachment points. The problem can be avoided by adopting the proposal of Launder and Spalding [2] in which the flow in the near wall region is assumed to be in local equilibrium. The logarithmic velocity and temperature laws are used with the non-dimensional parameters replaced with

$$\begin{aligned} y^+ &= \frac{c_\mu^{1/4}\, k_p^{1/2}\, y}{\nu} \\ u^+ &= \frac{c_\mu^{1/4}\, k_p^{1/2}\, u}{\tau_w/\rho} \\ T^+ &= \frac{(T - T_w)\,\rho c_p\, c_\mu^{1/4}\, k_p^{1/2}}{q_w} \end{aligned} \tag{63}$$

In the turbulent kenitic energy equation, the dissipation term used is the average over the control volume near the wall.

$$\int_0^{y_p} \varepsilon\, dy = c_\mu^{3/4}\, k_p^{3/2}\, \frac{\ln\,(E y_p^+)}{\kappa} \tag{64}$$

For the equation of dissipation rate ε , the value is evaluated under local equilibrium condition as

$$\varepsilon = c_\mu^{3/4} \frac{k_p^{3/2}}{\kappa y_p} \tag{65}$$

The above wall treatment has been tested in the present study for a backward-facing step problem, and the heat transfer rates in the neighborhood of reattachment points were poorly underpredicted (as has been shown by many investigators).

Ciofalo and Collins [23] extended the Johnson and Launder's proposal [4] of varying viscous sublayer thickness with the level of turbulent kinetic energy diffusing into the sublayer. Their approach is to relate the non-dimensional viscous sublayer thickness to the near-wall turbulence intensity rather than to the near-wall profile of the turbulent kinetic energy as in the proposal of Johnson and Launder. This proposal is implemented as follows. In the equilibrium boundary layer, the nondimensional turbulent kinetic energy, $k^+ \equiv k / u_\tau^2$, can be expressed as

$$k^+ = c_\mu^{-1/2} \left(\frac{y^+}{y_{vo}^+} \right)^2 \qquad y^+ \le y_{vo}^+ \tag{66}$$

$$k^+ = c_\mu^{-1/2} \qquad y^+ > y_{vo}^+ \tag{67}$$

where y_{vo}^+ is the nondimensional viscous sublayer thickness taken as 11.225.

Using the above profiles of k^+ and those of u^+ in the viscous sublayer and in the fully turbulent region, the turbulence intensity in the equilibrium boundary layer can be expressed as

$$\psi_e \equiv \frac{k^{1/2}}{u} = \frac{1}{c_\mu^{1/4} y_{vo}^+} \qquad Re_y \le y_{vo}^{+2} \tag{68}$$

$$\psi_e = \frac{\kappa}{c_\mu^{1/4} \ln(E\phi)} \qquad Re_y > y_{vo}^{+2} \tag{69}$$

where Re_y is the local Reynolds number, uy/v , and ϕ is the root of the equation

$$\frac{\phi}{\kappa} \ln(E\phi) = Re_y \tag{70}$$

The ratio of ψ_p/ψ_E is interpreted as an index of the distance from equilibrium in the near-wall region, and comparison with experimental data suggests a simple power law of the form

$$\frac{y_v^+}{y_{v0}^+} = \left(\frac{\psi_E}{\psi_P}\right)^c \tag{71}$$

where the exponent c is found to be a value between 1/3 and 2/3 .

The thermal sublayer is approximated for $0.5 < Pr < 2$ as

$$y_T^+ = y_v^+ \left(\frac{Pr_t}{Pr}\right)^{0.25} \tag{72}$$

With the calculated sublayer thicknesses, y_v^+ and y_T^+ , the constant E and the P function in the logarithmic laws can be reevaluated.

2.2.5 *Wall function method for variable properties flow*

Viegas and Rubesin [77] extended Chieng and Launder's wall function approach [3] to include the effect of compressibility for flow over adiabatic surface. Supersonic flow over a flat plate and two cases of normal shock-wave turbulent boundary layer interaction at transonic speed with and without separation were computed with $k-\varepsilon$ model of Jones and Launder [72] and of Chien [78], and $k-\omega^2$ model of Wilcox and Rubesin [79]. Computations were performed with both the wall function method and integration to the surface with all three models, and comparison with experiments were generally better with the wall function method, provided that the first two mesh points lie between the buffer layer and the wake.

Viegas et al. [80] improved the wall function approach to nonabiabatic conditions and relaxed the criteria for the placement of the near-wall mesh points so that they can lie in the viscous sublayer. Computations for attached and separated flows over both adiabatic and nonadiabatic surfaces with Mach numbers, $0.875 < \mathrm{Ma} < 2.85$, gave good agreement with the experimental data. However, they point out that the nonadiabatic contribution to the wall function had a small effect on the local temperature due to small surface heat fluxes and that the wall function can be in considerable error. They comment that improvements in shear and eddy viscosity modeling within the first mesh volume will be required for consideration of very cold wall cases.

Following Chieng and Launder's approach, Viegas et al. assumes that the turbulence Reynolds number, $Re_v = y_v k_v^{1/2}/v$, a universal constant equal to 20 which would require a cubic equation for k_v. This assumption has led to poor

prediction of heat transfer rates (20-30% lower than the experimental data) in abrupt pipe expansion flows [4]. In this study, the approach of Ciofalo and Collins [23] is used to calculate the viscous sublayer thickness, and the assumption of $Re_v = 20$ is abandoned. However, the calculation of P function from the thermal sublayer thickness is not used, and the surface heat flux is calculated from a reduced energy equation as will be shown later. The effects of compressibility was added following the approach of Viegas and Rubesin.

The conventional law of the wall is extended to compressible flow with the use of the van Driest transformation, and the effective u^+ is

$$u^+ = \frac{\int_0^u (\frac{\rho}{\rho_w})^{1/2} du}{u_\tau} \tag{73}$$

and the effective kinetic energy of turbulence is shown to have the density scaling as [79]

$$k_{eff} = \frac{\rho\, k}{\rho_w} \tag{74}$$

The nondimensional y coordinate is chosen as

$$y^+ = \frac{y\, u_\tau}{\nu_w} \tag{75}$$

and the friction velocity is defined as

$$u_\tau = (\frac{\tau_w}{\rho_w})^{1/2} \tag{76}$$

With the above relations, the mean velocity profile is given by

$$\frac{\left(\frac{\rho_p k_p}{\rho_w}\right)^{1/2}\int_0^u\left(\frac{\rho}{\rho_w}\right)^{1/2}du}{\tau_w/\rho_w} = \frac{1}{\kappa^*}\ln\left[E^*\frac{y_p\left(\frac{\rho_p k_p}{\rho_w}\right)^{1/2}}{\nu_w}\right] \tag{77}$$

where E^* and κ^* are 5.0 and 0.23 respectively. With the approximation of constant pressure between the wall and the first node point, the effective velocity can be evaluated as

$$\int_0^{u_p}\left(\frac{\rho}{\rho_w}\right)^{1/2}du = \int_0^{u_v}\frac{du}{(T/T_w)^{1/2}} + \int_{u_v}^{u_p}\frac{du}{(T/T_w)^{1/2}} \tag{78}$$

In order to evaluate the integral, the following analysis is employed. Neglecting the convection of heat near the surface, the temperature distribution in the viscous sublayer is obtained as

$$T = T_w - \frac{Pr}{c_p}q_w\left(\frac{1}{\tau}\right)_l u \tag{79}$$

where

$$\left(\frac{1}{\tau}\right)_l \equiv \frac{1}{u}\int_0^u\frac{du}{\tau} \tag{80}$$

and a mean value of τ was employed as

$$\left(\frac{1}{\tau}\right)_l = \frac{2}{\tau_v + \tau_w} \tag{81}$$

In the fully turbulent region, neglecting the molecular diffusion of heat leads to the following temperature distribution.

$$T = T_w - \frac{q_w}{c_p}\left[Pr_t(\frac{1}{\tau})_t(u - u_v) + Pr(\frac{1}{\tau})_l u_v \right] \tag{82}$$

where

$$(\frac{1}{\tau})_t \equiv \frac{1}{u - u_v}\int_{u_v}^{u} \frac{du}{\tau} \tag{83}$$

and a mean value of τ is taken as

$$(\frac{1}{\tau})_t = \frac{\tau_1 + \tau_v}{2\tau_1 \tau_v} \tag{84}$$

Substitution of Eq. (79) and Eq. (82) into Eq. (78) produces the following relationship for the effective velocity.

$$\begin{aligned}\int_0^u \left(\frac{\rho}{\rho_w}\right)^{1/2} du &= \frac{2c_pT_w}{Prq_w(\frac{1}{\tau})_l}\left[1 - \left(\frac{T_v}{T_w}\right)^{1/2}\right] \\ &+ \frac{2c_pT_w}{Pr_tq_w(\frac{1}{\tau})_t}\left[\left(\frac{T_v}{T_w}\right)^{1/2} - \left(\frac{T_p}{T_w}\right)^{1/2}\right]\end{aligned} \tag{85}$$

The velocity at the viscous sublayer is obtained from the momentum equation at the near-wall mesh as

$$u_v - \frac{Prq_w}{2c_pT_w}(\frac{1}{\tau})_l u_v^2 = \frac{\tau_w}{\mu_w}y_v + \frac{1}{\mu_w}(\frac{dp}{dx})\frac{y_v^2}{2} \tag{86}$$

If the near-wall grid point lies within the viscous sublayer, the wall shear stress is calculated using Eq. (79) and the assumption, $\mu/\mu_w = T/T_w$.

$$\tau_w = \left[u_p - \frac{Prq_w}{2c_pT_w}\left(\frac{1}{\tau}\right)_l u_p^2 - \frac{1}{\mu_w}\frac{y_p^2}{2}\left(\frac{dp}{dx}\right) \right]\frac{\mu_w}{y_p} \tag{87}$$

Given T_w, the wall heat flux can be obtained from Eq. (82), and iteration is required among u_v, T_v, τ_w , and q_w.

Next, the mean generation and dissipation rates of k are derived as proposed by Chieng and Launder [3]. A simple expression for the mean dissipation rate $\bar{\varepsilon}$ is obtained by neglecting the variation of k across the near-wall grid, but Chieng and Launder found that the prediction of local heat transfer rates were better with the variation of k taken into account. The turbulent shear stress is assumed zero in the viscous sublayer and undergoes an abrupt increase at the edge of the sublayer, varying linearly over the remainder of the near-wall grid. The mean generation of kinetic energy becomes

$$\overline{P} = \frac{1}{y}\int_0^{y_1}\left(\tau_w + (\tau_1 - \tau_w)\frac{y}{y_1}\right)\left(\frac{\partial U}{\partial y} + \frac{\partial V}{\partial x}\right)dy \tag{88}$$

where the subscript 1 denotes the north edge of the near- wall grid. Using the mean velocity distribution of Eq. (77) the integration leads to

$$\begin{aligned}\overline{P} = {} & \frac{\tau_w}{\rho_w \kappa^*(\rho_p k_p/\rho_w)^{1/2}}\left(\frac{\rho_w}{\rho_1}\right)^{1/2}\left(\tau_w \ln\frac{y_1}{y_v} + (\tau_1 - \tau_w)\left(1 - \frac{y_v}{y_1}\right)\right) \\ & + \frac{\partial V}{\partial x}\left(\tau_w\left(1 - \frac{y_v}{y_1}\right) + \frac{\tau_1 - \tau_w}{2}\left(1 - \frac{y_v^2}{y_1^2}\right)\right)\end{aligned} \tag{89}$$

For the evaluation of the mean dissipation, a linear variation of k is assumed between the edge of viscous sublayer and the second grid next to the wall, and a parabolic variation of k is assumed within the viscous sublayer as follows.

$$k = k_v \left(\frac{y}{y_v}\right)^2 \quad , \; y \le y_v \tag{90}$$

$$k = \frac{k_1 - k_v}{y_1 - y_v} y + \left(k_p - \frac{k_p - k_N}{y_p - y_N} y_p\right) = by + a \quad , \; y > y_v \tag{91}$$

The dissipation rate of k is not zero in the viscous sublayer unlike the generation. Use of the parablic profile of Eq. (90) gives

$$\varepsilon = \frac{2\nu_w k_v}{y_v} \tag{92}$$

where ν in the sublayer is assumed to be a constant and equal to its wall value. In the fully turbulent region, ε is evaluated as

$$\varepsilon = \frac{k^{3/2}}{c_l y} \tag{93}$$

where $c_l = \kappa / c_\mu^{3/4} = 2.55$

The mean dissipation rate of turbulent kinetic energy in the near-wall grid is evaluated as

$$\bar{\varepsilon}_p = \frac{1}{y_1}\left(\frac{\rho_w}{\rho_p}\int_0^{y_v} \varepsilon \, dy + \int_{y_v}^{y_1} \varepsilon \, dy\right) \tag{94}$$

Upon evaluating the integrals, the following expression is obtained.

$$\bar{\varepsilon}_p = \frac{2\nu_w \rho_w k_v}{y_1 y_v \rho_1} + \frac{1}{c_l y_1}\left(\frac{2}{3}(k_1^{3/2} - k_v^{3/2}) + 2a\,(k_1^{1/2} - k_v^{1/2}) + \lambda\right) \tag{95}$$

where

$$\lambda = a^{3/2} \ln\left[\frac{(k_1^{1/2} - a^{1/2})/(k_1^{1/2} + a^{1/2})}{(k_v^{1/2} - a^{1/2})/(k_v^{1/2} + a^{1/2})}\right] \quad , \quad a > 0$$
$$\lambda = 2(-a)^{3/2}\left[\tan^{-1}\left(\frac{k_1}{-a}\right)^{1/2} - \tan^{-1}\left(\frac{k_v}{-a}\right)^{1/2}\right] \quad , \quad a < 0 \tag{96}$$

Dissipation at the near-wall node is approximated under local- equilibrium condition as

$$\varepsilon_p = \frac{k_p^{3/2}}{c_l y_p} \tag{97}$$

2.2.6 *Algebraic stress model*

The algebraic form of Reynolds stress equation can be obtained by neglecting gradients of $\overline{u_i u_j}/k$, which is true when $\overline{u_i u_j}/k$ is constant, and approximately true when $\overline{u_i u_j}/k$ varies slowly across the flow field. The resultant equation proposed by Rodi [81] assumes that the convective and diffusive transport of $\overline{u_i u_j}$ are analogous to those of turbulent kinetic energy as follows.

$$U_k \frac{\partial \overline{u_i u_j}}{\partial x_k} = \frac{\overline{u_i u_j}}{k} U_k \frac{\partial k}{\partial x_k}$$
$$D_{ij} = \frac{\overline{u_i u_j}}{k} D(k) \tag{98}$$

where D_{ij} is the diffusive transport tensor and $D(k)$ is the diffusion of k. The transport equation for k and ε are modelled following Daly and Harlow [82], as follows:

$$U_j \frac{\partial k}{\partial x_j} = \frac{\partial}{\partial x_j}\left(\nu \frac{\partial k}{\partial x_j} + c_k \overline{u_i u_j} \frac{k}{\varepsilon} \frac{\partial k}{\partial x_i} \right) - \overline{u_i u_j} \frac{\partial U_i}{\partial x_j} - \varepsilon \tag{99}$$

$$U_j \frac{\partial \varepsilon}{\partial x_j} = \frac{\partial}{\partial x_j}\left(\nu \frac{\partial \varepsilon}{\partial x_j} + c_{\varepsilon 2} \overline{u_i u_j} \frac{k}{\varepsilon} \frac{\partial \varepsilon}{\partial x_i} \right) + c_{\varepsilon 1} \frac{\varepsilon}{k} P - c_{\varepsilon 2} \frac{\varepsilon^2}{k} \tag{100}$$

Combining the equations (98) and (99) with the Reynolds stress equation, the algebraic equation for $\overline{u_i u_j}$ is obtained as

$$\frac{\overline{u_i u_j}}{k}(P - \varepsilon) = P_{ij} - \frac{2}{3}\delta_{ij}\varepsilon + \phi_{ij} \tag{101}$$

where P is the production of k, and ϕ_{ij} is called the pressure-strain tensor. The generation tensor of $\overline{u_i u_j}$ is given by

$$P_{ij} = -\overline{u_i u_k} \frac{\partial U_j}{\partial x_k} - \overline{u_j u_k} \frac{\partial U_i}{\partial x_k} \tag{102}$$

The pressure strain term is modelled into two component, $\phi_{ij,1}$ which involves only turbulence quantities, and $\phi_{ij,2}$ which involves products of turbulence quantities and mean rates of strain. The component $\phi_{ij,1}$ has been refered to as the "return-to-isotropy" term, and is modelled by Rotta [83] as

$$\phi_{ij,1} = -c_1 \frac{\varepsilon}{k}\left(\overline{u_i u_j} - \frac{2}{3}\delta_{ij} k \right) \tag{103}$$

The mean strain part of the pressure strain term, $\phi_{ij,2}$ has been modelled by Launder et al. [84] as

$$\phi_{ij,2} = -c_2\left(P_{ij} - \frac{2}{3}\delta_{ij} P \right) \tag{104}$$

where c_1 and c_2 are 1.8 and 0.6 respectively. Shir [85] proposed that the term $\phi_{ij,1}$ be modified to account for the near-wall effects by adding to it the following correction:

$$\phi_{ij,1}' = c_1' \frac{\varepsilon}{k}(\overline{u_k u_m} n_k n_m \delta_{ij} - \frac{3}{2}\overline{u_k u_i} n_k n_j - \frac{3}{2}\overline{u_k u_j} n_k n_i) f(\frac{l}{n_i r_i}) \quad (105)$$

where n_i is the unit vector normal to the wall, r_i is the distance from the wall, and l is the length scale, $k^{3/2}/c_l \varepsilon$. The f function acts as to diminish the influence of the near-wall correction as the distance r increases. Shir's idea was extended by Gibson and Launder [86] to model a near-wall correction for the term $\phi_{ij,2}$.

$$\phi_{ij,2}' = c_2' (\phi_{km,2} n_k n_m \delta_{ij} - \frac{3}{2}\phi_{ik,2} n_k n_j - \frac{3}{2}\phi_{jk,2} n_k n_i) f(\frac{l}{n_i r_i}) \quad (106)$$

The final algebraic equation for the Reynolds stresses is

$$\overline{u_i u_j} = \frac{2}{3}\delta_{ij} k + \frac{(1-c_2)k}{P + (c_1 - 1)\varepsilon} \left[\left(P_{ij} - \frac{2}{3}\delta_{ij} P\right) + \frac{1}{(1-c_2)}\left(\phi_{ij,1}' + \phi_{ij,2}'\right)\right] \quad (107)$$

A proposal was made by Launder [87] to produce better prediction of turbulent shear stress in a free jet. His proposed equation is

$$\overline{u_i u_j} = \frac{2}{3}\delta_{ij} k + \frac{(1-c_2)}{(\lambda - 1)(1+\alpha) + (\alpha - \beta)\Lambda + c_1}\frac{k}{\varepsilon} \left[\left(P_{ij} - \frac{2}{3}\delta_{ij} P\right) + \frac{1}{(1-c_2)}\left(\phi_{ij,1}' + \phi_{ij,2}'\right)\right] \quad (108)$$

where

$$\lambda = P/\varepsilon \quad \text{and} \quad \Lambda = D(k)/\varepsilon \tag{109}$$

α and β are empirical constants with values of 0.3 and -0.8 respectively.

2.2.7 *Closure*

The wall function approaches were tested in the present study for abrupt pipe expansion flow and flow downstream of a backward-facing step, and proved to be inadequate(especially when the step height is too small to locate sufficient number of grid points). The low-Reynolds number model with modification by Yap has received most attention in the present study.

It has been known that the Boussinesq-viscosity hypothesis cannot simulate the level of anisotropy of normal stresses resulting from curvature in flow. A related example is the turbulence-driven secondary motions causing bulging of the velocity contours towards the corners in straight, non-circular ducts and open channel. The motions has been known to have a pronounced effect on the shear stress and heat transfer in the corner region and cannot be predicted by an isotropic eddy-viscosity model. Numerical studies are currently under progress with the algebraic stress model.

Chapter III

NUMERICAL SOLUTION

3.1 PHOENICS

The present study uses PHOENICS(Parabolic Hyperbolic Or Elliptic Numerical Integration Code Series) developed by CHAM Ltd. It is a general purpose computer program for the analysis of fluid-flow, heat transfer, chemical-reaction and related phenomena. PHOENICS can solve single-phase or two-phase parabolic and elliptic problems in cartesian, cylindrical polar, and curvilinear body-fitted coordinate systems. Dependent variables in the governing equations are allowed to vary in one, two or three dimensions and in time.

PHOENICS consists of two main computer codes and an auxiliary code. The main codes are a pre-processor called SATELLITE and a processor called EARTH. SATELLITE is an interpreter that converts instructions provided by the user into a data file for EARTH. EARTH is the main flow-simulating software that executes the corresponding computations. Various data-setting can be made by the user in GROUND which is a subroutine of EARTH. The auxiliary code is called PHOTON. It is a graphics program that presents the computed grid and flow pattern on the screen.

3.2 SOLUTION ALGORITHM

3.2.1 *Grid configuration*

In PHOENICS, staggered grids are used. Pressure and other scalar dependent variables including the turbulence kinetic energy and dissipation rate are stored at the cell nodes whereas velocities are located at the cell faces. For U velocities, the control volumes are displaced in the positive x direction by one half cell so that, for U_p , the west boundary of the cell passes through the node point P, and the east boundary passes through the node point E. Grid node locations and the staggered grids for velocities are shown in Figures 3.1 and 3.2. The V velocity control volume is similarly displaced by one half cell in the y direction.

The grid nodes are placed in the center of the control volume, rather than the control volume faces being placed half way between grid points. This grid arrangement is convenient with the solution domain containing porosities, since the control volume faces can be located along the boundaries of the blockage, whereas the latter grid arrangement would require setting up the grid nodes first and cell boundaries to coinside with the boundaries of blockage.

The governing equations are integrated over individual control volume or grid cell to arrive at the discretised equations.

3.2.2 *Discretisation of the governing equations*

PHOENICS provides solutions to the discretized versions of sets of differential equations having the general form [88] :

$$\frac{\partial}{\partial t}(r_i \rho_i \phi_i) + \nabla \cdot (r_i \rho_i \vec{V} \phi_i - r_i \Gamma_{\phi i} \nabla \phi_i) = r_i S_i \qquad (110)$$

where,

t stands for time

r_i stands for volume fraction of phase i

ρ_i stands for density of phase i

ϕ_i stands for any conserved property of phase i , such as enthalpy, velocity, mass fraction of a chemical species, etc.

$\vec{V}$ stands for velocity vector

$\Gamma_{\phi i}$ stands for the exchange coefficient of ϕ in phase i

S_i stands for the source rate of ϕ_i

Integration of Equation (110) for a single phase over the whole volume of the domain of surface area A, followed by application of the divergence theorem yields:

$$\int_A \int \left(\rho \vec{V} \phi - \Gamma_\phi \nabla \phi\right)_n dA = \iiint_\forall S_\phi d\forall \qquad (111)$$

Rewriting the convective and diffusive fluxes normal to the surface area at e, w, n, s (east, west, north, and south of the control volume faces), the equation in two-dimensions becomes:

$$J_e - J_w + J_n - J_s = \iint S_\phi d\forall \tag{112}$$

with

$$\begin{aligned}
J_e &= (\rho U)_e (r_p^j \delta y_{ns})\, \phi_e - \Gamma_{\phi,e} (r_p^j \delta y_{ns}) \frac{\partial \phi}{\partial x}\Big|_e \\
J_w &= (\rho U)_w (r_p^j \delta y_{ns})\, \phi_w - \Gamma_{\phi,w} (r_p^j \delta y_{ns}) \frac{\partial \phi}{\partial x}\Big|_w \\
J_n &= (\rho V)_n (r_n^j \delta x_{ew})\, \phi_n - \Gamma_{\phi,n} (r_n^j \delta x_{ew}) \frac{\partial \phi}{\partial y}\Big|_n \\
J_s &= (\rho V)_x (r_x^j \delta x_{ew})\, \phi_x - \Gamma_{\phi,x} (r_x^j \delta x_{ew}) \frac{\partial \phi}{\partial y}\Big|_x
\end{aligned} \tag{113}$$

and δy_{ns} and δx_{ew} indicate the distance between cell volume walls, n and s, and the distance between cell volume walls, e and w respectively, as shown in Figure 3.1. $j = 0$ and 1 corresponds to cartesian and cylindrical coordinates respectively. For the convective and diffusive flux at the west face, J_e, the transport properties at e can be evaluated either by arithmetic averages of those on either side of the cell faces, or by harmonic mean averaging. In the present study, arithmetic averages have been used to approximate the transport properties.

The value of ϕ is assumed to vary linearly between grid nodes in the approximation of $\partial\phi/\partial x\,|_e$, and the use of central difference scheme results in:

$$\frac{\partial \phi}{\partial x}\Big|_e = \frac{(\phi_E - \phi_P)}{\delta x_{EP}} \tag{114}$$

In the evaluation of ϕ_e in the convective flux term in J_e, there are many alternatives. In the upwind scheme, a stepwise variation of ϕ is used, and the flux

of variable ϕ across the east cell face is taken as the product of the mass flux and the value of ϕ at the upwind node. Thus the flux is:

$$\begin{array}{ll} \rho_P U_e \delta y_{ns} \phi_P & \text{for} \quad U_e > 0 \\ \rho_E U_e \delta y_{ns} \phi_E & \text{for} \quad U_e < 0 \end{array} \tag{115}$$

In the hybrid scheme that was developed by Spalding [89] , the value of ϕ_e is evaluated by the central difference scheme when the cell Peclet number, Pe, is less than 2 as follows.

$$\phi_e = \frac{\phi_P + \phi_E}{2} \quad , \quad \left| \frac{(\rho U)_e \delta x_{PE}}{\Gamma_{\phi, e}} \right| < 2 \tag{116}$$

de Vahl Davis and Mallinson [90] have shown that the false diffusion coefficient, arising from the use of upwind differencing scheme when flow cuts across grid lines at an angle, is given approximately by

$$\Gamma_f = \frac{\rho U \triangle x \triangle y \sin 2\theta}{4 (\triangle y \sin^3\theta + \triangle x \cos^3\theta)} \tag{117}$$

where θ is the angle made by the velocity vector with the x direction. The false diffusion is the largest where the velocity vector is at an angle of 45^o with the grid lines.

A better approximation of the exact solution using a quadratic interpolation equations called QUICK was proposed by Leonard [91]. For a uniform grid spacing, the resulting formula is

$$\begin{array}{ll} \phi_e = \dfrac{\phi_P + \phi_E}{2} - \dfrac{1}{8}(\phi_W - \phi_P + \phi_E) & \text{for} \quad U_e > 0 \\ \phi_e = \dfrac{\phi_P + \phi_E}{2} - \dfrac{1}{8}(\phi_P - \phi_E + \phi_{EE}) & \text{for} \quad U_e > 0 \end{array} \tag{118}$$

where the second term is like a correction to a linear interpolation proportional to the upstream-weighted curvature. EE is the east neighbor grid point of the grid E. PHOENICS only has the hybrid scheme and the upwind scheme as options, and the present results were obtained with the hybrid scheme. The algebraic stress model with the QUICK scheme is currently under investigation.

Substitution of the approximations for the profile of ϕ at the cell face into the Equation (112) yields the set of equation of the following form.

$$a_P \phi_P = \sum a_i \phi_i + \int\int S_\phi d\forall \tag{119}$$

where $i = E, W, S, N$ for the hybrid differencing scheme. For scalar variables, the formula for the coefficients become

$$\begin{aligned}
a_E &= \max\left(0, \frac{\Gamma_e \delta y_{ns}}{\delta x_{PE}} - \alpha \left| \rho_e U_e \delta y_{ns} \right| \right) + \max\left(0, -\rho_e U_e \delta y_{ns}\right) \\
a_W &= \max\left(0, \frac{\Gamma_w \delta y_{ns}}{\delta x_{WP}} - \alpha \left| \rho_w U_w \delta y_{ns} \right| \right) + \max\left(0, \rho_w U_w \delta y_{ns}\right) \\
a_N &= \max\left(0, \frac{\Gamma_n \delta x_{ew}}{\delta y_{PN}} - \alpha \left| \rho_n V_n \delta x_{ew} \right| \right) + \max\left(0, -\rho_n V_n \delta x_{ew}\right) \\
a_S &= \max\left(0, \frac{\Gamma_s \delta x_{ew}}{\delta y_{SP}} - \alpha \left| \rho_s V_s \delta x_{ew} \right| \right) + \max\left(0, \rho_s V_s \delta x_{ew}\right)
\end{aligned} \tag{120}$$

For $\alpha = 0$, diffusive effects contribute irrespective of the value of cell Peclet number, and the upwind difference scheme is obtained. The hybrid difference scheme corresponds to $\alpha = 0.5$. In the variable properties flow, the cell-face densities are evaluated using the upwing convention. Thus

$$\begin{aligned} \rho_e &= \rho_P \quad \text{for} \quad U_e > 0 \\ \rho_e &= \rho_E \quad \text{for} \quad U_e < 0 \end{aligned} \tag{121}$$

The expression used for the coefficient a_E of U - velocity equation is

$$a_E = \max(0, d_E - \alpha \mid m_E \mid) + \max(0, -m_E) \tag{122}$$

where

$$\begin{aligned} m_E &= \frac{\rho_e \delta y_{ns} (U_e + U_{eE})}{2} \\ d_E &= \frac{\Gamma_E \delta y_{ns}}{\delta x_{eeE}} \end{aligned} \tag{123}$$

eE is the east cell face of the grid point E, and other coefficients have the similar form.

In the present study, the sets of linear equations are solved by the TDMA(tridiagonal matrix algorithm) which is described in section 3.5.

3.2.3 *Source term linearization and boundary condition*

The source term needs to be a linear function of ϕ in order to have the whole discretised equation in the linear form. The nodal value of source terms are supposed to prevail over the whole of the cell volume, and the source term over a control volume can be written as

$$\iint S_\phi d\forall = S_c + C_\phi \phi \tag{124}$$

The proper linearization is to have the coefficient C_ϕ be less than or equal to zero in order to assure that the coefficient a_P remain positive to avoid divergence of solution iterations. For the momentum equations, the pressure gradient is added to the source term, and all the boundary conditions also enter the discretised equations by way of the source terms.

The boundary condition on the wall for the momentum equations enters the source term as the product of wall shear stress and the surface area of a wall bounded cell face. For the laminar flow problem or a low-Reynolds number turbulence models, the wall shear stress is simply the product of the near wall velocity gradient and the fluid viscosity. In the case of wall functions approach, the wall shear stress can be evaluated from the law of the wall as in section 2.2.3.

The constant wall temperature boundary condition enters the source term similarly as the product of temperature gradient and the fluid thermal conductivity near the wall. For the constant wall heat flux boundary condition, the coefficient C_ϕ is set to a small number, 10^{-10}, to prescribe a fixed-flux source term.

In PHOENICS, the source term is always expressed as a linear function of the dependent variable ϕ as [92]

$$S_\phi = C_\phi (V_\phi - \phi) f_t \tag{125}$$

where C_ϕ is a link coefficient which relates the source term to the difference between in-cell value of ϕ and the boundary value, and V_ϕ is the boundary value for variable ϕ. f_t represents some geometric factor such as area of the

computation cell. This equation is appropriate for a boundary across which there is no mass flow, and source or sink terms only arise due to diffusion.

For an inflow boundary, the mass source is expressed as a linear function of pressure:

$$\dot{m} = C_p(V_p - p)f_t \tag{126}$$

The source of any other dependent variable ϕ is

$$S_\phi = \dot{m} V_\phi + C_\phi (V_\phi - \phi)f_t \tag{127}$$

where the first term represents the amount of ϕ convected into the computation domain, and the second term represents the source of ϕ due to diffusion. $C_\phi = 0$ is appropriate if diffusion effects are negligible. In order to prescribe a flux boundary condition with Eq. (125) C_ϕ is set to a small number, 10^{-10}, and V_ϕ is multiplied by 10^{+10}.

3.2.4 *Solution of hydrodynamic equations*

There exists various methods of treating the pressure-velocity coupling between the mass and momentum conservation equations. PHOENICS uses a variant of the SIMPLE algorithm [93] called SIMPLEST. The major difference between the SIMPLEST and SIMPLE algorithm is that in the former the coefficients for the momentum equations contain only diffusion contributions, and the convection terms are added to the linerized source terms. This implies that, in the absence of diffusion, the momentum equations are solved by a Jacobi point-by-point procedure instead of the line-by-line procedure [94].

The essential idea is to use the continuity equation to derive an equation for pressure correction to be added to the current iteration value of pressure which will tend toward the correct pressure and also satisfy continuity equation. This is summarized below.

The discretized momentum equation with the staggered grid for the velocity components can be written as

$$a_e u_e = \sum a_i u_i + b + (p_P - p_E) A_e \tag{128}$$

An incorrect pressure field in the momentum equation yields a velocity field that will not satisfy the continuity equation. In order to correct the guessed pressure, the following steps of the SIMPLE algorithm are used, as proposed by Patankar and Spalding [93].

The correct pressure and velocity are assumed to be in the form:

$$\begin{aligned} p &= p^* + p' \\ u &= u^* + u' \\ v &= v^* + v' \end{aligned} \tag{129}$$

where the starred variables are imperfect values and the primed variables are correction terms. Subtracting the discretized momentum equation based on incorrect pressure and velocity fields from Eq. (128) results in :

$$a_e u_e' = \sum a_i u_i' + (p_P' - p_E') A_e \tag{130}$$

The first term on the right hand side of Eq. (130) is neglected since the converged solution given by this algorithm does not contain any error resulting from its omission. The resulting velocity correction formula is

$$u_e' = \frac{A_e}{a_e}(p_P' - p_E') \tag{131}$$

Equation (131) can also be written as

$$u_e = u_e^* + \frac{A_e}{a_e}(p_P' - p_E') \tag{132}$$

Equation (132) can be used to correct velocity from the pressure corrections. Substitution of Eq. (132) and the corresponding equation for the velocity component, v_n, into the discretized continuity equation of the following form .

$$[(\rho u)_e - (\rho u)_w]\,\delta y - [(\rho v)_n - (\rho v)_s]\,\delta x = 0 \tag{133}$$

yields the pressure correction equation.

$$a_p p_P' = \sum a_i p_i' + b' \tag{134}$$

where

$$b' = [(\rho u^*)_w - (\rho u^*)_e]\,\delta y + [(\rho v^*)_s - (\rho v^*)_n]\,\delta x \tag{135}$$

b' is a mass imbalance in the control volume due to the fact that the current velocities do not satisfy continuity.

The overall solution procedure consists of the following steps.

1. Guess the pressure field.
2. Solve the momentum equations to obtain the velocity field based on the guessed pressure field.
3. Solve the pressure correction equation.

4. Solve for the new velocity field using the velocity correction formula.
5. Solve the discretized equation for other variables (temperature and turbulence quantities).
6. With the new pressure field, return to step 2 and repeat the procedure until a converged solution is obtained.

3.2.5 *Tridiagonal matrix algorithm*

The tridiagonal matrix algorithm can be used to solve any set of equations when the matrix of the coefficients of the equations consists of nonzero coefficients aligned along three diagonals of the matrix. The discretised equation (119) can be rearranged in the following form.

$$a_j \phi_j = b_j \phi_{j-1} + c_j \phi_{j+1} + d_j \tag{136}$$

where the subscript j refers to the grid node P and varies along a chosen line. The recurrence relations are

$$\begin{aligned} C_j &= \frac{c_j}{a_j - b_j C_{j-1}} \\ D_j &= \frac{d_j + b_j D_{j-1}}{a_j - b_j C_{j-1}} \end{aligned} \tag{137}$$

and the second stage consists of a back-substitution by

$$\phi_j = C_j \phi_{j+1} + D_j \tag{138}$$

For the first equation

$$C_1 = \frac{c_1}{a_1} \quad , \quad D_1 = \frac{d_1}{a_1} \tag{139}$$

and

$$\phi_N = D_N \tag{140}$$

A sweep along the line of nodes in the transverse direction is performed, and the calculation is performed on the next parallel line of nodes with updated values of ϕ. Upon completion of sweeps in the transverse direction, a similar procedure may be performed in the sweep direction.

3.3 COMPUTATIONAL ASPECTS

3.3.1 *Convergence criterion*

The criterion of convengence of the numerical solution is based on the absolute normalized residuals of the equations that was summed for all cells in the computation domain. The mass residual, or the imbalance of the continuity equation, is defined as

$$RES = \frac{\sum | b' |}{\dot{m}_{in}} \tag{141}$$

where b' is defined in the Equation (135). The residuals associated with other dependent variables are defined as

$$RES = \frac{\sum | \sum a_i \phi_i + S - a_P \phi_P |}{M_{in,\phi}} \tag{142}$$

where, for the momentum equations, $M_{in,\phi}$ is the total inflow of momentum and for the equations of the turbulence kinetic energy and dissipation rate, it is the product of total volumetric inflow and the inlet value of k and ε respectively. The solutions are regarded as converged when these normalized residuals become less than 10^{-3} for the continuity equation and 10^{-2} for other variables.

In the case of the turbulent flow in a channel with ribs, a typical output had the normalized absolute residuals of $7e-5$, $7e-2$, $1.5e-3$, 1.67, 1.67, $4.4e-3$, for continuity, V momentum, U momentum, k, ε, and energy equation respectively, after 1500 sweeps.

In addition to the whole-field residuals, the average friction factor and the average heat transfer coefficient were monitored at every 50 sweeps for the problem of flow in channel with ribs. The relative errors of the average friction factor and the average heat transfer coefficient defined below was less than 1% for all cases studied.

$$\text{rel. error} = \frac{\phi^n - \phi^{n+1}}{\phi^n} \tag{143}$$

In the case of flow in an abrupt pipe expansion, flow over a backward-facing step, and the impingement cooling, the local heat transfer coefficients were also monitored at every 100 sweeps. When the solutions were well converged, the computed local heat transfer coefficients were almost invariant.

For example, the change in the stagnation heat transfer coefficient for the impingement cooling problem was less than 1% over 1000 sweeps once the heat transfer coefficient profile was converged.

For the flow in a tube with transverse rectangular ribs, an increase in the number of grids in the axial direction of 30% changed f and St by about 4% and 3% respectively, and improved agreement with experiment. For the most of the computation domain, at least 3 grid nodes were placed within the viscous sublayer, and the grid was stretched in x or y direction by a factor of 1.1-1.5 carefully over various parts of solution domain. The effect of further grid refinement near the wall was negligible for the prediction of flow field. For the computations with wall function methods, most of the near-wall grids were placed in the fully turbulent region, $y^+ > 30$, and extensive grid refinement tests were not performed.

3.3.2 *Under-relaxation*

The present computation involves equations that are nonlinear and strongly coupled, and under-relaxation is required to achieve the overall convergence to a solution. In the present calculations under-relaxation was applied in the following manner involving the false time step δt_f.

$$\left(a_P + \frac{\rho \forall}{\delta t_f}\right)\phi_P = \sum a_i \phi_i + S + \frac{\rho \forall}{\delta t_f}\phi_P^{\times} \tag{144}$$

where $\phi_P^{\times}$ is the previous sweep value of ϕ at point P. If δt_f is small the terms containing it will be large and tend to dominate the equation, implying

$$\phi_P = \phi_P^{\times} \tag{145}$$

Thus, the smaller the value of δt_f the less ϕ can change from sweep to sweep.

An alternative form of under-relaxation called linear under- relaxation was used for pressure as

$$p = p^{\times} + \alpha (p - p^{\times}) \tag{146}$$

The turbulent viscosity was also under-relaxed in the similar manner.

$$\mu_t = \mu_t^{\times} + \alpha (\mu_t - \mu_t^{\times}) \tag{147}$$

3.3.3 *Computational time*

For the flow in the abrupt pipe expansion of $d/D = 0.8$ and $Re = 20{,}130$, a grid of 71x37 for the low- Reynolds number turbulence model required about 620 seconds on the IBM ES/9000 model 900 in order to achieve the convergence criteria. The RES of the turbulence kinetic energy and the dissipation rate were not lowered below 0.5, but the local Nusselt number prediction was almost invariant, and the iteration was terminated at 1500 sweeps. A grid of 59x21 for the wall function methods and the same problem required less than half the time required for the low-Reynolds number model to achieve approximately the same convergence criteria.

In the case of channel with ribs, the average friction factor and the average Stanton number were monitored, and a typical run with a grid of 96x66 re-

quired about 1300 seconds. About the same amount of computing time was required for the jet impingement cooling problem with a grid of 58x74.

3.4 COMMENTS ON PHOENICS CODES

PHOENICS has many capabilities for simulation of various fluid-flow, heat transfer, and related phenomena. For example, curvilinear body-fitted coordinates option can be used to generate grids for complex geometry. However, the code is weak in turbulence modelling; the standard $k - \varepsilon$ model is the most advanced one provided. For the low Reynolds number $k - \varepsilon$ model, the additional terms in the transport equations of k and ε have to be coded as a source term. The two-dimensional algebraic stress model formulation requires as many as ten extra source terms to be coded in each of the momentum equations. Due to inaccessibility of the source code and its large size, modification can become very difficult. The advantage of PHOENICS over other specific codes may be its capability to solve diverse problems, but due to its large applications the code is difficult to debug. In addition, the upwind scheme and hybrid scheme are the only differencing schemes available in the current version of PHOENICS(1.4). Thus, the code may also suffer from lack of solution accuracy due to numerical diffusion in many problems.

3.5 BOUNDARY CONDITIONS

3.5.1 *Flow in a sudden pipe expansion*

Inlet conditions were fully developed profiles for k, ε, and the axial velocity, U, obtained from the straight pipe flow solutions of the standard $k-\varepsilon$ model with wall function boundary conditions of Eqs. (54), (57), (59), and (60). The inlet condition for enthalpy was a uniform profile. The outlet was located about $200h(= 60D)$ downstream from the step so that its influence on the main flow would be negligibly small. The boundary conditions imposed were

outlet :

$$p = 0$$

$$\frac{\partial \phi}{\partial x} = 0 \ for \ \phi = u, v, k, \tilde{\varepsilon} \ and \ T$$

symmetry :

$$\frac{\partial \phi}{\partial r} = 0 \ for \ \phi = u, v, k, \tilde{\varepsilon} \ and \ T$$

wall :

$$u, \ v, \ k, \ \tilde{\varepsilon} = 0$$

constant wall heat flux

The wall boundary conditions were an adiabatic wall on the entry pipe ($-0.5D < x < 0$) and on the side wall of the step, and constant wall heat flux on the expansion tube as in Baughn's [9] experimental setup.

3.5.2 *Flow over a backward-facing step*

The same boundary conditions for the flow in a sudden pipe expansion apply to this problem with cylindrical coordinates replaced by cartisian coordinates. The inlet profiles for k , ε, and the axial velocity U were obtained from the two-dimension channel flow solutions of the standard $k-\varepsilon$ model with wall function boundary conditions.

3.5.3 *Flow in channel with rectangular ribs*

The fully developed condition of $\partial u/\partial x = 0$ and $v = 0$ cannot be applied to this problem since u varies continuously with x and v is not zero. But, the flow field will repeat itself in a succession of cross sections that are separated by the pitch length, L, as shown in Figure 3.3, sufficiently far downstream. One possible approach is to use periodicity boundary conditions as proposed by Patankar et al. [31]. Their approach is summarized below.

The velocity components are assumed to behave periodically as

$$u_i(x,y) = u_i(x+L,y) = u_i(x+2L,y) = \ldots\ldots \tag{148}$$

The periodicity condition for pressure is

$$p(x,y) - p(x+L,y) = p(x+L,y) - p(x+2L,y) = \ldots\ldots \tag{149}$$

and the pressure is assumed to be composed of

$$p(x,y) = -\beta x + P(x,y) \tag{150}$$

where β is defined as

$$\beta = \frac{p(x,y) - p(x+L,y)}{L} \tag{151}$$

The βx term is related to the global mass flow, and $P(x,y)$ is related to the detailed local motion, and is assumed to be periodic as

$$P(x,y) = P(x+L,y) = P(x+2L,y) = ... \tag{152}$$

The fully developed temperature profile condition of $\partial T/\partial x = 0$ for constant wall heat flux boundary condition cannot be applied to the present problem for two reasons. The first is the non-uniform heat transfer surface area which precludes uniform heat addition to the fluid, and the second is the nonzero axial conduction term, $\partial^2 T/\partial x^2$. The temperature field is assumed to be composed of a component due to the heat flux plus a periodic component.

$$T(x,y) = \gamma x + \hat{T}(x,y) \tag{153}$$

where γ is defined as

$$\gamma = \frac{T(x+L,y) - T(x,y)}{L} = \frac{Q}{\dot{m}\, c_p L} \tag{154}$$

and $\hat{T}$ is periodic as

$$\hat{T}(x,y) = \hat{T}(x+L,y) = \hat{T}(x+2L,y) = ... \tag{155}$$

Substitution of the Eq. (150) and Eq. (153) into the momentum and energy equation yields a β term on the right hand side of the x-momentum equation and a $-u\gamma$ term on the right hand side of the energy equation respectively.

The pressure gradient β generates a corresponding mass flow, and its first value is assigned as

$$\beta = f\frac{\rho u_b^2}{2D} \tag{156}$$

where f is obtained from the flow in a pipe with repeated- rib roughness [26]. The value of β can be iterated upon until the solution converges, as proposed by Lee [30].

$$\beta = \beta_o\left(1 + \alpha\left(\left(\frac{Q_o}{Q}\right)^2 - 1\right)\right) \tag{157}$$

where the subscript o refers to the value of the previous iteration, and α is an overrelaxation factor.

Patankar et al. have used this approach for the laminar flow problem, but with at least two more equations(turbulent kinetic energy and dissipation rate) in the present problem, further complication of the convergence problem was avoided, and a simpler approach to the periodic boundary condition was used. A fixed number of inner iterations were performed for given inlet conditions, and the calculated outlet values of velocities, enthalpy, kinetic energy, and dissipation rates were substituted as inlet conditions for the next outer iteration. A 1/7th power law profile was given for the axial velocity for the entire field as an initial guess in order to accelerate convergence to a fully developed condition. For this approach, the computation domain in Figure 3.3 was modified such that the inlet was located at six slabs before the right end of the first rib for the flow in a channel. The values at slab NX-1 were substituted

as the inlet conditions after each outer iteration. For the flow between parallel plates with wider ribs, the inlet was located 6 slabs before the right end of the first rib. The following boundary conditions were imposed.

outlet :

$$p = 0$$

$$\frac{\partial \phi}{\partial x} = 0 \; for \; \phi = u, v, k, \tilde{\varepsilon} \; and \; T$$

symmetry :

$$\frac{\partial \phi}{\partial y} = 0 \; for \; \phi = u, v, k, \tilde{\varepsilon} \; and \; T$$

wall :

$$u, \; v, \; k, \; \tilde{\varepsilon} = 0$$

constant wall heat flux or constant wall temperature

3.5.4 *Jet impingement cooling*

For the present numerical computations, the following boundary conditions were used.

outlet :

$$p = 0$$

$$\frac{\partial \phi}{\partial x} = 0 \; for \; \phi = u, v, k, \tilde{\varepsilon} \; and \; T$$

symmetry :

$$\frac{\partial \phi}{\partial r} = 0 \; for \; \phi = u, v, k, \tilde{\varepsilon} \; and \; T$$

wall :

$$u, \; v, \; k, \; \tilde{\varepsilon} = 0$$

constant wall heat flux

At the jet inlet, uniform profiles of turbulent energy, and energy dissipation rates were

$$k_{in} = i\, u_{in}^2 \tag{158}$$

$$\varepsilon_{in} = k_{in}^{1.5} / (\lambda\, d_j) \tag{159}$$

where i is the turbulence intensity and λ is the length scale constant. Typical values used were 0.5% and 30% for i and λ respectively. Fully developed profiles of velocity, k, and ε obtained from pipe solutions were also used for the inlet condition. A schematic diagram of the computation domain is shown in Figure 3.4.

3.6 COMPUTATION OF FRICTION FACTOR AND STANTON NUMBER

For the flow in a channel with rectangular ribs, The average friction factor is calculated from the pressure drop over one pitch length,

$$f = \frac{\triangle p}{\rho u_b^2 L / D_h} \tag{160}$$

The local Stanton number is defined as

$$St = \frac{q_w}{\rho\, u_b\, c_p (T_w - T_b)} \tag{161}$$

where

$$T_b = \frac{\int_0^H T\,u\,dy}{\int_0^H u\,dy} \tag{162}$$

The bulk temperature calculated by Eq. (162) was compared to that obtained from an energy balance in the abrupt pipe expansion flow, and they were almost identical. Along the front and rear faces of the ribs, T_b is taken as an average of the values at the upstream and downstream slabs.

An average Stanton number is calculated as

$$St_{av} = \frac{q_w}{\rho\, u_b\, c_p (\overline{T_w - T_b})} \tag{163}$$

where the average value of $(T_w - T_b)$ was obtained as

$$\overline{T_w - T_b} = \frac{\int_0^L (T_w - T_b)\,dx}{L} \tag{164}$$

where L is the rib pitch. Use of this definition of St_{av} for a uniformly heated surface may give good agreement with average Stanton numbers obtained with a uniform temperature boundary condition, as described by Mills [95]. The average Stanton number including the front and back faces of ribs was also calculated using the entire length of the heated surface for L in Eq. (164). The difference between the two average St was found to be less than 5% in the present computations.

3.7 VARIABLE PROPERTIES FLOW

The assumption of constant fluid properties is not adequate for large heat fluxes into the fluid, since all the physical properties depend on temperature and pressure. Fluid properties for the numerical calculation can be entered as power law approximations. The properties for low-pressure air can be approximated within 4% in the temperature range of about 273K $< T <$ 1500K. approximated as follows [96]

$$\frac{\mu}{\mu_{in}} = \left(\frac{T}{T_{in}}\right)^{0.67}, \quad \frac{k}{k_{in}} = \left(\frac{T}{T_{in}}\right)^{0.805}, \quad \frac{c_p}{c_{pin}} = \left(\frac{T}{T_{in}}\right)^{0.095}, \quad \frac{\rho}{\rho_{in}} = \frac{T_{in}}{T} \tag{165}$$

Due to decrease in density with temperature, there is continuous acceleration of the flow, and also another effect is the increase of the fluid resistance at the wall with heating that causes thickening of wall boundary layer, thus reducing the core flow area. These effects must be taken into account in evaluating the wall shear stress. Assuming static pressure is uniform across the flow section and treating the momentum flux as one-dimensionl, the wall shear stress becomes

$$\tau_w = -\frac{D}{4}\frac{d(p + \rho u_b^2/2)}{dx} \tag{166}$$

In the present computation, the friction induced by the momentum change was taken into account in calculating the average friction factor over one pitch length.

The specific heat was taken as a constant, and average viscosity and temperature ratio over the length of a pitch was taken as the average of the inlet

and outlet values. A fixed number of inner iterations were performed with a constant wall heat flux boundary condition, and the calculated values of velocities and turbulence quantities at the outlet of the computation domain were substituted as inlet conditions for the next outer iteration.

Supercritical hydrogen properties are strongly dependent on temperature and pressure. Convenient curve-fits have been supplied by Baek [97]. These curve-fits have been incorporated in PHOENICS and can be used in the future study of complex turbulent flow involving supercritical hydrogen.

Chapter IV

RESULTS AND DISCUSSION

4.1 FLOW IN A SUDDEN PIPE EXPANSION

For the present computations, expansion ratios of 0.4 and 0.8 and a downstream Reynolds number range from 10570 to 76080 were chosen to study the effect of Reynolds number and the expansion ratio on the performance of the turbulence models. The inlet conditions were fully developed profiles for all the variables obtained using wall function boundary conditions, except enthalpy, which was uniform. Air was chosen as the fluid, and properties were evaluated at 293 K. The wall heat flux used was $700 W / m^2$ which was in the range of Baughn's experiment [9]. The turbulent Prandtl number was fixed at 0.9. A typical grid used for $d/D = 0.4$ was NY = 59 and NX = 71 with 75% of the grids located between the wall the the top of the step in the radial direction.

Figure 4.1.1 shows the velocity profiles for the expansion ratio of 0.4 and 0.8. The local Nusselt number distribution normalized by the Dittus- Boelter relation for $d/D = 0.4$ and $Re = 12310$ computed by three methods, the low-Re model with modification by Yap, wall function method of Collins, and the standard wall function method are shown in Figure 4.1.2a The low-Re model predicts the overall Nusselt number distribution the best except for an underprediction of reattachment length. The standard wall function and the method of Collins underpredict the maximum Nu at the reattachment point by about

40% and 23% respectively. The heat transfer rates in the recirculation zone are predicted better by the wall function methods, as have been reported by other investigators.

Figure 4.1.2b shows that the corner eddy near the step can be predicted by the low-Re model, but the maximum wall shear stress in the recirculation region is about 2 times larger than that by the methods of Collins. Experimental data for the wall shear was not available, and a comparision could not be made. The skin friction and the Nusselt number are both low near the step. However the skin friction approaches a maximum about 5 step heights upstream of reattachment and declines to zero at reattachment while the Nusselt number reaches to a maximum near the reattachment. The skin friction and the heat transfer coefficient behave differently in a recirculating flow, and the Reynolds analogy does not hold in a reattaching or recirculating flow. Thus, the wall function approach of relating the flow with the wall shear stress fails in the neigborhood of reattachment.

Figure 4.1.3 shows the predictions of local Nu distribution for Re = 23,210 and 40,750. The low-Re model overpredicts the maximum Nu of the experiment data by about 25% for Re = 40,750, whereas the Collins method gives a good prediction at the reattachment and in the recirculation region. However, the predictions by wall function methods are consistently poor in the redevelopment region. The values of Nu_{db} for Re = 12,310, 23,210, and 40,750 are 37.6, 62.4, and 97.8 respectively. Figure 4.1.4 shows the computation results by the low-Re model for Re = 10750 and d/D = 0.8. For this expansion ratio, the step height is only 20% of the pipe radius whereas for d/D = 0.4 the

step height is 60% of the pipe radius. Also, use of the wall function boundary conditions was not practical for this low Reynolds number, because not enough grid points could be placed below the step if the first grid point adjacent to the wall was to be selected to lie within the fully turbulent part of boundary layer. The prediction of local Nusselt number shows a good aggreement with the experimental data over the entire field. Figure 4.1.5 shows predictions by the three methods for Re = 20,130 and 39,300. The wall function methods perform poorly for this small step height and the Reynolds number range. Prediction for Re = 76,080 in Figure 4.1.6 shows that the low-Re model overpredicts the maximum Nu by about 18% and again indicates the need for correction at high Reynolds number.

4.2 FLOW OVER A BACKWARD-FACING STEP

Vogel and Eaton [19] have performed a detailed study of fluid flow and heat transfer for flow over a backward-facing step. Numerical computations have been performed to investigate the performance of the low-Re model and the wall-function methods. The experiment of Vogel and Eaton was performed had a development section of length 2.5m, and transpiration was used to vary the boundary layer thickness. For the present computations, inlet profiles for the computations were obtained from the solution of the standard $k-\varepsilon$ model at the end of a channel of the length of 2.5m (16.5D) , and a boundary-layer thickness of 1.1e was obtained, where e is the step height. The outlet was lo-

cated at $54e$ downstream from the step. The expansion ratio was 1.25 and the Reynolds number based on the step height was 28,000.

Figure 4.2.1 shows the vector plot, and Figure 4.2.2 shows the mean velocity profiles at various nondimensional streamwise coordinates, $x^* = x - x_r / x_r$ where x_r is the reattachment length. Predictions by the low-Re model and the wall function method of Collins are almost identical and are generally in good agreement with the experimental data. Figure 4.2.3 shows the comparison with the experimental data for the mean velocity profiles in the near-wall region that were measured by the traversing pulsed wall probe with two orientations. The experimental data at $x^* = 0.4$ indicate an almost vertical profile whereas the profile at $x^* = 0.33$ in Figure 4.2.2 shows a gradual increase of the streamwise velocity with y. There is also a discrepancy in the data for the streamwise velocities at the reattachment point in Figure 4.2.2 and 4.2.3. The cause of this discrepancy between the two data sets is not certain. However, comparison of the computed results with the data very close to the wall, $y < 0.2h$, shows generally good agreement.

Mean temperature profiles at various streamwise locations downstream of the step in Figure 4.2.4 show the steepest temperature gradients in the region very close to the wall. The large temperature gradient across the shear layer near the step far from the wall is generally well predicted by the present computations. The dark markers at $y = 0$ indicate the wall temperatures measured by Vogel and Eaton, and the vertical lines indicate numerical results of wall temperatures by the two methods, for $x^* = -0.35$, 0.05 and 0.45. The prediction by the low-Re model shows closer agreement to the experimental data

than that by the wall function method of Collins. Figure 4.2.5 shows an enlarged plot of the mean temperature profiles at $x^* = -0.95$ and -0.75. The wall temperature prediction by the low-Re model is again better than that of wall function method, except the large overprediction by the methods very near the step, at $x^* = -0.95$.

Figure 4.2.6 shows the static pressure profiles on the top and bottom walls for $Re_e = 28{,}000$ and $\delta/e = 1.1$. The gradual increase of the static pressure on the top wall and the rapid increase in the bottom wall static pressure through reattachment to the downstream are well predicted by the present computations. The computation by the low-Re model shows correctly the slightly accelerating flow in the upstream near the step. Pressure recovery downstream of reattachment is predicted better by the low-Re model than by the wall function method.

Figure 4.2.7 shows that the computed St at the reattachment point is about 22% overpredicted by the low-Re model whereas the wall function method of Collins gives a 13% underprediction. The temperature difference, $T_w - T_\infty$, at the reattachment point was about 4^0C in the data of Vogel and Eaton, and if the reference condition is taken at 20^0C , the maximum St is 0.00494 with their condition of $U_{ref} = 11.3\ m/s$ and $q_w = 270\ W/m^2$. There is also a discrepancy in the profile of St for $\delta/e = 1.1$ and $Re_e = 28{,}000$ in their report. These uncertainties in the experimental data will have to be resolved. The present computation by the wall function method gives a peak St that is 13% lower than that reported by Collins, and the cause of this disagreement is not certain. The wall shear stress profile in Figure 4.2.7 shows that the computa-

tion by the low-Re model gives poor prediction in the recirculation region whereas prediction in the redeveloping region is much better than the wall function method.

4.3 FLOW IN CHANNEL WITH RECTANGULAR RIBS

Parametric studies for repeated rib roughness were performed for

$$e/D = 0.056$$

$$e/b = 0.67,\ 1$$

$$L/e = 5,\ 7.5,\ 10,\ 15,\ 20$$

$$Re = 5{,}200 - 41{,}800$$

Air was chosen as the fluid, and properties were evaluated at 293 K. The wall heat flux used was $700 W/m^2$. A typical grid used for $L/e = 10$ was NX = 84 and NY = 74 with 60% of the grids located between the wall and the rib top.

Figure 4.3.1 shows the velocity distribution for $L/e = 5, 10$, and 20 at $Re = 20{,}900$. For $L/e = 5$, a large recirculation is present between the ribs and there is no flow reattachment. Though not shown in the figures, a small counterrotating vortex was observed in the corner behind the first rib. A large vortex near the second rib is shown in Figure 4.3.1d, and the velocity plot shows rapid acceleration of fluid along the front face of the rib. The static pressure contours for $L/e = 5$ and 15 are shown in Figure 4.3.2. The turbulent kinetic energy contours in Figure 4.3.3 show maxima at the sharp edge of the second rib where flow impinges and a highly turbulent shear layer is generated. A second maximum occurs near the flow reattachment for $L/e = 10$, as observed in experiments.

Isotherms for $L/e = 5$ and 10 in Figure 4.3.4 show high temperature regions where recirculations occur. Figure 4.3.5 shows the prediction of temperature along the channel wall including the front and back side of the rib for $L/e =$

5. The region between the first two vertical markers in the figures corresponds to the front side of the rib, and that between the second and third markers corresponds to the top of the rib. The temperature is the lowest at the top of the front side of the rib where there is a flow impingement, and the highest heat transfer coefficient is obtained. The boundary-layer development at the top of the second rib also leads to low wall temperature, and there is a sudden increase in temperature at the back side of the rib. Another maximum in local heat transfer coefficient between the ribs lies close to the second rib where the faster moving fluid above the ribs has penetrated. The temperature and local St distribution along the wall for $L/e = 10$ are shown in Figures 4.3.6-9, and those for $L/e = 15$ are shown in Figures 4.3.10-13. The figures show the lowest wall temperature and the highest heat transfer coefficient between the ribs at the reattachment point.

Figure 4.3.14 shows a comparison of the average friction factor with the experimental data of Han et al. [27]. The agreement of the friction factor with experiment is generally good, except for the underprediction of about 10% for both $L/e = 10$ and 15 at Re of about 20,000. For $L/e = 5$ and 7.5, well converged results for $Re < 20{,}000$ were difficult to obtain, and they are not presented at this point. The prediction of the average St shows fair agreement with experimental data, except for generally low predictions. As shown in Figure 4.3.1, a large portion of area near the wall contains velocity vectors that are at some angle with the grid lines. Though the angles may be small, numerical diffusion effects are expected to be appreciable at higher Reynolds numbers. The heat transfer prediction is also sensitive to the details of near-

wall flow field such as the location and length of reattachment. Higher order models, such as the algebraic stress model, might give a superior simulation of this complex flow. A higher order differencing scheme such as QUICK method, may reduce the numerical error.

Prediction of the average friction factor and Stanton number with each outer iteration are shown in Figure 4.3.15 for three cases. The average values for both f and St are stabilized after about 10 outer iterations. Figure 4.3.16 is a typical plot of local Stanton number along the tube wall after each outer iteration. The total number of outer iterations shown is 20, and gradual convergence is obtained, though the behavior is erratic.

Figure 4.3.17 shows a comparison of local Nusselt number distribution with the experimental data of Liou and Hwang [98]. The experiment was performed in a rectangular channel with an aspect ratio of 4:1, but the present computations were performed for a 2-dimensional channel. N in the figure indicates the index of the rib in the heated section of the channel in their experiment. The comparison shows a fairly good prediction by the present results except the front and top of the rib where large overprediction occurs.

4.4 FLOW IN TUBE WITH RECTANGLAR RIBS

Computation of flow in a channel with rectangular cross section is more appropriate in the design of a heat exchanger for active cooling, and thus the focus of the present work was on a 2-dimensional channel. The well known experiments by Webb et al. [26] using rectangular rib roughness were per-

formed in a tube, with parameters which were very different to those in the experiment of Han et al. [27]. The tube had a larger pitch to rib height ratio and a smaller rib height to the channel height ratio compared to the channel of Han et al., and thus presented a different test for the turbulence model. This problem was actually investigated first, and is included here for completeness.

Parametric studies for repeated rib roughness were performed for

$$e/D = 0.02$$

$$e/b = 1$$

$$L/e = 20 \quad \text{and} \quad 40$$

$$Re = 18{,}940 - 56{,}810$$

The ratio of roughness height to width, e/b, was 1.94 in the experiments of Webb et al. [26]. For the large pitch to roughness height ratio, this variation of e/b should have negligible effect on pressure drop and overall heat transfer rate in the fully rough regime. With the outlet at the edge of a rib, the wider rib shape of $e/b = 1.0$ gave more stable numerical solutions. Air was chosen as the fluid, and properties were evaluated at 300 K. The wall heat flux used was $700 W/m^2$. The typical grid used for $L/e = 20$ was $NY = 85$, $NX = 84$ with 30 grids in the radial direction between the wall and rib tip.

Figure 4.4.1 show the prediction of temperature and the local Stanton number distribution along the pipe wall for $L/e = 20$. Results are shown between two slabs before the first rib and the slab $NX - 1$ on the second rib. Near-symmetry of wall temperature and Stanton number was obtained between the inlet and outlet. The maximum temperature occured in the corner

of the first rib. The maximum in local Stanton number between two ribs occurs at the flow reattachment point. A second maximum heat transfer occurs at the sharp edge of the second rib where there is flow impingement and boundary-layer development.

Figure 4.4.2 show a comparision of the average friction factor and Stanton number with experimental data of Webb et.al. [26]. The agreement with experiment was generally quite good, except for the heat transfer prediction for $L / e = 40$. A stabilized heat transfer coefficient was difficult to obtain at high Reynolds number for this pitch over roughness height ratio.

4.5 JET IMPINGEMENT COOLING

Numerical computations were performed for turbulent axisymmetric jets impinging on a heated flat plate for various values of Re and H/d. The Reynolds number was varied from 23,750 to 80,400, and H/d was varied from 2 to 22. The typical grid of the computation domain for $H/d = 6$ was 58X74 cells in the x and r directions with about 44% of the grids located within the normal distance of one jet diameter from the impingement wall and dense grids located around the stagnation point. The outlet was located at either 10 or 20 jet diameters downstream from the stagnation point depending on the distance from the jet outlet to the impingement surface. Either fully developed profiles for velocity, turbulent energy, and dissipation rates obtained from the numerical solution of the turbulent flow in a pipe, or uniform profiles were used at the jet outlet.

Figure 4.5.1 shows the velocity vector plots for $H/d = 2$ and 6 computed with a low-Re turbulence model and Yap's correction. The jet grows by entrainment of the stagnant fluid and deflects into a radial wall jet. The decay of the jet centerline velocity in Figure 4.5.2a shows that the jet flow is not much affected by the impingement wall up to about one jet diameter from the wall. About 95% of the flow deceleration occurs within one nozzle diameter from the wall for $H/d = 6$. Comparison of the jet centerline velocity decay with the experimental data of Giralt et al. [43] for several nozzle heights is shown in Figure 4.5.2b. Rapid decay of the centerline velocity to zero at the stagnation point is shown for $H/d = 6.67$. Computations for larger nozzle heights show characteristics of the free jet data, and predicts correctly the in-

fluence of the impingement wall on the oncoming flow(which extends further upstream as the nozzle height increases). The slightly faster decay near the impingement wall for $H/d = 22$ as compared to the experimental data could be due to greater spreading rate of the free jet.

Figure 4.5.3a shows the computed results for the axial velocities, u/u_m plotted against the nondimensional parameter, r/δ_u , where δ_u is the radial distance r where $u = 1/2\, u_m$. Similar profiles at different axial locations compare fairly well with the experimental data, except farther away from the center of the jet, for $r/\delta_u > 1.5$. The experimental data of Beltaos and Rajaratnam [42] were found to agree well with the theoretical solution of Tollmien [70] that is based on Prandtl's mixing-length hypothesis. Tollmien's solution is known to describe accurately the velocity distribution in a two-dimensional turbulent jet, and thus the present numerical computation seems to give fairly good prediction of flow field in the jet development region.

The distribution of the axial velocities at various locations in Figure 4.5.3b shows the continuous decay of the centerline velocity as the impingement wall is approached. Though not plotted in the figure, the radial velocity near the center of the jet is positive causing the jet to spread out, and the radial velocity further from the center is negative and flow entrainment occurs.

Dimensionless profiles of mean radial velocities are shown in Figure 4.5.4. V_m is the maximum velocity at each station and δ_v is the height where $V = 0.5\, V_m$. Comparison with experimental data of the classical wall jet obtained by Schwarz and Cosart [99] is in good agreement except that the lo-

cation of the maximum radial velocities are slightly underpredicted. Only portion of the experimental data are plotted in the figure.

The distribution of the static pressure along the impingement wall for $H/d = 6$ is shown in Figure 4.5.5. Due to the uncertainty of the outlet condition of the jet in the experiment by Giralt et al., two different jet outlet profiles, one which was obtained numerically at 50 diameters downstream in a tube, and one with uniform profiles, were employed. The uniform jet nozzle outlet condition fits the experimental data more closely than the fully developed condition. Giralt et al. investigated the pressure distributions over the range $1.2 < H/d < 20$ at $30{,}000 < Re < 80{,}000$ and narrower distribution of the wall static pressure was obtained with increasing jet height, for $H/d < 8$. They attributed this to the more concentrated kinetic energy of the jet near the centerline with more non-uniform velocity profiles at the start of the jet impingement region. The present computations with a fixed jet height and two different jet outlet conditions show the same trend. About 35% increase in the wall shear stress due to probably the steeper pressure gradient for the fully developed jet nozzle condition is shown in Figure 4.5.5b. This trend is consistent with Amano and Brandt [50] whose prediction for $H/d = 18$ and $Re = 180{,}000$ show 26% increase in wall shear stress when 5.5 power velocity profile was used. Amano attributed this to the higher turbulent kinetic energy at the edgy of the jet in the case of 5.5 power velocity profile. Figure 4.7.5b also shows a shift in the location of the maximum shear stress toward the stagnation point, a decrease of about 18%.

Comparison with the experimental data of Baltaos and Rajaratnam is made for H/d = 21.2 and Re = 80,400 in Figure 4.5.6a. The pressure distribution along the impingement wall show a fairly good agreement except for overall overprediction. The radial location where the pressure is 10% of the stagnation pressure is at about 3.6 d compared to about 1.1 d for H/d = 6 as shown in Figure 31.a. The centerline static pressure in Figure 4.5.6b shows good agreement with the data of Beltaos. Predictions for both H/d = 6 and 21.2 show no effect of the impingement wall on the jet up to 0.8 H downstream. For H/d = 21.2, computation shows slightly negative static pressure indicating that pressure in the free-jet region is below the ambient pressure.

The wall shear stress prediction in Figure 4.5.7a shows about 31% overprediction in the maximum shear stress, whereas good agreement is achieved away from the stagnation region, $r/H > 0.15$. Comparison with more experimental data is needed to resolve the discrepancy in the stagnation region. Baltaos and Rajaratnam indicate that the error in the shear stress for r/H less than about 0.08 could be greater than 6% due to the presence of large pressure gradients. Prediction of the maximum radial velocity along the impingement wall in Figure 4.5.7b shows that the peak is only about 22% of the jet outlet velocity.

Figure 4.5.8a shows the half-width spreading rate of the round free jet for H/d = 21.2 and Re = 74,000. Numerical results for $0.4 < x/H < 0.9$ predicts the spreading rate, $d\delta_u / dx$, equal to 0.103, compared to 0.093 of the data of Baltaos. Malin [54] reported the spreading rate of round free jet equal to 0.113 with the standard $k - \varepsilon$ model. The half-width spreading rate of the

radial wall jet is shown in Figure 4.5.8b. The spreading rate, $d\delta_v / dr$, for $H/d = 10$ and $Re = 23750$ was 0.09, and that for $H/d = 21.2$ and $Re = 74000$ was 0.085 over the range of $0.4 < r/H < 1.0$. The combined correlation for both $H/d = 10$ and 21.2 indicate the average spreading rate of 0.09, or δ_v / H is expressed as

$$\delta_v / H = 0.0948 (r / H)^{0.903} \tag{167}$$

Porch et al. [40] investigated turbulent radial wall jet for $8 < H / d < 24$ and $64{,}000 < Re < 288{,}000$,and the increase of jet thickness for $0.5 < r / H < 3$ was correlated by

$$\delta_v / H = 0.098 (r / H)^{0.9} \tag{168}$$

Comparing the two correlations shows that the prediction by the low-Re model is fairly good, and the average spreading rate of 0.9 compared to the experimentally excepted value of 0.085 - 0.095 is superior to the computed value of 0.068 by the standard $k - \varepsilon$ model.

Similarity profiles for k and $\overline{uv}$ in a free jet computed for $H / d = 21.2$ show fair agreement with the experimental data of Wygnanski and Fiedler [44] in Figure 4.5.9. The $\overline{uv}$ profile has the maximum value at about $r = 0.65\,\delta_u$ from the center of the jet where the velocity gradient $\partial U / \partial r$ is the largest. The present results are also in very close agreement with the numerical results of the standard $k - \varepsilon$ model that was reported by Malin who computed free and wall jets with various modifications to $k - \varepsilon$ and $k - W$ model. Figure 4.5.10 shows computed profiles of the turbulent kinetic energy and the turbulent

shear stress for $H / d = 10$ and 21.2 at various radial locations. Computed results of the turbulent intensity is underpredicted by about 17% compared to the data of Ng [100], but Malin points out that the data of Ng cannot be regarded as definitive, and that Poreh et al. measured a peak intensity of $k^{1/2} / U_m = 0.35$. (The experimental data of Ng was reproduced from the paper of Malin due to unavailability of Ng's thesis at present). The predicted profiles for $H / d = 10$ is very close to the numerical results of the standard $k - \varepsilon$ model that was reported by Malin, except that the present computation of $\overline{uv}$ with the low-Re model gives up to 20% improvement near the wall, $x \leq 0.5\,\delta_v$. In the case of the radial wall jet, the similarity profiles for k and $\overline{uv}$ are not quite obtained for $x > 0.5\,\delta_v$, and since only one computed profile for each case is given from Malin, it was not possible to compare the degree of similarity. However, the experimental data of Poreh et al. show scatter in measurement of both k and $\overline{uv}$, and they summarized that it was difficult to conclude from the data whether the turbulent shear stress in the wall jet is similar.

Figure 4.5.11 shows the Nusselt number profile for $H / d = 2, 6, 10, 14$, and $Re = 23{,}750$. The outlet profiles for the jet were obtained from the numerical solution from a pipe with the length of 72 diameters to simulate the experimental condition. Comparison with the experimental data of Baughn and Shimizu shows poor agreement near the stagnation point, as much as 56% overprediction for $H / d = 6$. In the case of $H / d = 2$, the minimum Nu at r / d of about 2 are well produced by the computation. The predicted profiles are in good agreement with the data for the downstream region. Figure 4.5.13

and 4.5.14 show the results when the extra source term in the ε equation is damped more than in the origional proposal of Yap. The predicted profiles of the local Nu show significant improvements except for the absence of the second peak for $H / d = 2$. The extra source term had to be about 1.6 to 6 times larger depending on H / d. More detailed investigation is needed to produce the necessary correction term to improve the heat transfer prediction in the vicinity of the stagnation point.

4.6 VARIABLE PROPERTIES CHANNEL FLOW USING THE LOW-RE MODEL

The effect of variable properties on heat transfer augmented by ribs in channel flow can be deduced from empirical equations, such as that of Vilemas and Simonis [38],

$$Nu_b = 0.029\, Re_b^{0.84}\, Pr_b^{0.6} \left(\frac{T_w}{T_b}\right)^n \tag{169}$$

where n depends on geometry and Reynolds number, and is given by Eq.(29). Thus

$$St_b \propto \mu_b^{0.16} \left(\frac{T_w}{T_b}\right)^n \qquad ; \quad n < 0 \tag{170}$$

With heating μ_b increases and T_w/T_b decreases in the axial direction, thus both terms contribute to the increase of St_b along the channel.

The friction factor for flow over sand-grain roughness is known to be function of geometry only, and independent of Reynolds number in the fully rough regime where form drag is the dominant mechanism. But, the friction factor for flow over repeated-rib roughness involves more geometric parameters, namely the height of roughness e, the width of the roughness w, and the pitch of roughness elements L. For widely spaced ribs, the flow reattaches behind each rib, and a viscous layer grows. This viscosity dependent shear stress should be dominant as L/e approaches infinity. Savage and Myers [101] performed experiments with water flow in a tube with rectangular rib roughness. They investigated the contribution of form drag to the total forces

retarding flow for different roughness configurations and Reynolds numbers. For $L/e = 1$, the total pressure drop was entirely due to a skin-friction effect. The relative contribution of skin friction decreased almost linearly as L/e increased and appeared to pass through a minimum at about $L/e = 13$. For $e/D = 0.04$ and $Re = 10^5$, the minimal contribution of skin friction was 30 % of the total retarding force at $L/e \simeq 10$. For the repeated-rib roughness, it seems that form drag may not be the dominant mechanism and skin friction may not be negligible, depending on the spacing of ribs. Consequently the friction factor may depend on viscosity in a variable properties flow even though the equivalent sandgrain roughness indicates the fully rough regime. The variation of friction factor downstream along the channel wall may be difficult to correlate since the relative contribution of skin friction depends on the rib spacing.

As a preliminary study, a channel with $L/e = 15$, $e/D = 0.056$ was chosen to observe the effect of variable physical properties. The low-Re model with the Yap's modification was employed. The inlet Reynolds number was varied from 11,500 to 20,000, and the calculated temperature ratio, T_w/T_b, was between 1.42 and 1.88. Pr and c_p were assumed constant for these initial calculations. Iterations were performed until a stabilized value of friction factor and Stanton number were obtained. In the present computation, the calculated variables at the outlet after an outer iteration were substituted as inlet conditions for the next outer iteration. Thus, the temperature level is increasing in the computation domain for successive outer iterations, and the process is very similar to marching in the flow direction. A slight increase in f and St were

observed in the course of iteration at high heat fluxes, and it is suspected that the heat transfer coefficient may not have stabilized due to flow laminarization in this low Reynolds number range.

Figure 4.6.1 shows a plot of f/f_c versus T_w/T_b for Re = 10,000 and 15,000, where f_c is the constant property value. The Reynolds number is an average value calculated with bulk properties over a pitch. The present calculation shows about 13% and 21% reduction in f at Re = 15,000 and 10,000 respectively, when the air was heated to about T_w/T_b = 1.7. The results also show an increase in f with increasing Re , and the effect of Re on f seems not negligible. The experimental data of Vilemas and Simonis [38] showed a large effect of temperature ratio on friction at low range of Re but smaller effect of Re on friction. They found a 20% decrease in f in the Reynolds number range of 10,000 to 20,000 when the channel was heated to T_w/T_b = 1.8 from an adiabatic flow condition. The effect of Reynolds number on f was negligible for heating up to T_w/T_b = 1.8 in the range of Reynolds number less than about 60,000. However the data for the influence of temperature ratio on friction is for one channel only (e/D = 0.013, L/e = 9.5), and the effect of the parameter e/d_e could not be discerned. The friction factor measured in the experiment of Vilemas and Simonis was the overall friction factor with an outer smooth wall and inner rough wall, whereas the present computation is performed with the both walls of identical roughness. Thus an exact comparison cannot be made. The channel of the present computation also has much larger pitch to roughness height ratio than the test section of Vilemas and Simonis, and the ratio of the roughness height to the channel height of flow passage is about

11% compared to only 2.6% in the experiment. Thus, the channel of the present study has larger flow recirculation and redeveloped region than the experimental setup.

Figure 4.6.2 shows the plot of St/St_c versus T_w/T_b. There is about 5% reduction in heat transfer rate for both Re = 10,000 and 15,000 when the air is heated to $T_w/T_b \simeq 1.7$. There is no apparent effect of Reynolds number on heat transfer for the small range of Reynolds number in the present computation. This seems to be supported by the experimental results of Vilemas and Simonis which show only about 5% difference in Nu/Nu_c from Re = 11,000 to 31,000 when the air was heated to $T_w/T_b \simeq 1.7$. However, their results show a large reduction in heat transfer with heating in the low Reynolds number range: about 19% at Re = 11,000 when the gas was heated to $T_w/T_b \simeq 1.7$. More computations need to be performed in order to investigate the effect of Reynolds number and the parameter e/D_e.

4.7 VARIABLE PROPERTIES FLOW WITH WALL FUNCTIONS

In the present computations, Pr and c_p are assumed constant, and ρ and μ are assumed to vary as

$$\frac{\mu}{\mu_{in}} = \left(\frac{T}{T_{in}}\right)^{0.67}, \qquad \frac{\rho}{\rho_{in}} = \frac{T_{in}}{T} \tag{171}$$

The wall function approach for variable properties flow described in section 2.2.5 was used to calculate the flow in channel with ribs, and the prediction of heat transfer showed opposite trend with heating: an increase of heat

transfer with temperature. As stated by Viegas and Rubesin, it seems that improvements in eddy viscosity modeling and careful consideration of the mean values of velocity and temperature in the first mesh volume are required in case of large wall heat fluxes. But, more importantly it seems that the increase of the viscous sublayer with heating should be incorporated into the Ciofalo and Collins approach. The proposed approach is to include the temperature ratio in case of variable properties flow as below.

$$\frac{y_v^+}{y_{vo}^+} = \left(\frac{\psi_e}{k^{1/2}/u}\right)^a \left(\frac{T_w}{T_b}\right)^b \tag{172}$$

where ψ_e and y_{vo} are the turbulence intensity and the non-dimensional sublayer thickness respectively in the equilibrium boundary layer, and a and b are empirical constants. This modification will make the P - function in the law of the wall for temperature a function of heating. Even though, this is possible with experimental data of variable properties flow, it would be similar to the derivation of the standard wall functions. Another drawback of the wall function approach was an inability to predict the recirculation zone at the top of the forward-facing rib, causing a low pressure zone above the rib which in turn gave a larger overall pressure drop.

Though this is less important, a possible improvement over Eq. (97) would be to adopt Amano's approach of evaluating the production and destruction terms in the ε equation, taking into account the variation of k in the near wall layer. A simpler approach would be to use Eq. (95) as a mean value. These possible improvements need to be further investigated.

4.8 EFFECT OF WALL THERMAL BOUNDARY CONDITIONS.

The computations presented were all performed with a constant wall heat flux boundary condition to correspond with the majority of the experiments that were used for comparison purposes. Subsequently flow in a channel with transverse rectangular ribs was solved with a constant wall temperature boundary condition, and an approximately four-fold increase of heat transfer coefficient at the top edge of the forward-facing rib was found. In the recirculating region behind the rib, the prediction of heat transfer was comparable with that for a constant wall heat flux boundary condition.

In order to investigate this unexpected results further, a simpler problem was chosen, namely a laminar flow over a forward-facing step. Figure 4.8.1 shows a velocity field for $Re = 550$ and $e/H = 0.13$. The grid employed was 52x28 with 10 grid nodes placed below the step. Figure 4.8.2 shows the local Nusselt number distributions along the channel wall including the front face of the step. For the both boundary conditions, the Nusselt number reaches a minimum in the corner of the step, and there is a gradual increase in Nusselt number along the front face of the step reaching a maximum on the top of the step. For a constant T_w, the minimum is much smaller and the maximum much larger(2 times) than for a constant q_w boundary condition.

Grid refinement tests are shown in Figure 4.8.3 for four different grid arrangements. The solutions are practically identical for all cases except for the overprediction of heat transfer coefficient on the top of the step with the grid of 40x20. The prediction over the face of the step is invariant for all the grid arrangements.

Isotherms for the both wall boundary conditions are plotted in Figure 4.8.4 where the scale of y coordinate has been enlarged to have a better view of temperature profiles below the step. The temperature contour has been plotted from the inlet to the forward-facing step, and from the wall to the top of the step only. The solution with the constant wall temperature boundary condition produces a steeper temperature gradients along the front face of the rib compared to that with wall heat flux boundary condition. In the corner of the step, the velocity of fluid is very small. Thus the fluid next to the wall retains a temperature very close to the wall temperature in the case of constant T_w boundary condition, and the fluid acts as an insulating layer. This leads to the very low heat transfer coefficient in the corner of the step as shown in Figure 4.8.2. The constant q_w boundary condition establishes wall temperature gradient along the face of the step, and this leads to steeper temperature gradient of fluid layer along the step wall , and subsequently higher heat transfer coefficient in the corner of the step than that for the constant T_w boundary condition. Whereas the wall temperature at the top of the step for the constant q_w boundary condition has cooled to about 80% of the wall temperature at the base of the step, the wall temperature along the front face of the step for the constant T_w boundary condition is fixed at a constant value. This effect seems to be similar to the entrance region problem where the temperature gradient at the wall is theoretically infinite. In fact, the temperature gradient at the top edge of the step is almost identical to that at the wall of the second slab from the entrance in the present computation domain. These effect of wall bound-

ary conditions on heat transfer was not observed in either abrupt pipe expansion flow or in jet impingement cooling.

Chapter V

CONCLUSIONS

5.1 OVERALL CONCLUSIONS

The flow downstream of a sudden pipe expansion and over a backward-facing step were solved with both high and low Reynolds number $k-\varepsilon$ model. The standard wall function method proved to be inadequate in the calculation of heat transfer rates for flow with reattachment. The wall function approach of Ciofalo and Collins that relates the viscous sublayer thickness to the near-wall turbulence intensity gave better heat transfer prediction than the standard approach, but the overall performance was poor. The best prediction of heat transfer was obtained with the Yap modified Jones and Launder low Reynolds number $k-\varepsilon$ model.

The large part of computations were performed on two elliptic flows: the flow in a channel with rectangular transverse ribs and jet impingement on a flat plate. The objectives were the application of turbulence models to these flows to facilitate the design of active cooling in hypersonic flight, and further improvement in the turbulence model for better prediction of heat transfer.

A simple periodicity boundary condition was used to compute the fully developed flow in a channel with repeated rib roughness. The low-Reynolds number $k-\varepsilon$ model with Yap's modification gave an adequate agreement with experiment for constant property flow. The results for average heat transfer rates were generally lower than the experimental data. For jet impingement

cooling, there were overprediction of heat transfer rates in the neighborhood of reattachment, and modification to the extra source term in the dissipation rate equation was required.

Investigation of the variable property flow in a channel with ribs with the same turbulence model showed reduction in both friction and average heat transfer rates with heating. The effect of Reynolds number on the friction was not negligible in contrast to heat transfer rates. The computation domain of the present study was different from the test section of the experiment, and exact conclusion could not be made. The wall function method was modified to account for the effect of variable properties with non-adiabatic surface, and results showed that a further near-wall modelling is required to incorporate the increase of the viscous sublayer with heating.

There was a large increase in heat transfer rate at the top edge of the rib when the wall boundary condition was changed to constant wall temperature from constant wall heat flux. A laminar flow over a forward-facing step was chosen to further investigate the effect of wall thermal boundary condition. The Nusselt number at the edge of the step for the constant T_w boundary condition was about two times higher than that for the constant q_w boundary condition.

5.2 RECOMMENDATIONS

Various turbulence models have been shown to perform fairly well in prediction of mean flow by many investigators, but there needs to be a more intensive investigation to improve the turbulence models for better prediction of heat transfer in complex flows. More experimental measurements of turbulence quantities and heat transfer rates are needed especially for the stagnation point region of the jet impingement flow, and for variable property flow with heating. These will facilitate for better modelling of turbulence models.

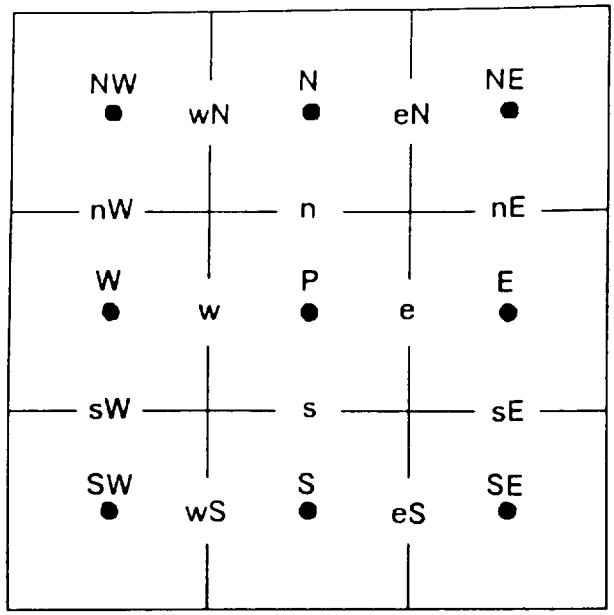

Figure 3.1 Grid nomenclature for the x-y plane.

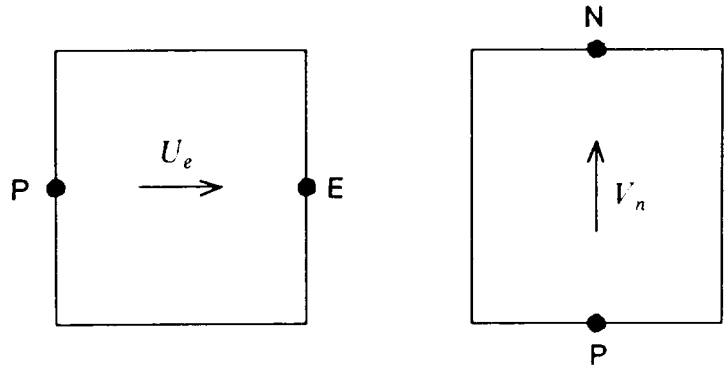

Figure 3.2 The staggered control volume in the x-y plane.

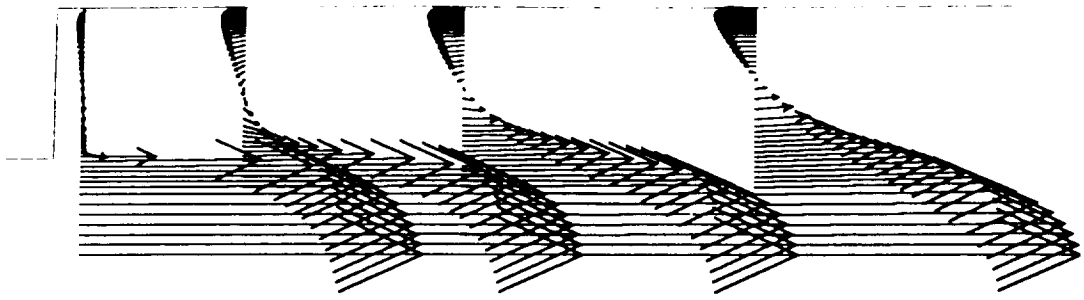

(a)

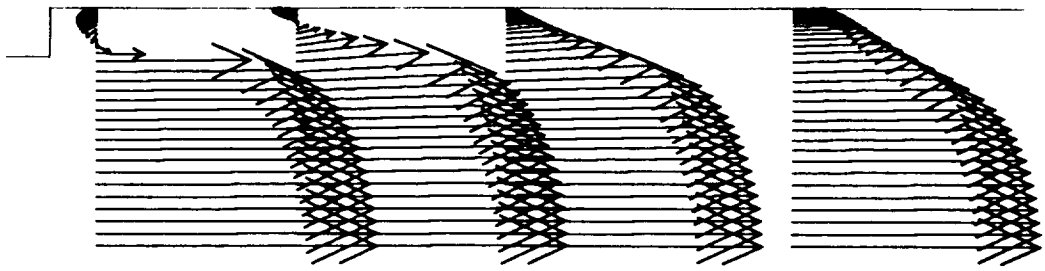

(b)

Figure 4.1.1 Velocity profiles for (a) $d/D = 0.4$, $Re = 12{,}310$ (b) $d/D = 0.8$, $Re = 20{,}130$.

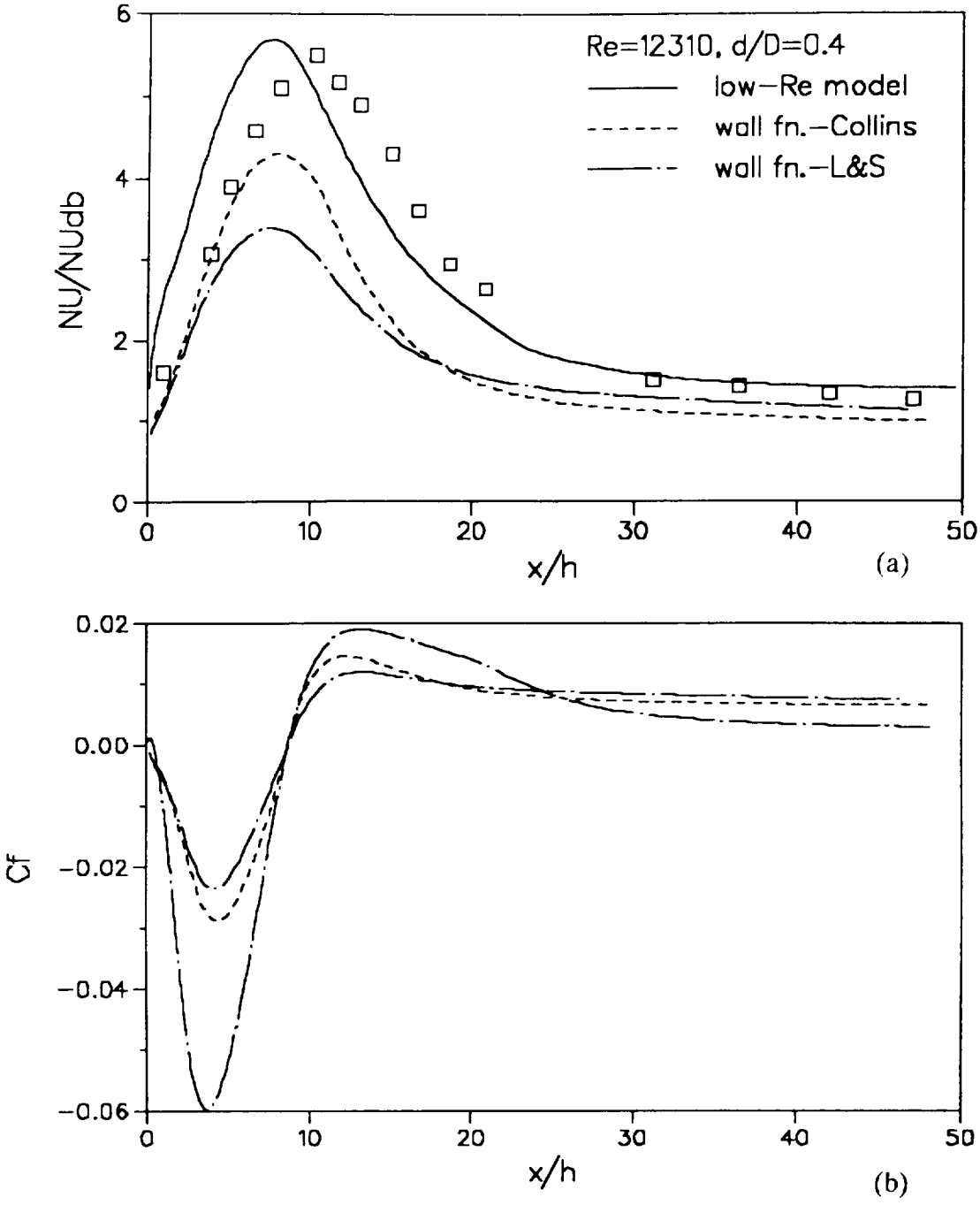

Figure 4.1.2 Comparison of Nusselt number and skin-friction coefficient with the data of Baughn et al. $d/D = 0.4$, $Re = 12{,}310$.

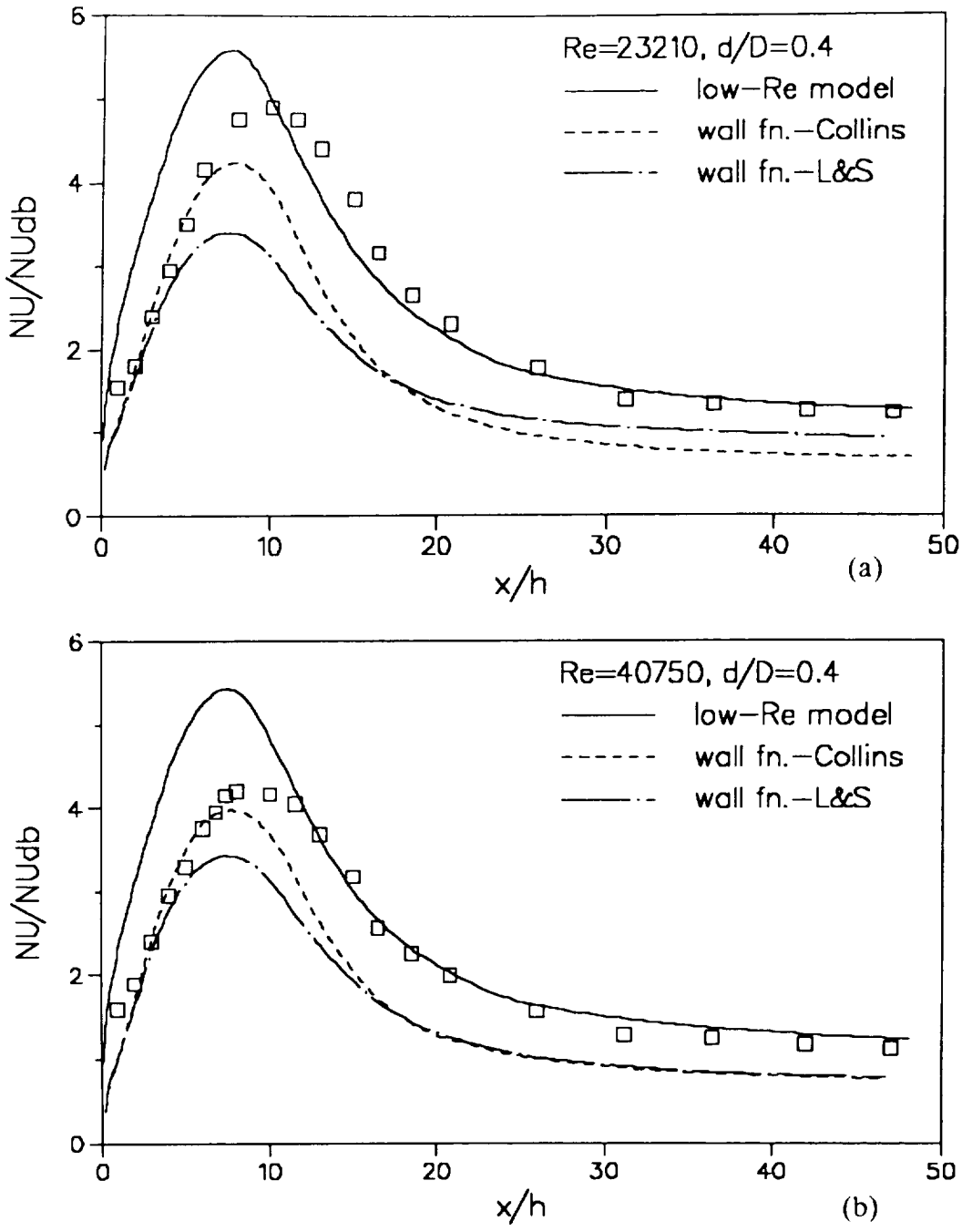

Figure 4.1.3 Comparison of Nusselt number for (a) Re = 23,210, (b) Re = 40,750 with the data of Baughn et al.

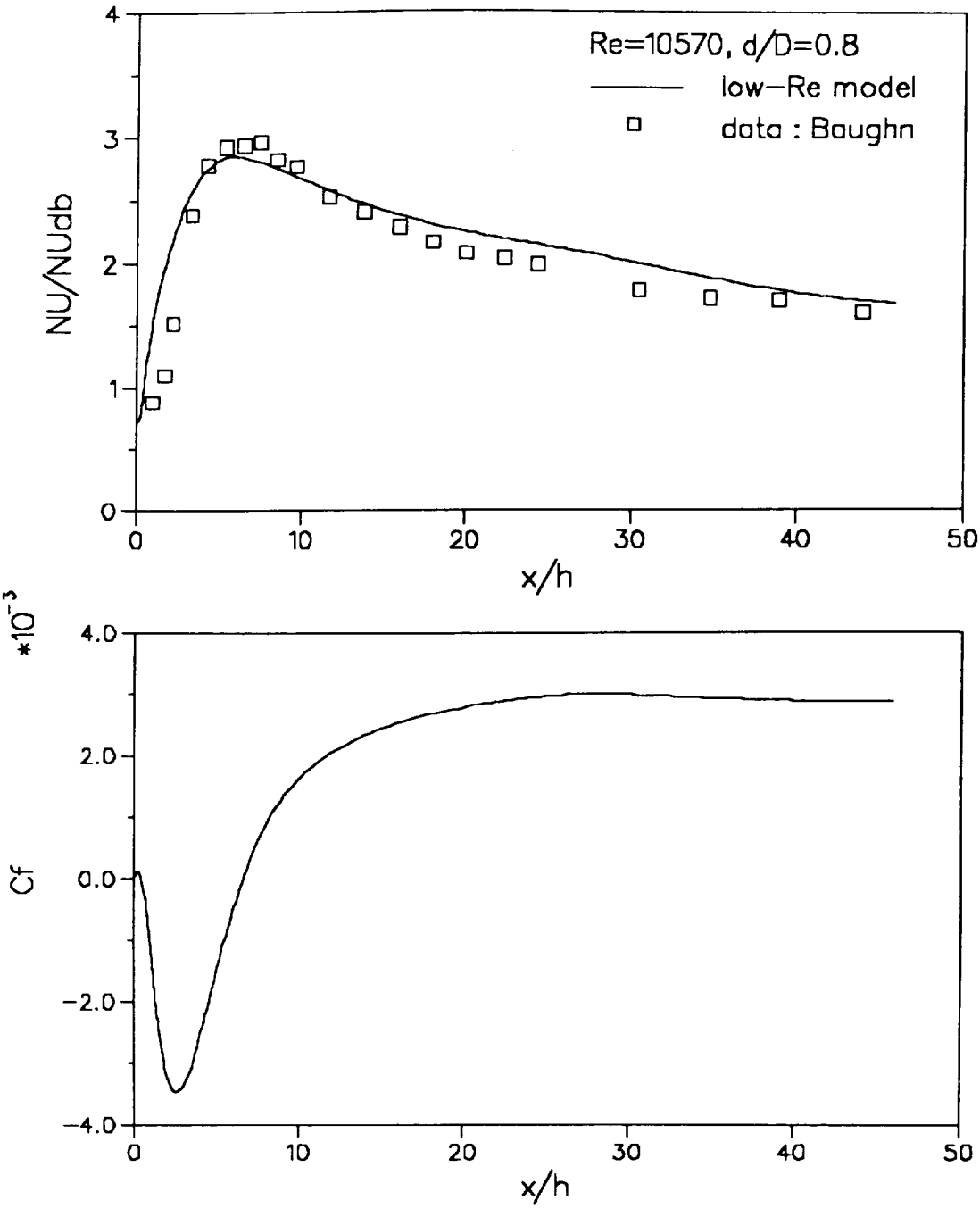

Figure 4.1.4 Comparison of Nusselt number and skin-friction coefficient with the data of Baughn et al. $d/D = 0.8$, $Re = 10{,}570$.

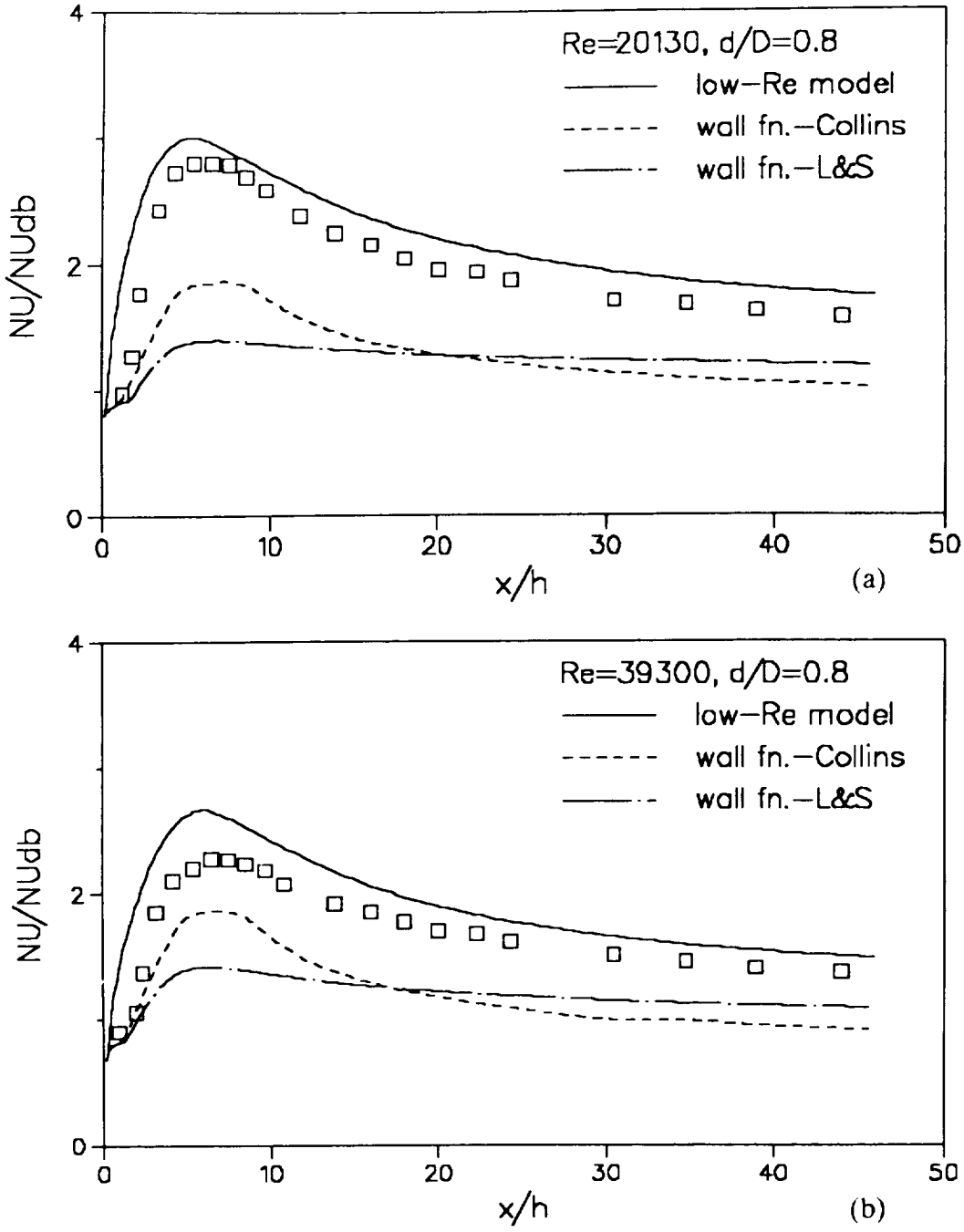

Figure 4.1.5 Comparison of Nusselt number for $d/D = 0.8$ (a) $Re = 20{,}130$ (b) $Re = 39{,}300$.

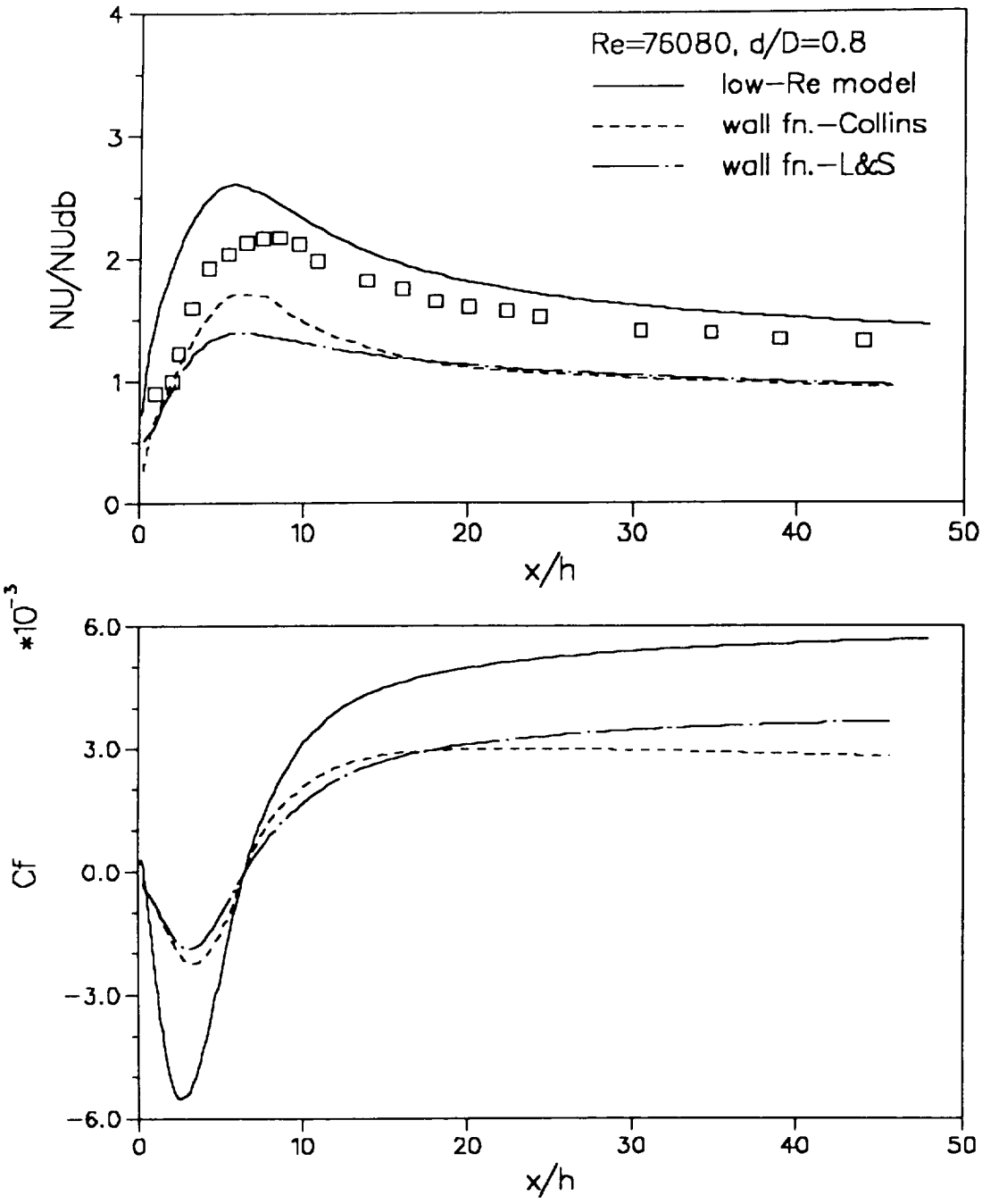

Figure 4.1.6 Comparison of Nusselt number and skin-friction coefficient with the data of Baughn et al. for d/D = 0.8, Re = 76,080.

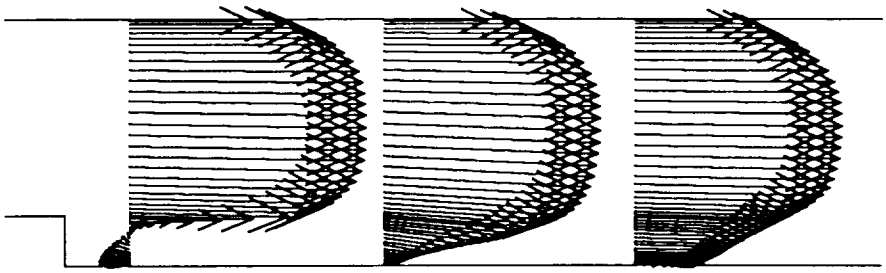

Figure 4.2.1 Vector plot for flow over a backward-facing step. expansion ratio = 1.25. Re_e = 28,000.

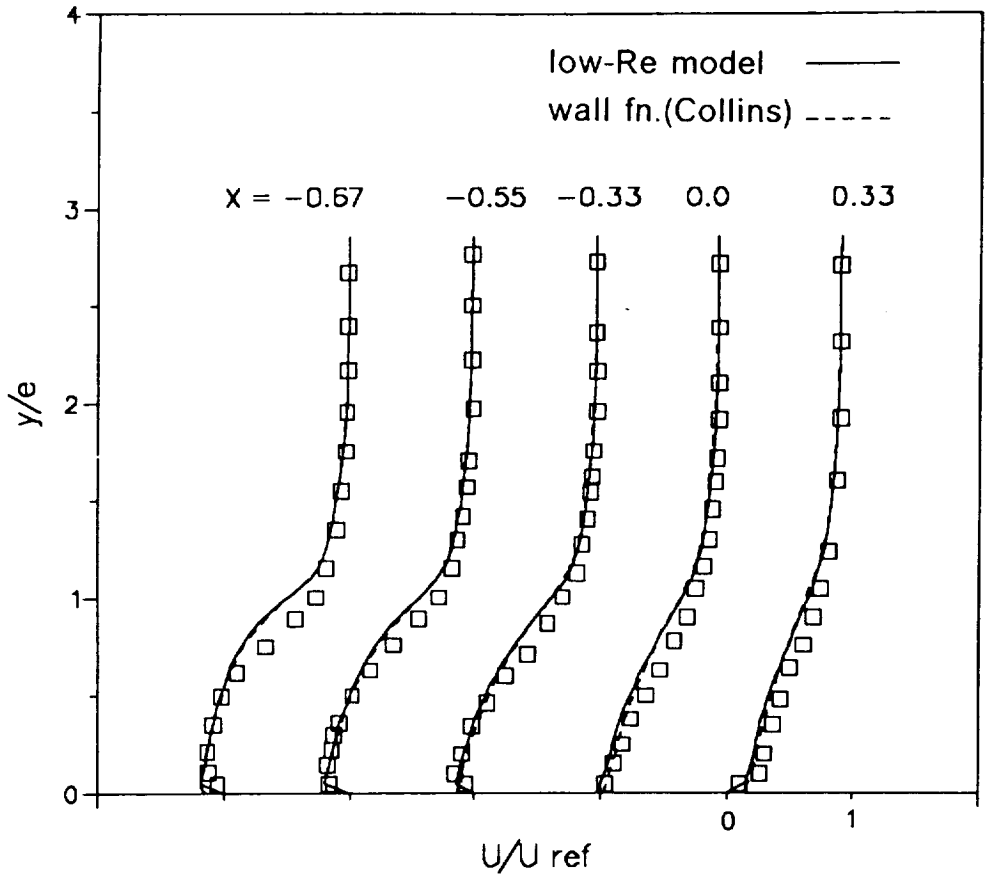

Figure 4.2.2 Mean velocity profile for flow over a backward-facing step. Re_e = 28,000.

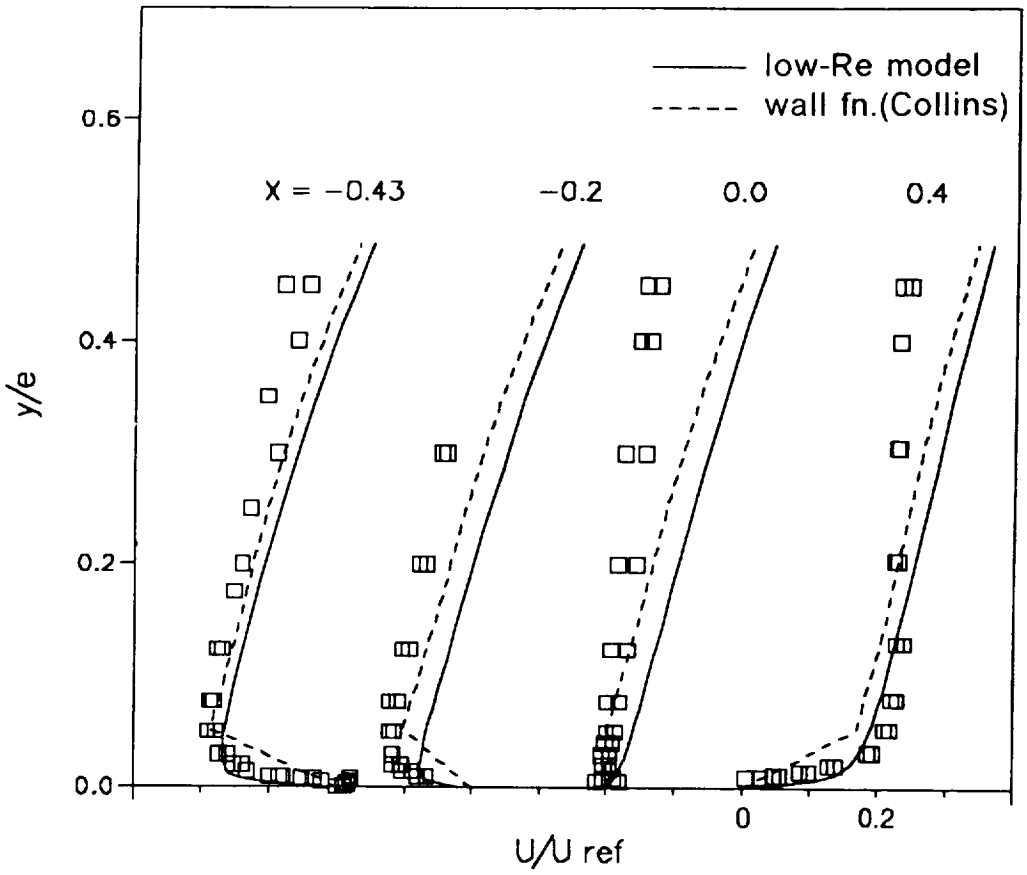

Figure 4.2.3 Mean velocity profile in the near-wall region. Re_e = 28,000.

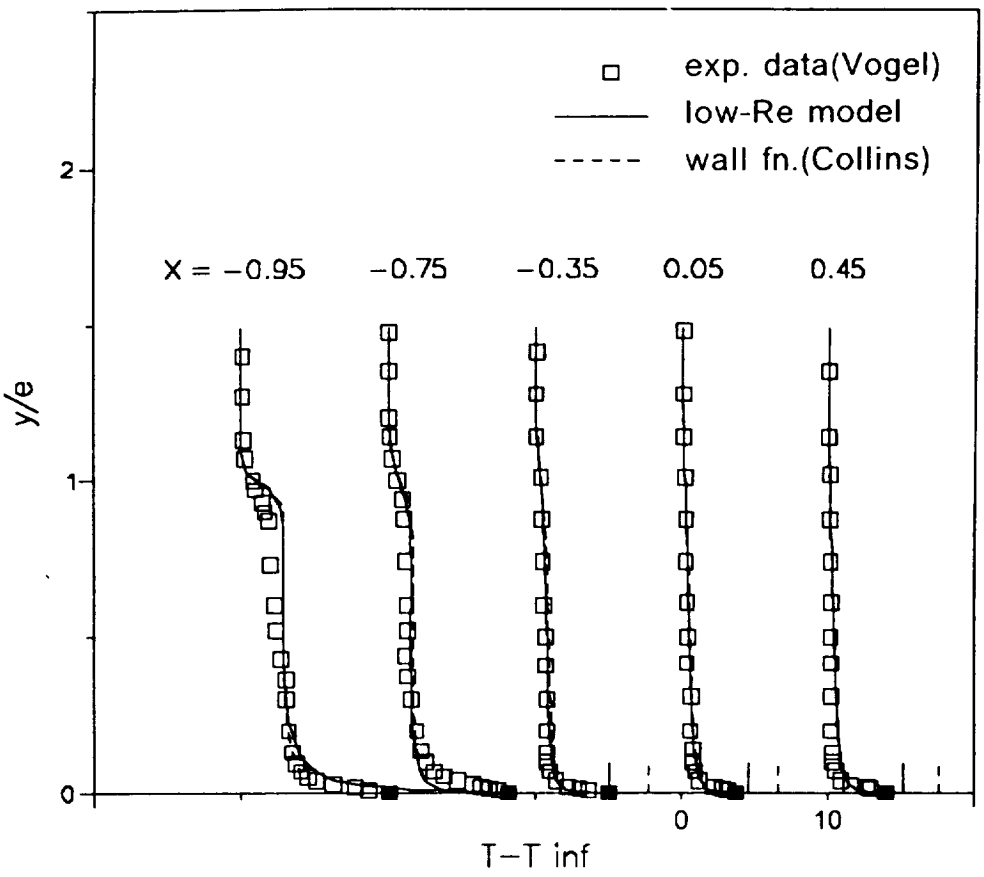

Figure 4.2.4 Temperature profile for flow over a backward-facing step. Re_e = 28,000.

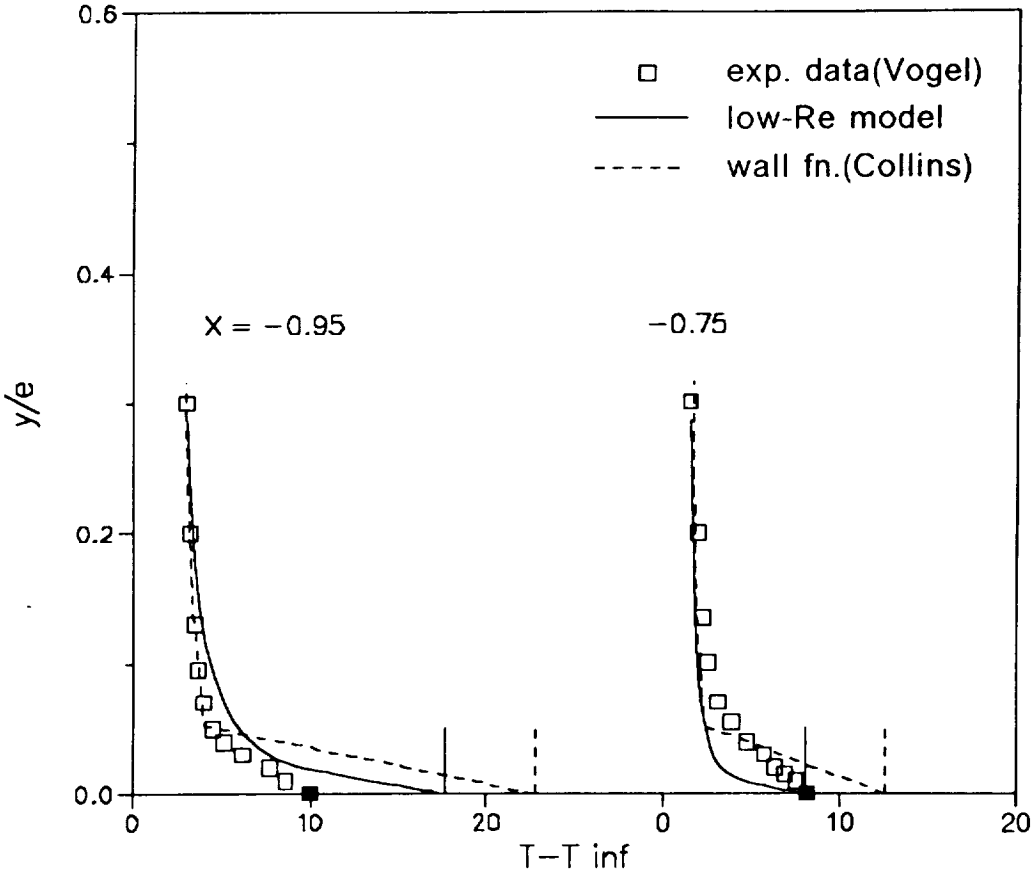

Figure 4.2.5 Temperature profile in the near-wall region. Re_e = 28,000.

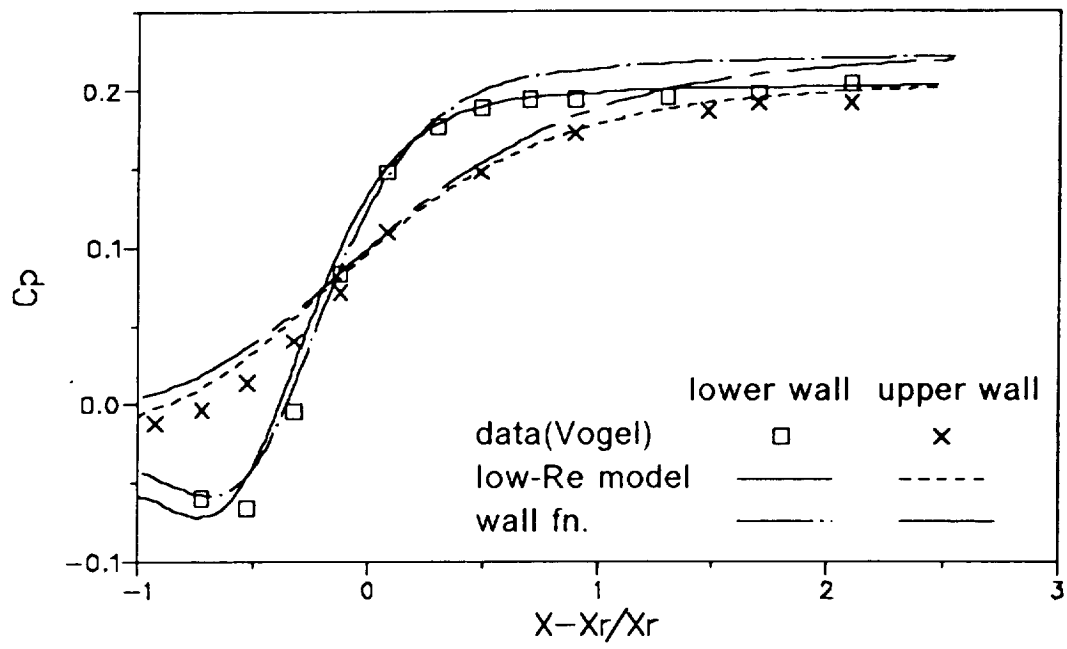

Figure 4.2.6 Wall static pressure profile for flow over backward-facing step. Re_e = 28,000.

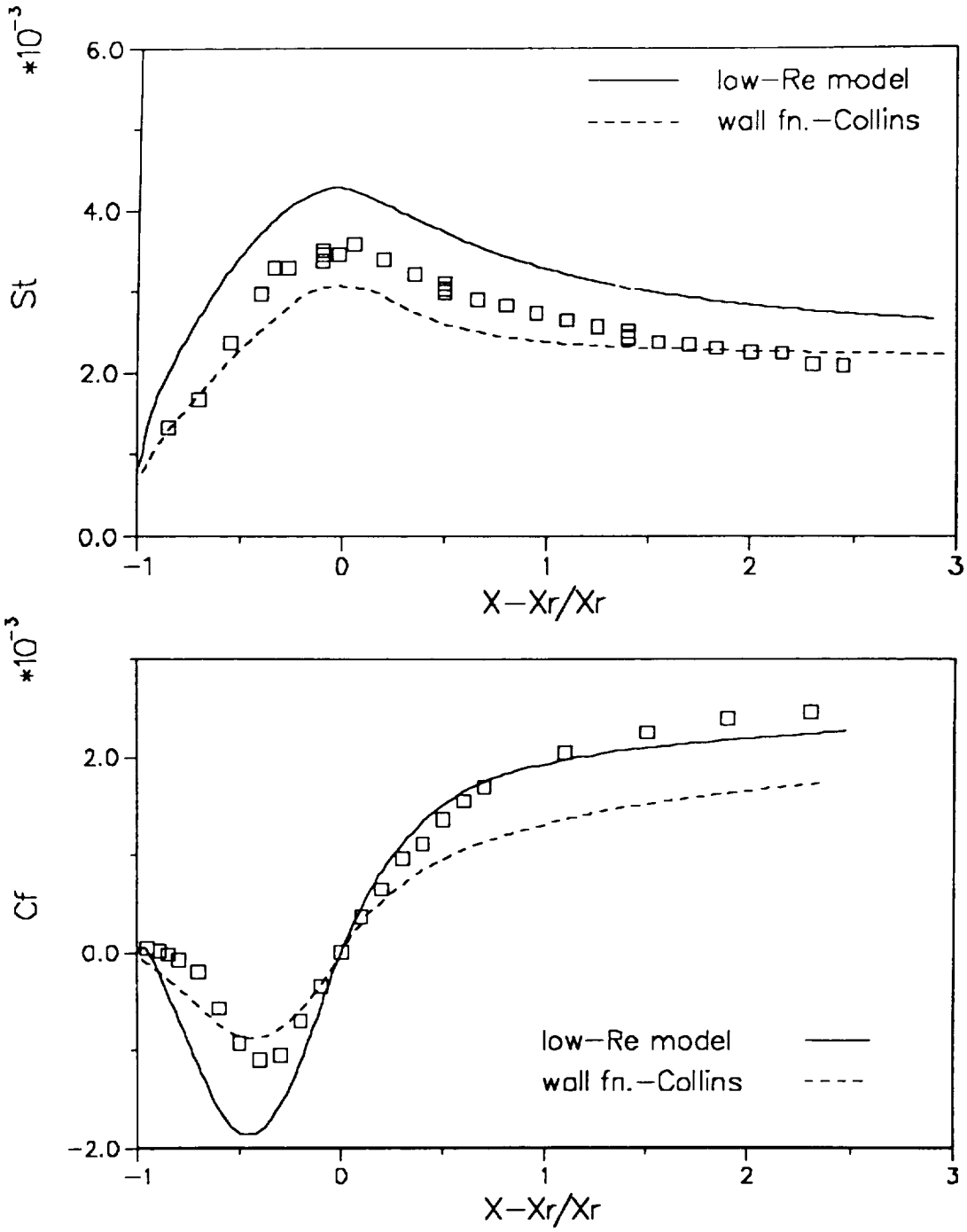

Figure 4.2.7 Predictions of Stanton number and skin-friction coefficient for backward-facing step. Re_e = 28,000.

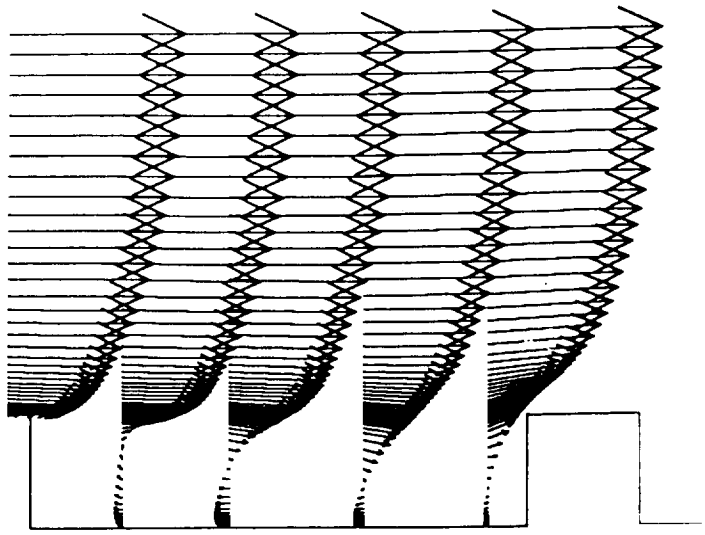

(a)

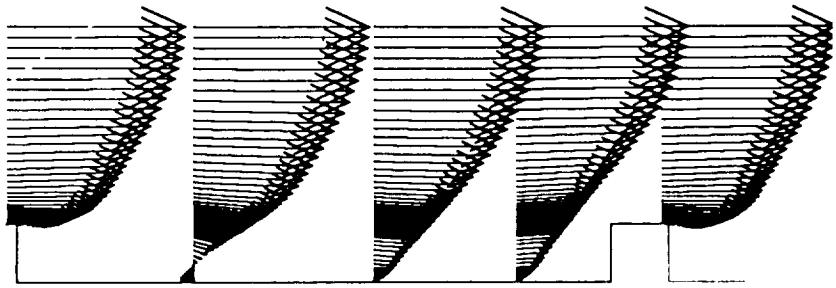

(b)

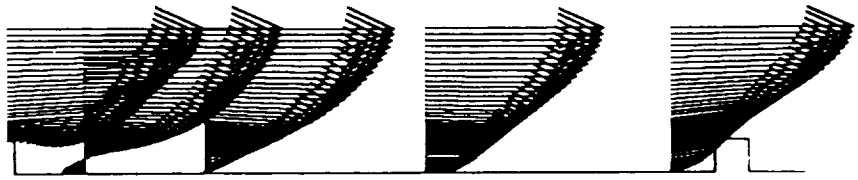

(c)

Figure 4.3.1 Vector plots for flow in a channel with ribs for $Re = 20{,}900$. (a) $L/e = 5$, (b) $L/e = 10$. (c) $L/e = 20$.

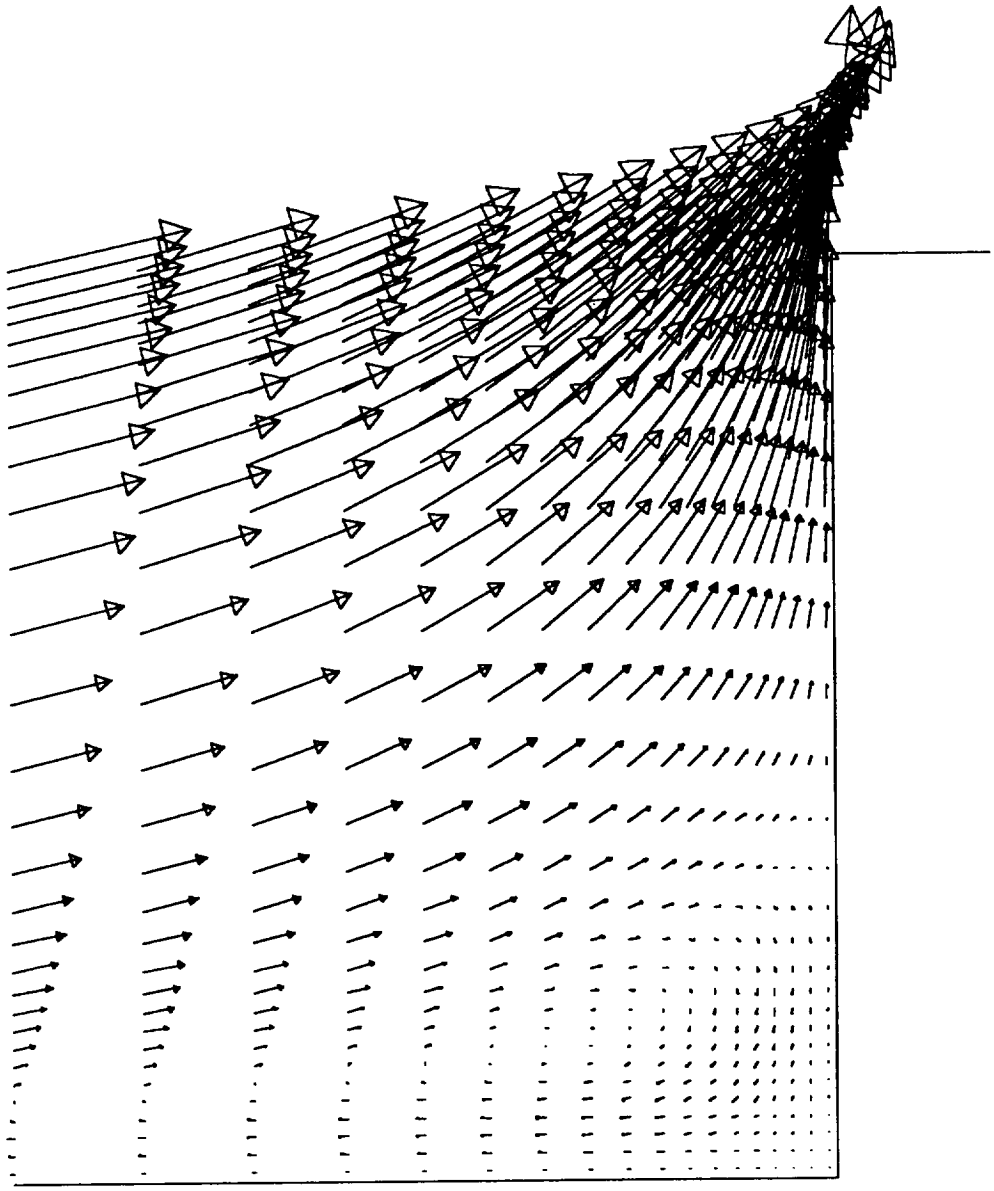

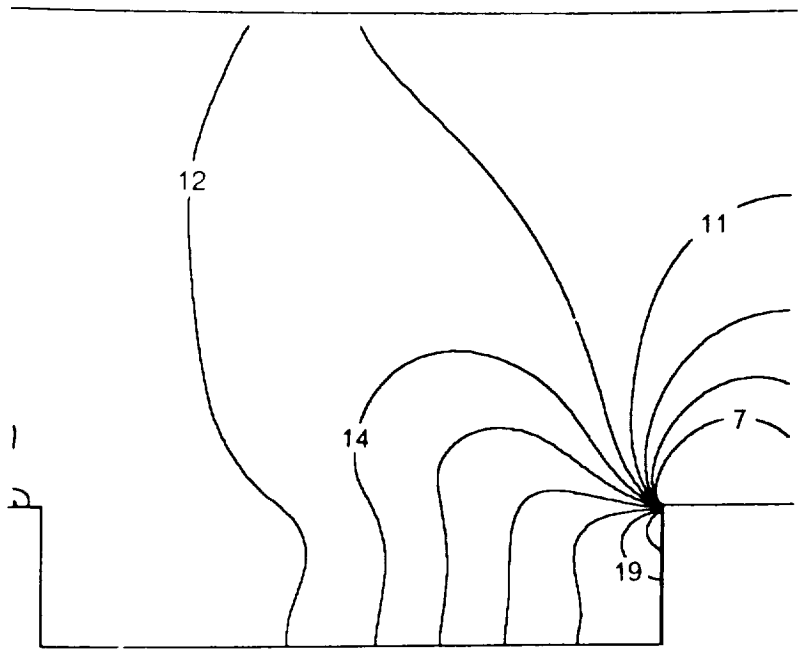

(a)

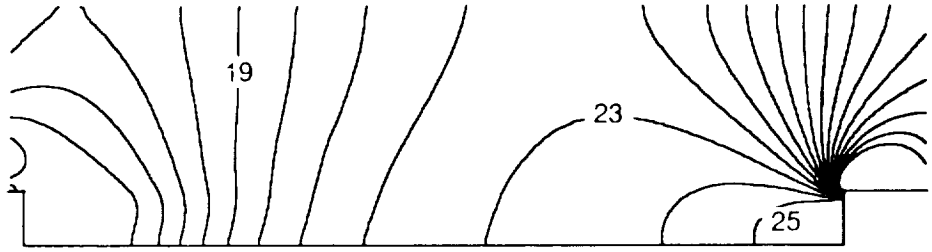

(b)

Figure 4.3.2 Static pressure contour for Re = 20,900. (a) L/e = 5, (b) L/e = 15.

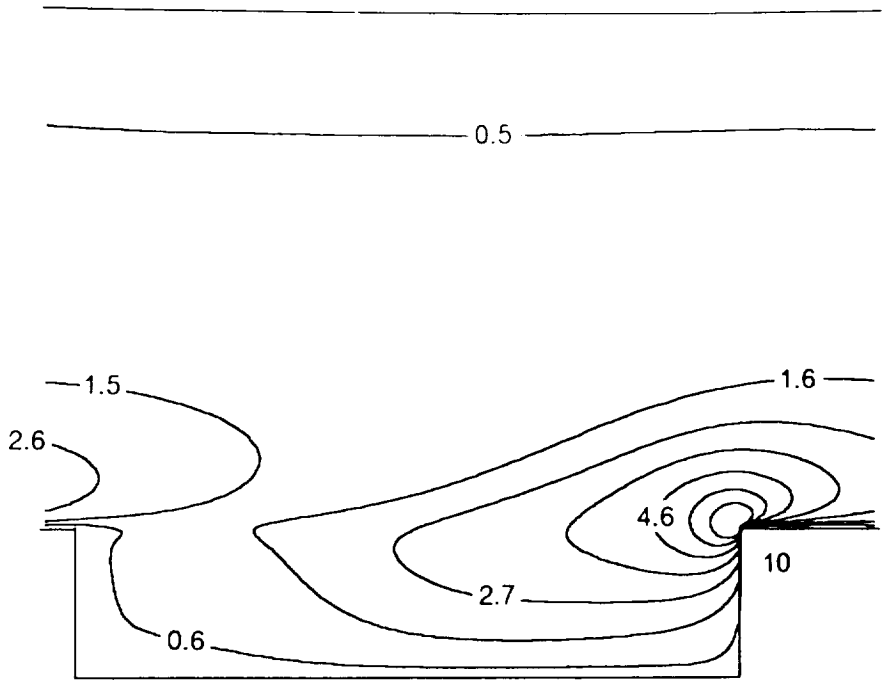

(a)

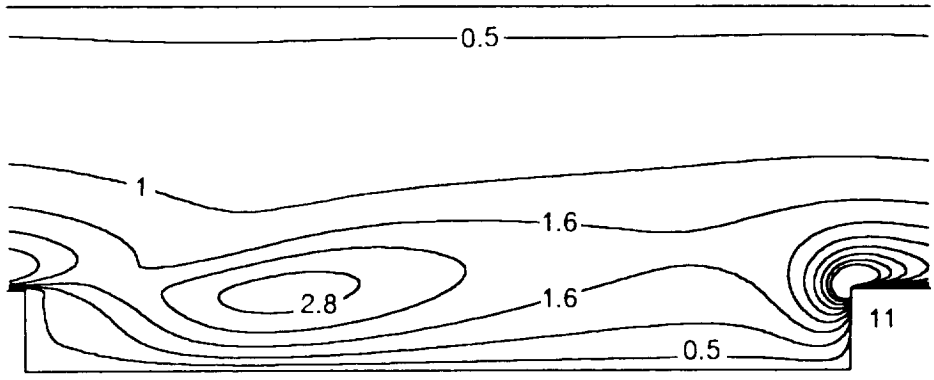

(b)

Figure 4.3.3 Turbulent kinetic energy contour for Re = 20,900. (a) L/e = 5, (b) L/e = = 10.

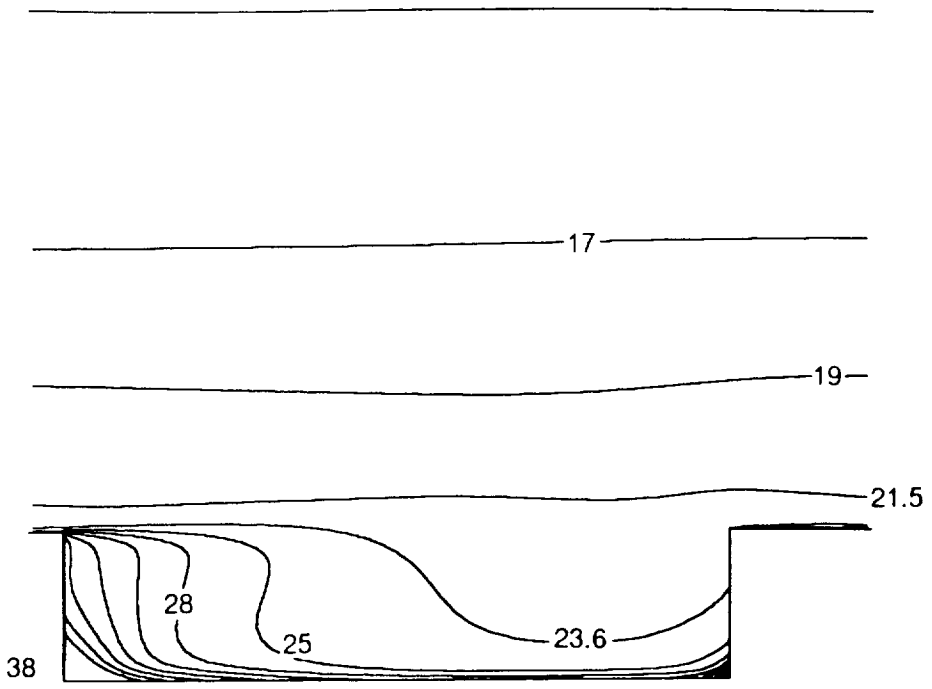

(a)

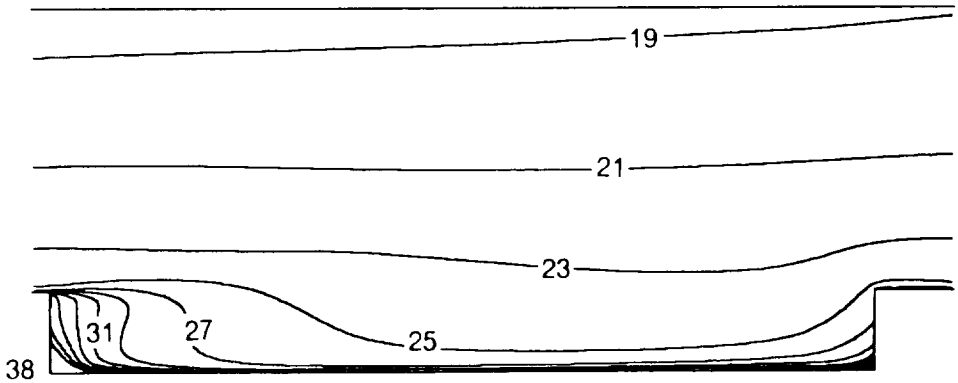

(b)

Figure 4.3.4 Isotherms for Re = 20,900. (a) L/e = 5, (b) L/e = 10.

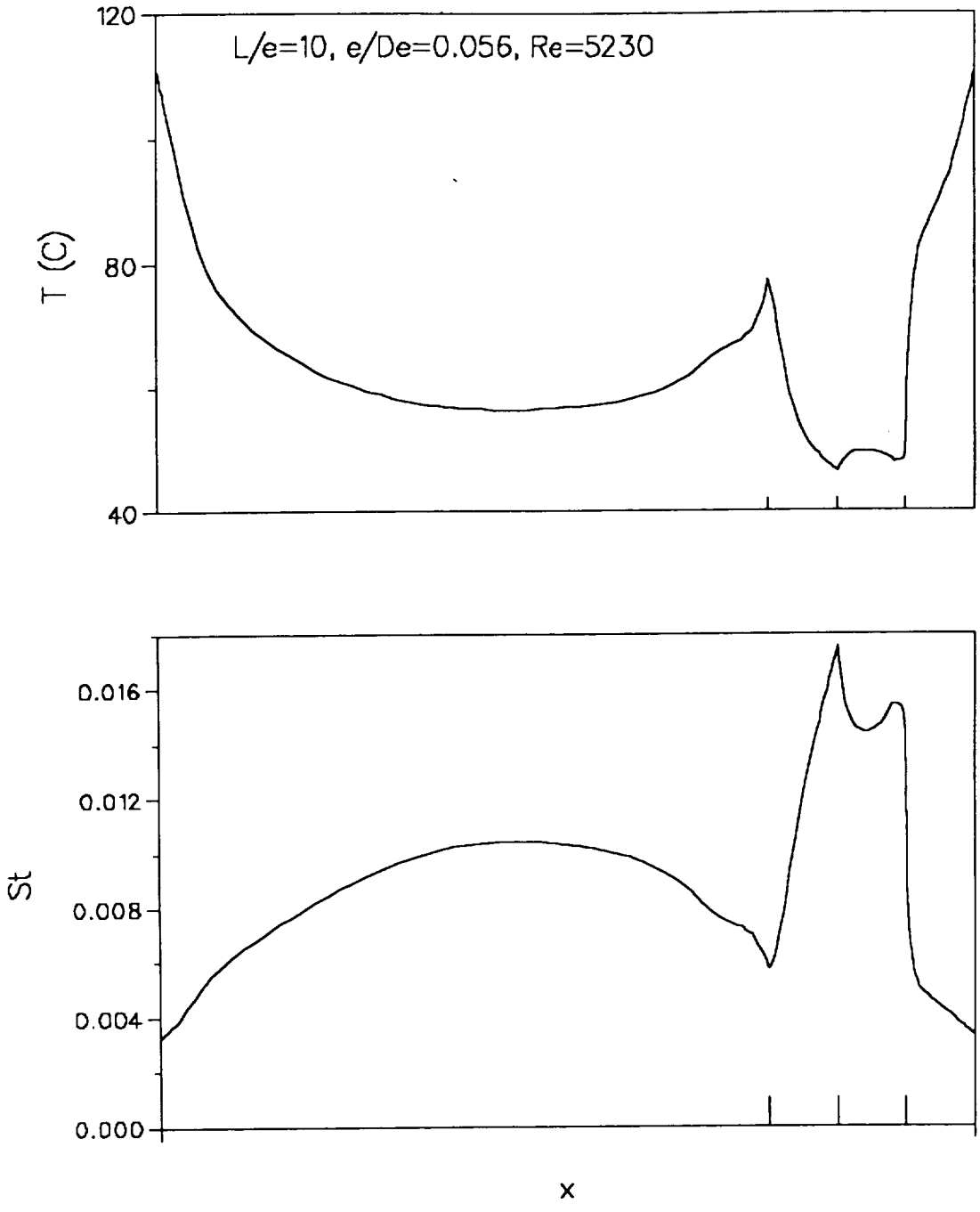

Figure 4.3.6 Prediction of wall temperature and Stanton number for L/e = 10, Re = 5,230.

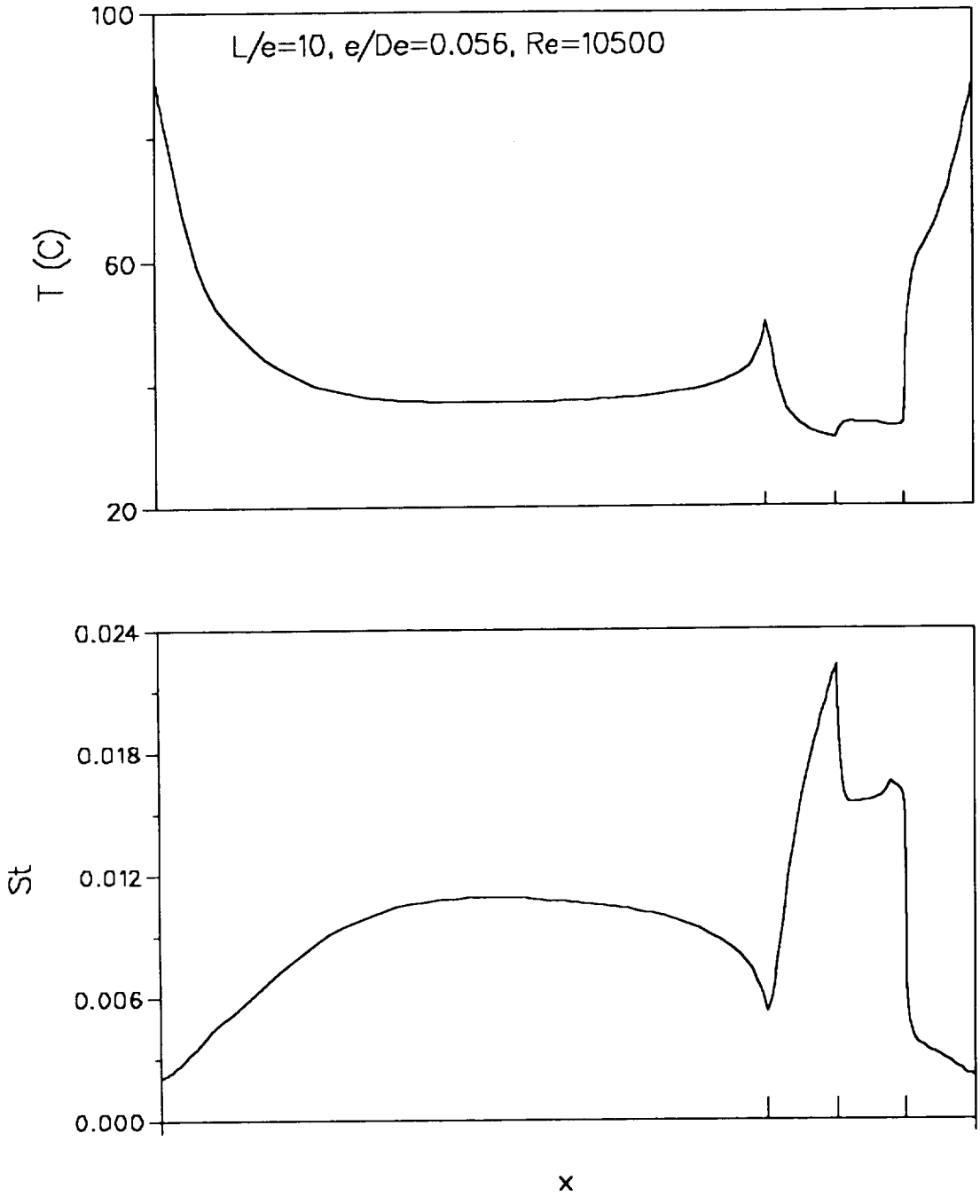

Figure 4.3.7 Prediction of wall temperature and Stanton number for L/e = 10, Re = 10,500.

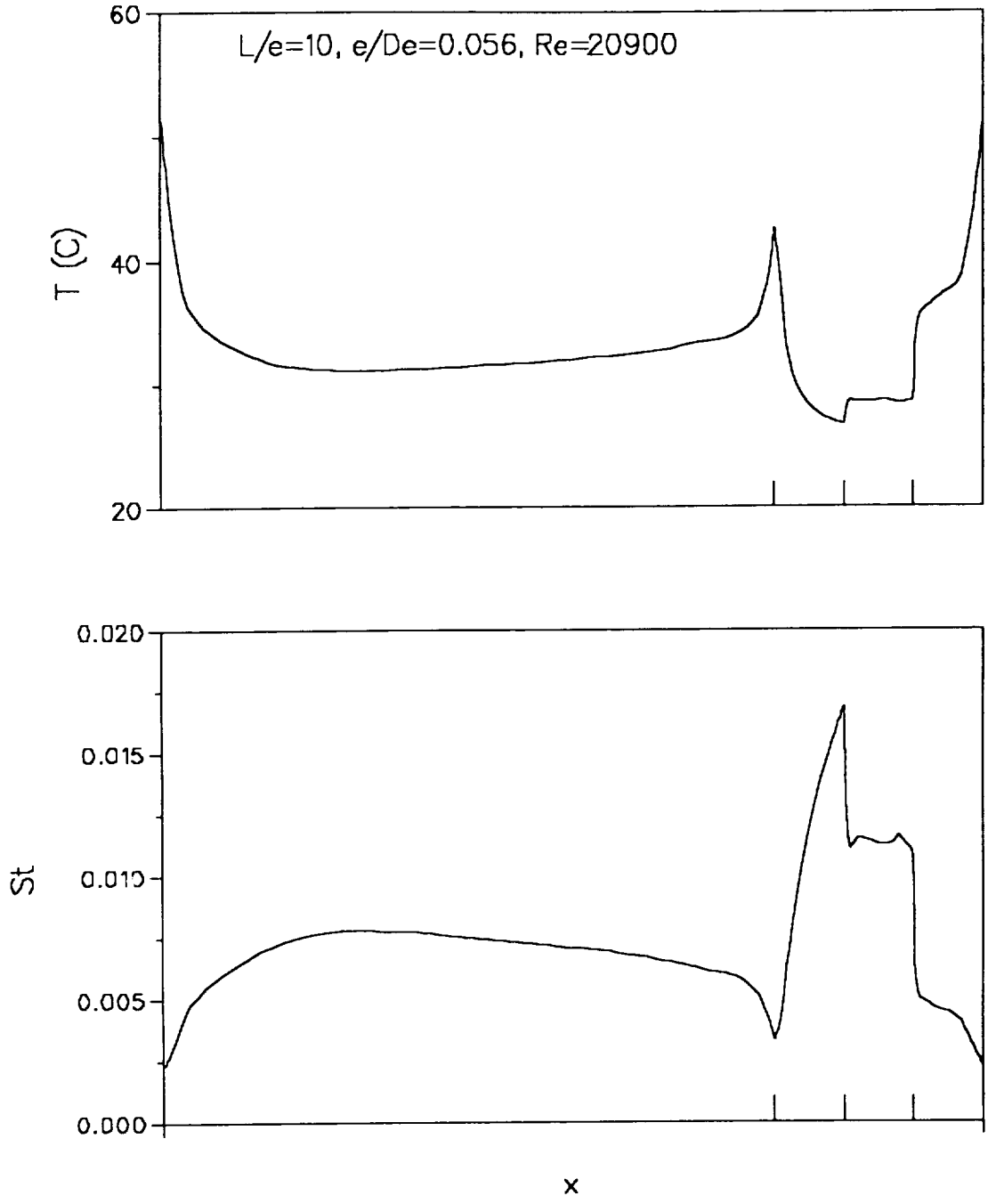

Figure 4.3.8 Prediction of wall temperature and Stanton number for L/e = 10, Re = 20,900.

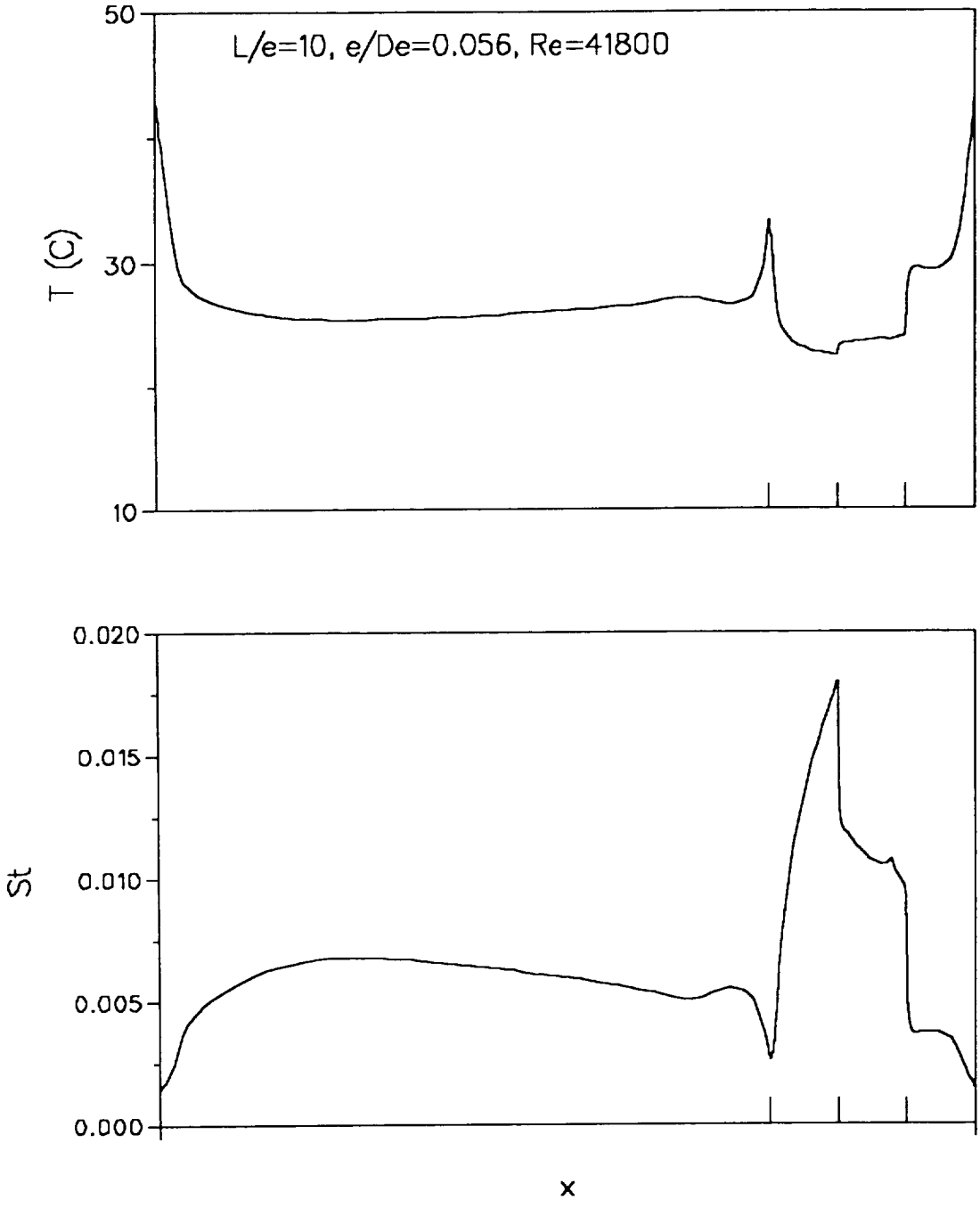

Figure 4.3.9 Prediction of wall temperature and Stanton number for L/e = 10, Re = 41,800.

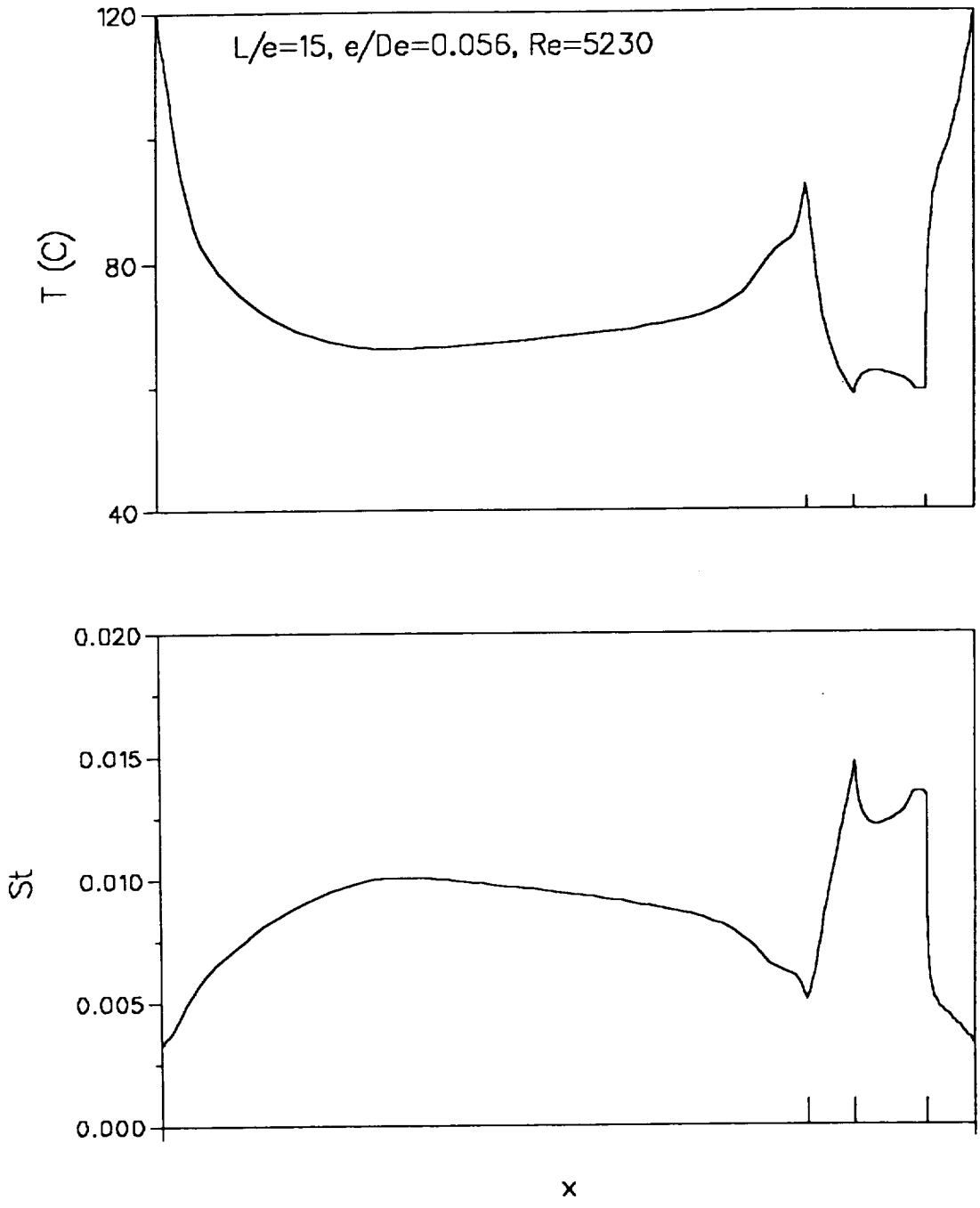

Figure 4.3.10 Prediction of wall temperature and Stanton number for L/e = 15, Re = 5,230.

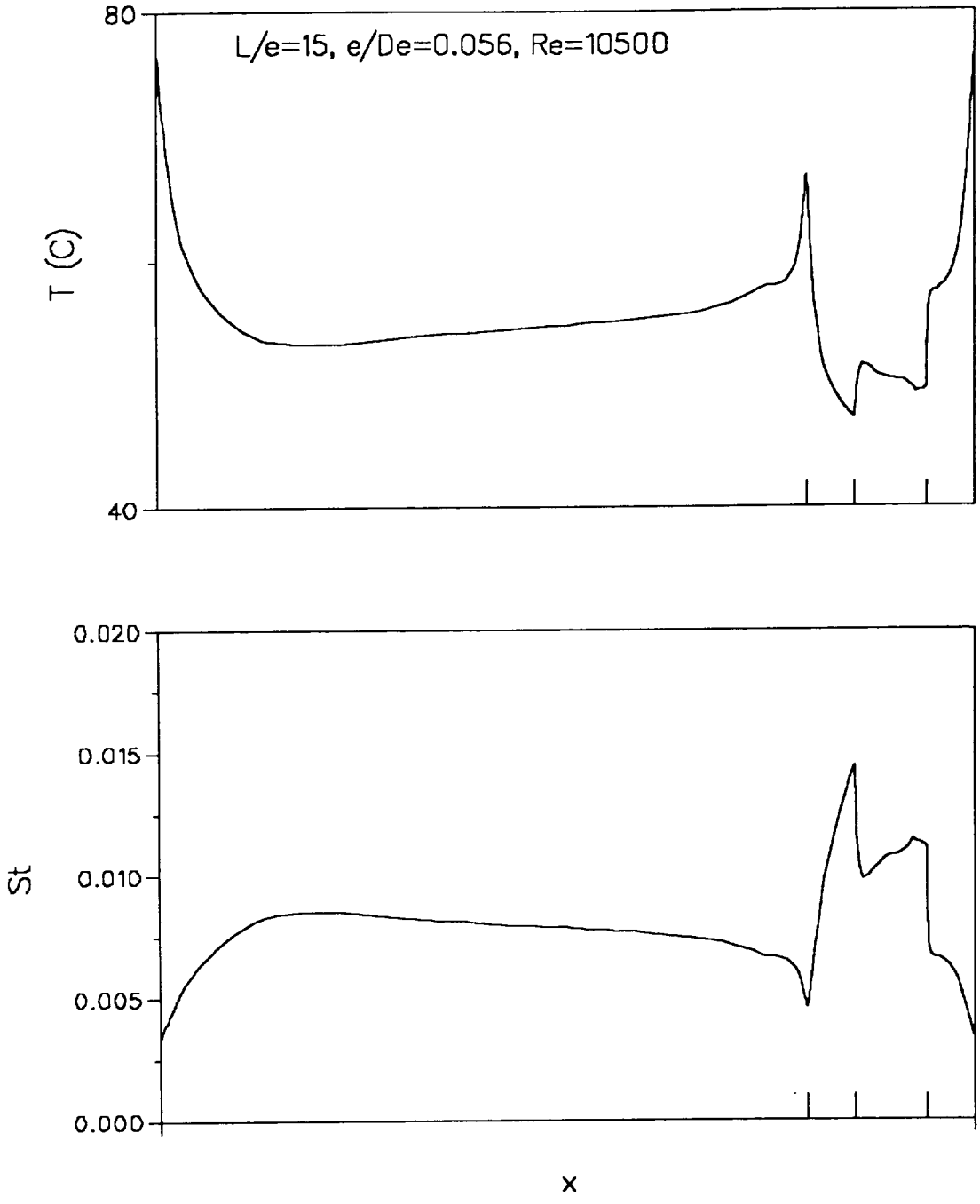

Figure 4.3.11 Prediction of wall temperature and Stanton number for L/e = 15, Re = 10,500.

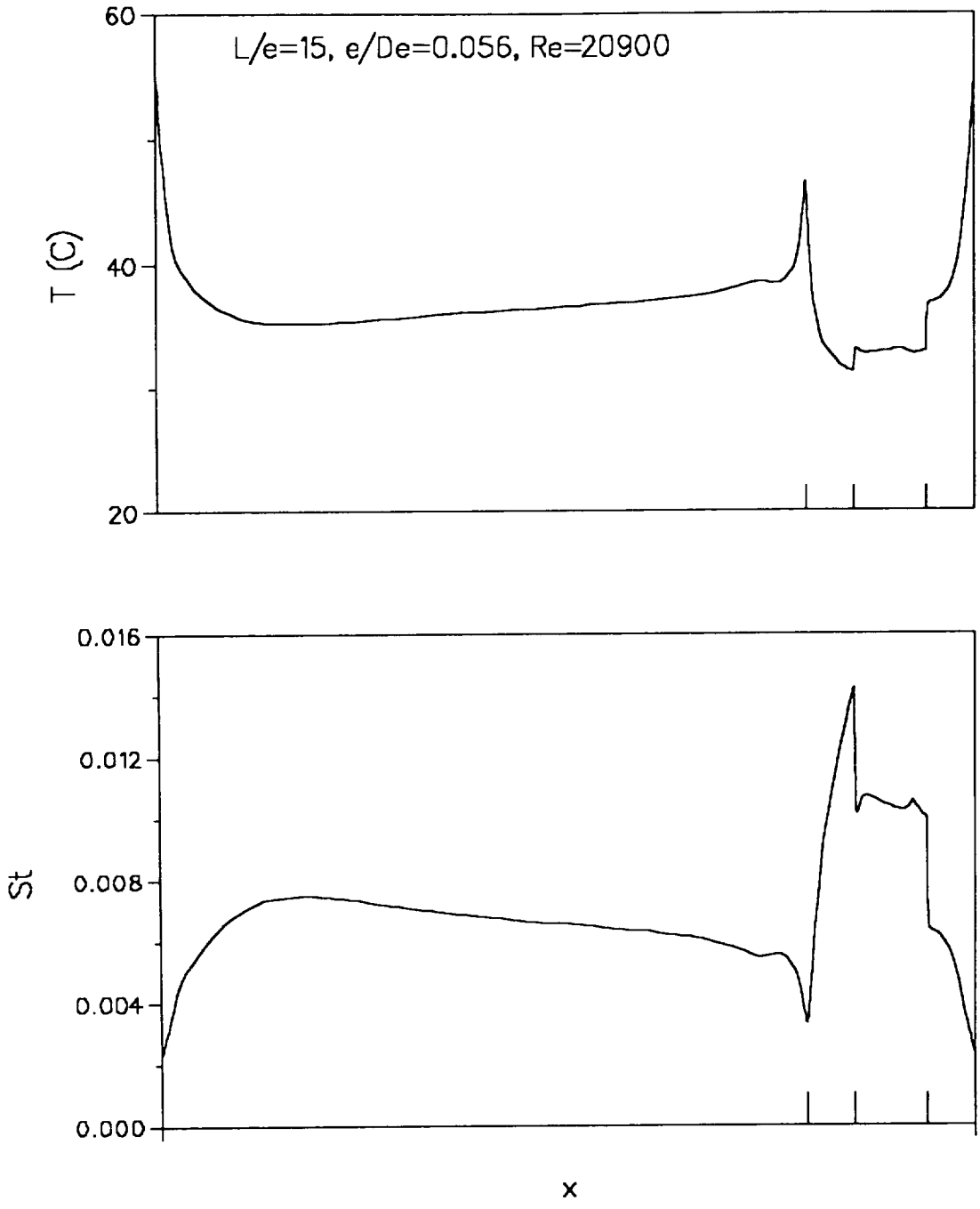

Figure 4.3.12 Prediction of wall temperature and Stanton number for L/e = 15, Re = 20,900.

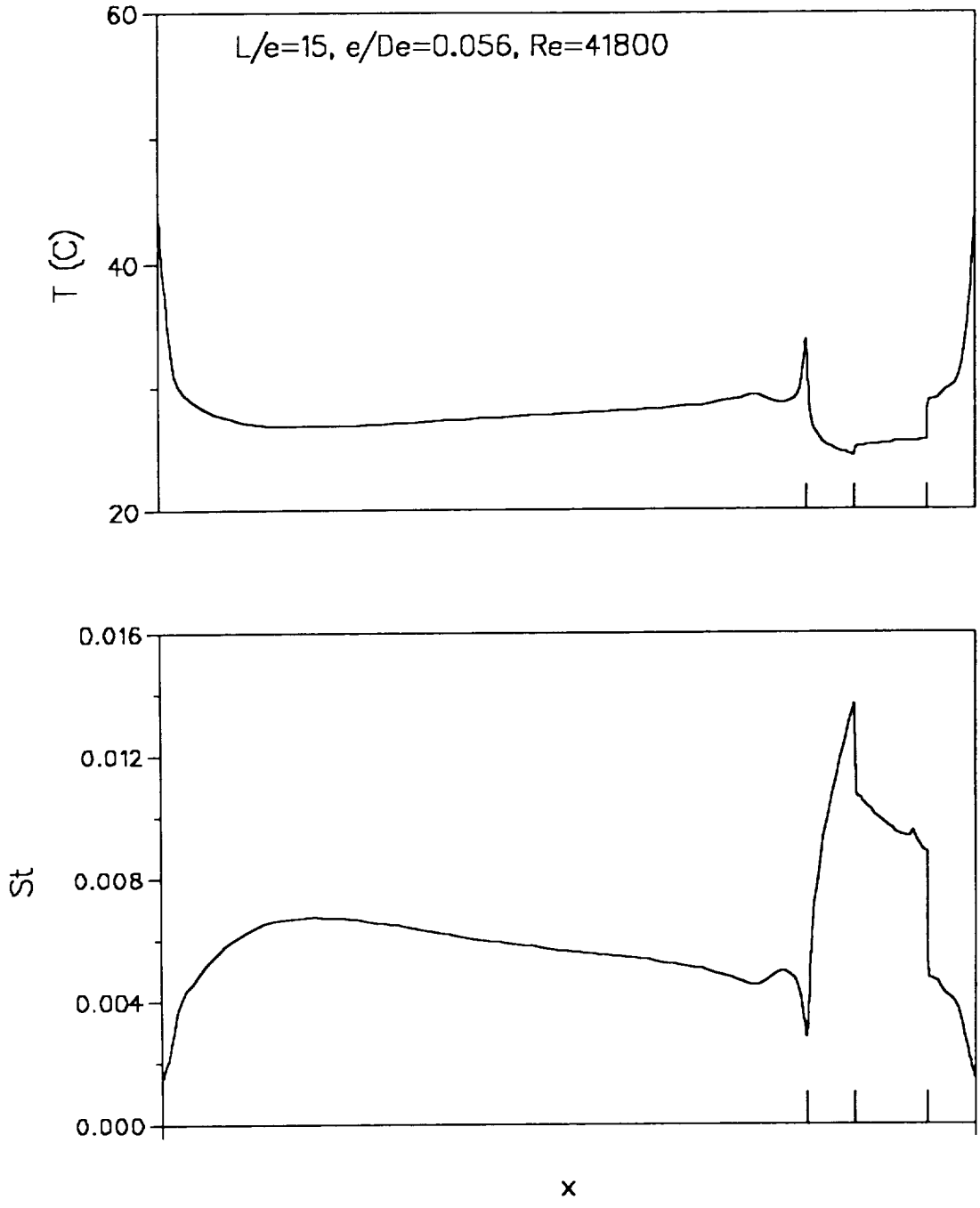

Figure 4.3.13 Prediction of wall temperature and Stanton number for L/e = 15, Re = 41,800.

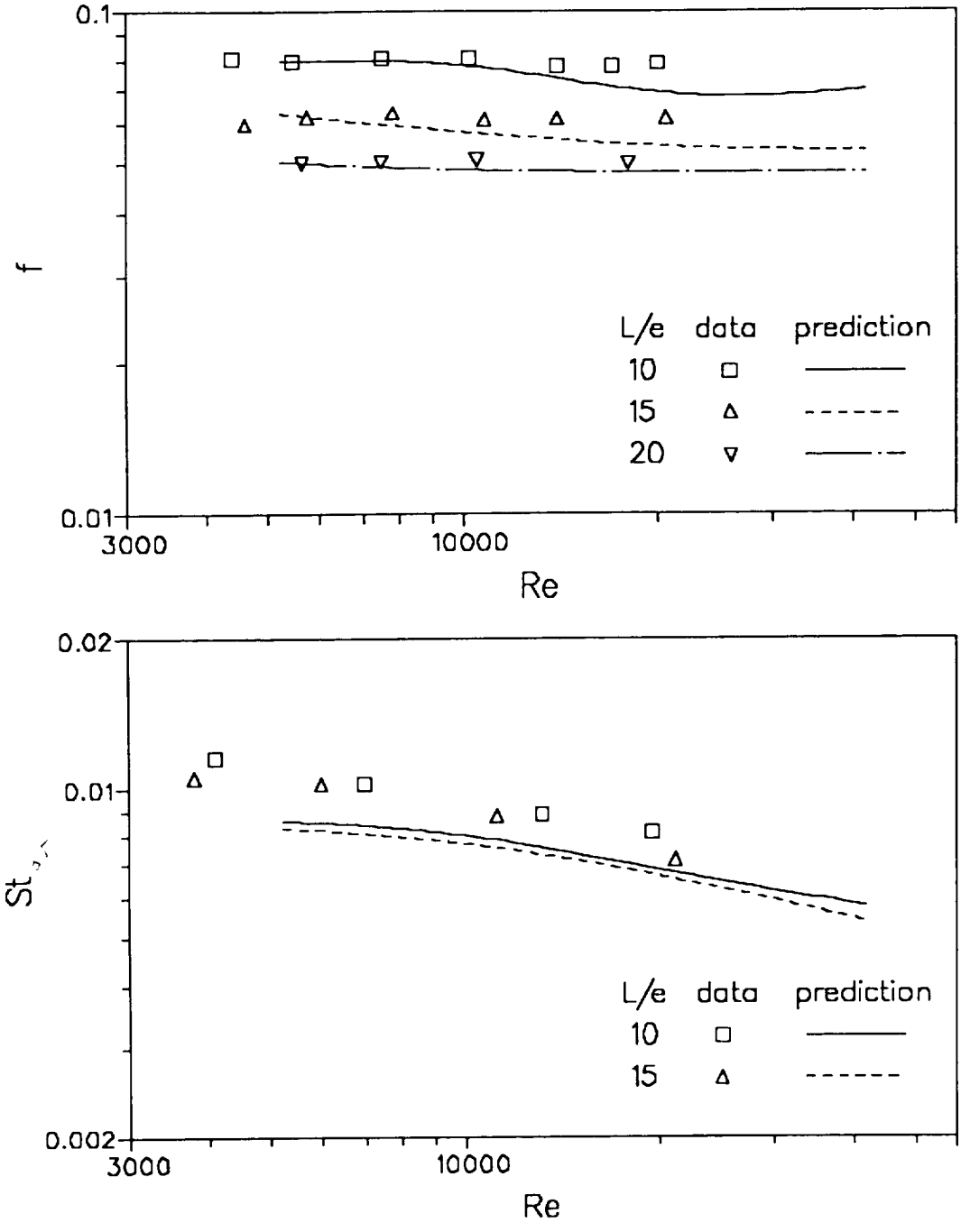

Figure 4.3.14 Comparision of average friction factor and Stanton number with the data of Han et al.

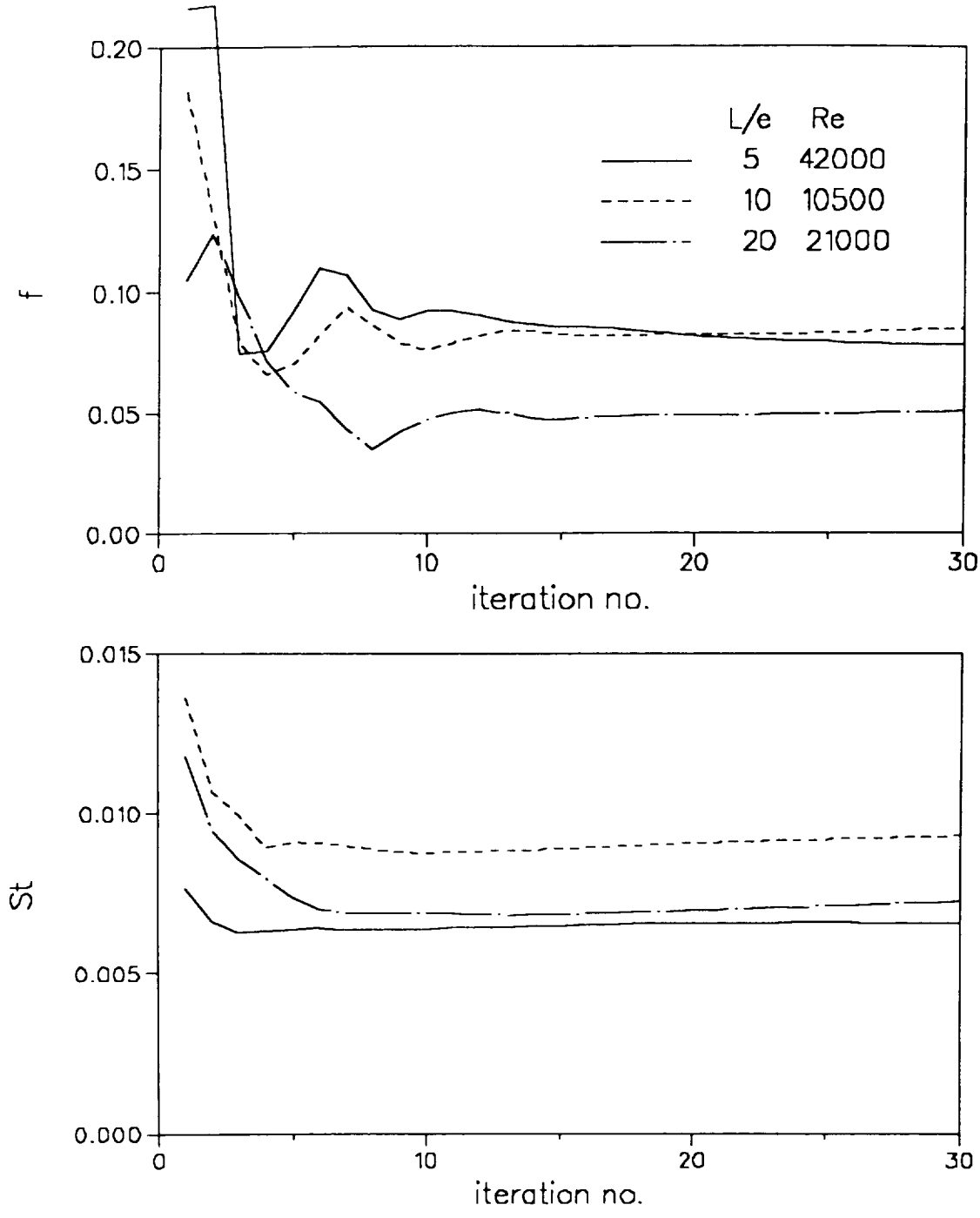

Figure 4.3.15 Average friction factor and Stanton number with outer iteration.

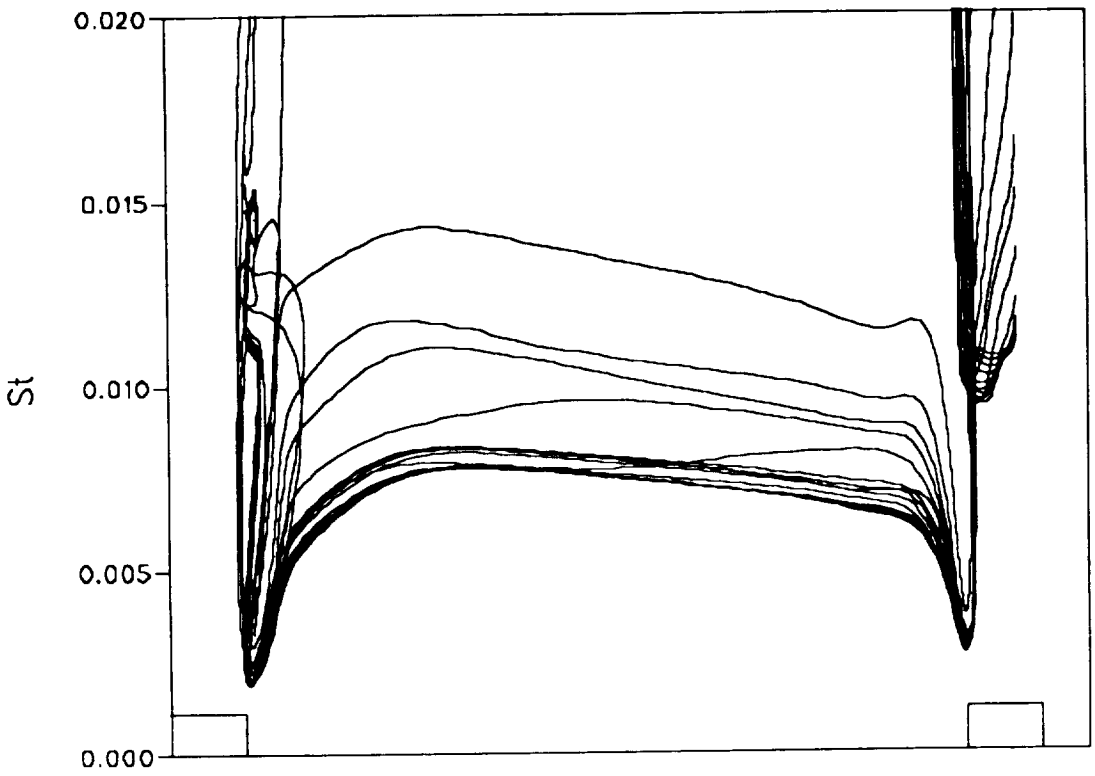

Figure 12. Local Stanton number distribution with outer iteration. $L/e = 10$, $Re = 20{,}900$.

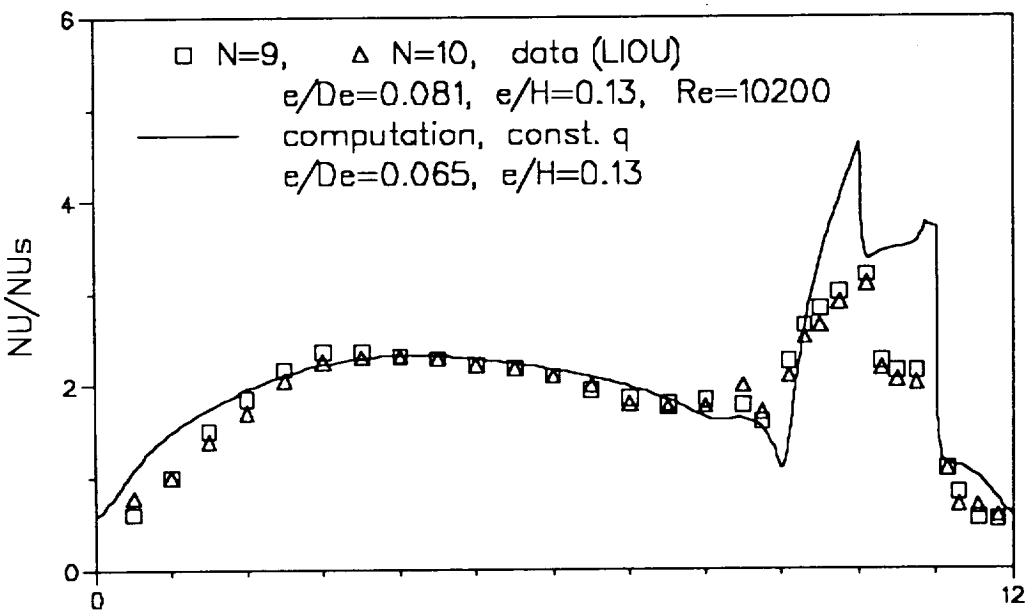

Figure 4.3.17 Comparison of local Nusselt number distribution for $L/e = 10$, $Re = 10{,}200$. $Nu_s = 0.023Re^{0.8}\,Pr^{0.4}$

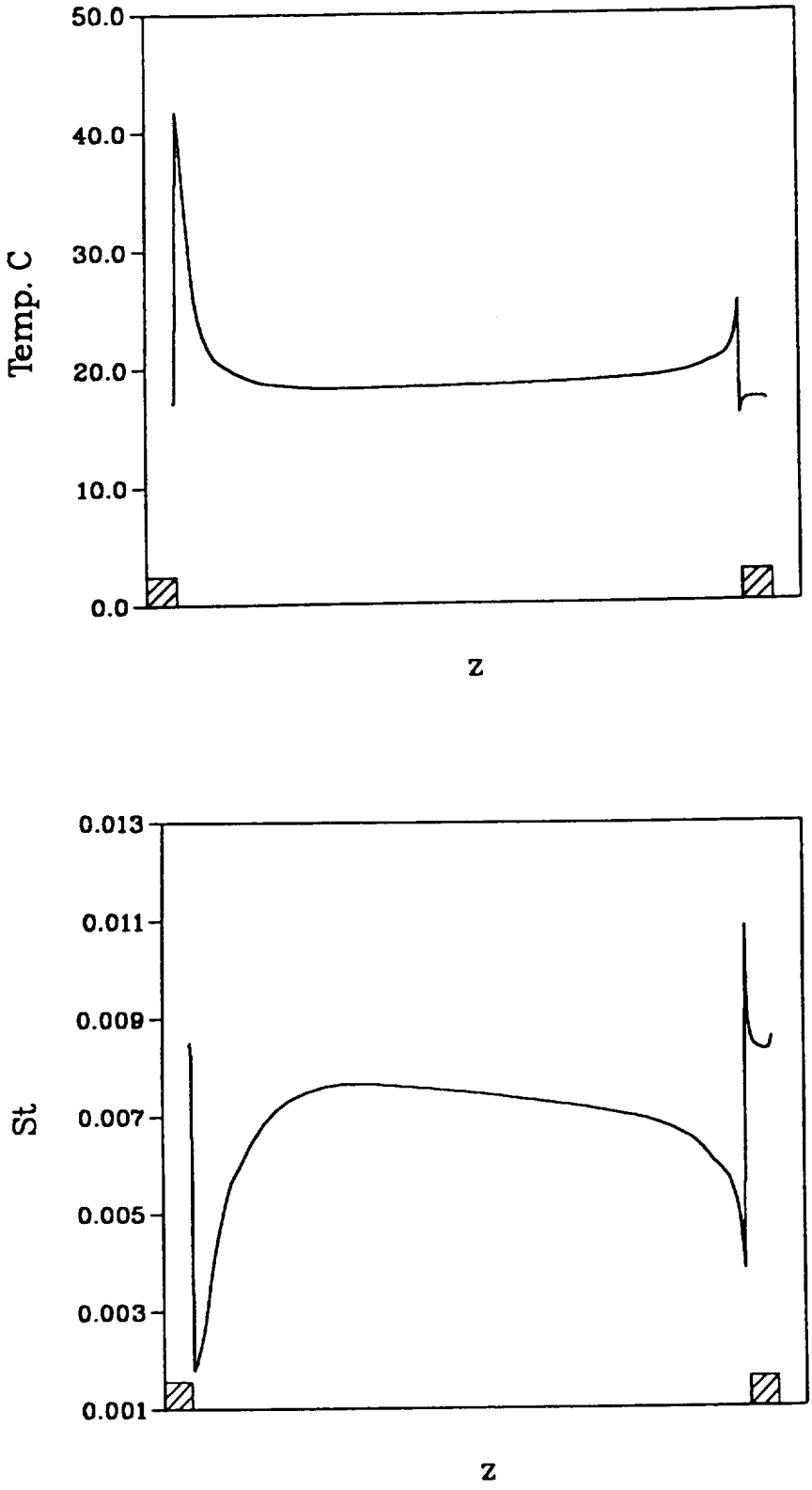

Figure 4.4.1 Prediction of wall temperature and Stanton number for e/D = 0.02, L/e = 20, Re = 37,900.

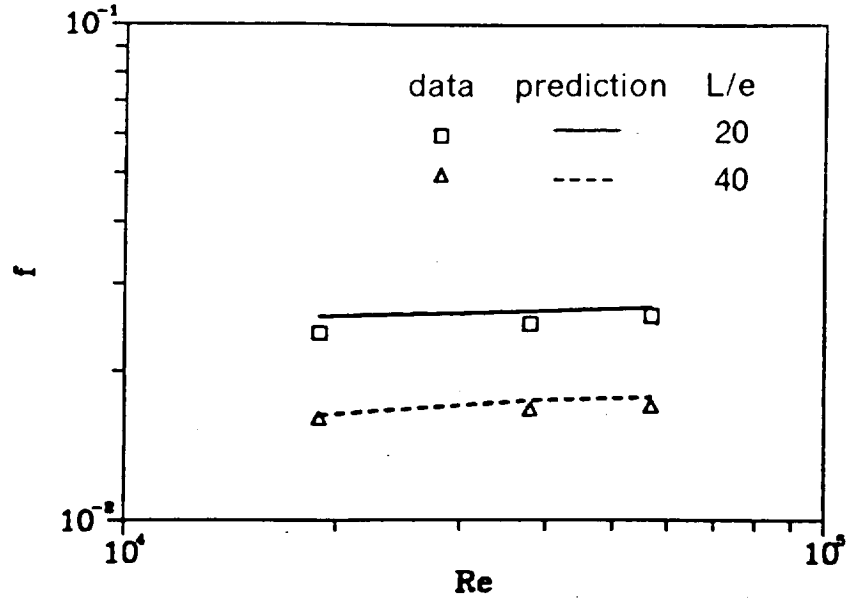

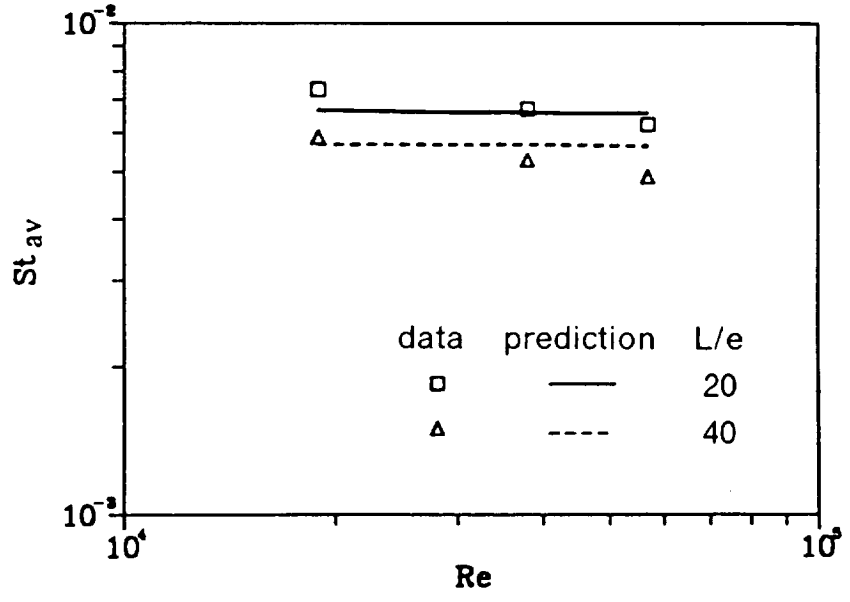

Figure 4.4.2 Prediction of friction factor and Stanton number for $e/D = 0.02$.

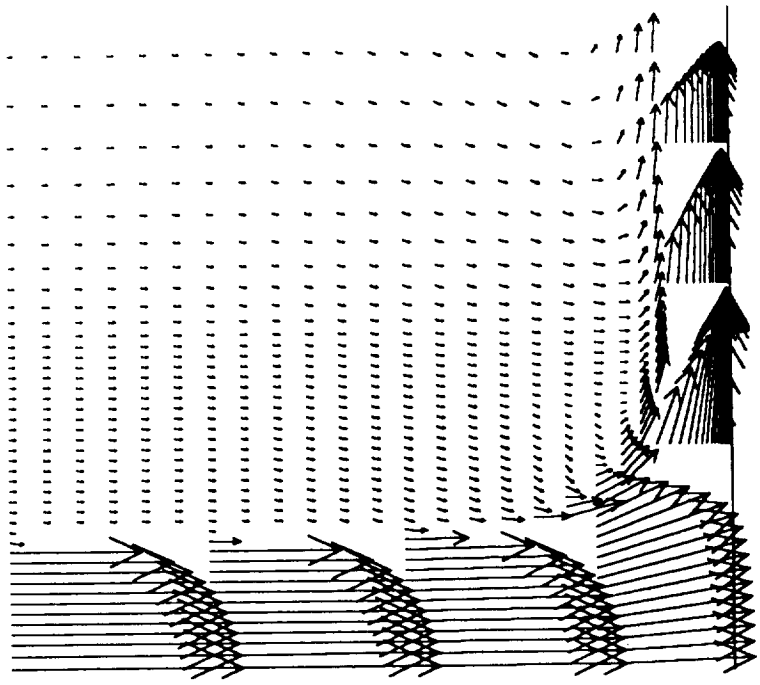

(a)

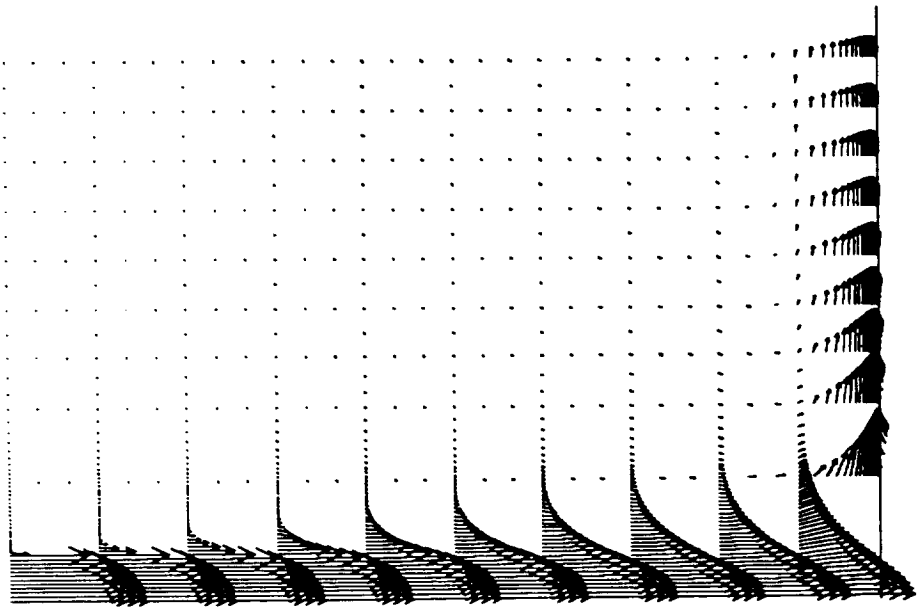

(b)

Figure 4.5.1 Vector plots for axisymmetric jet impingiment on a flat surface for $Re = 23{,}750$. (a) $H/d = 2$, (b) $H/d = 6$.

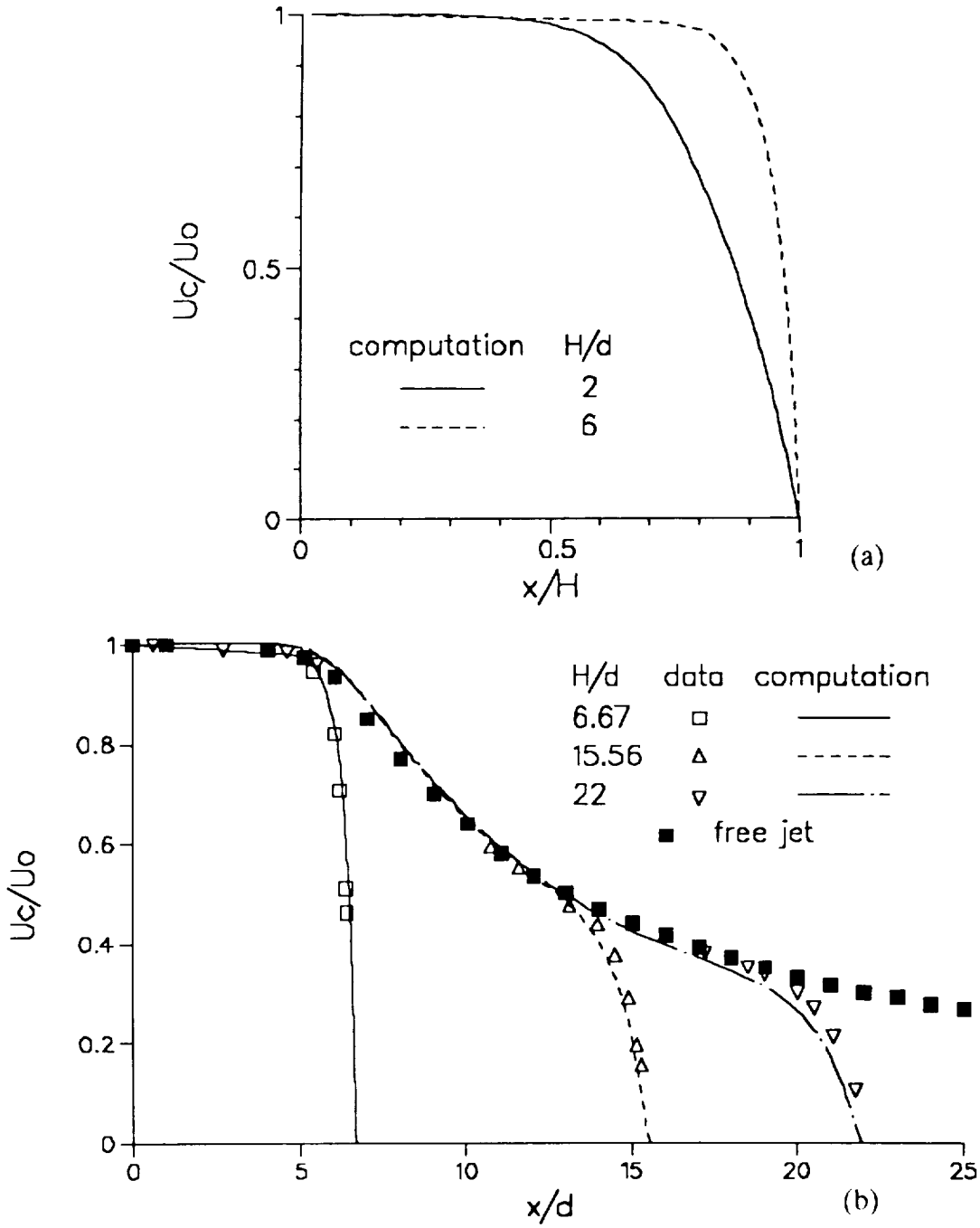

Figure 4.5.2 Comparison of the centerline velocity decay for (a) H/d = 2 and 6 at Re = 23,750. (b) H/D = 6.67 and Re = 23,750. H/D = 15.56 and Re = 40,000. H/D = 22 and Re = 80,400.

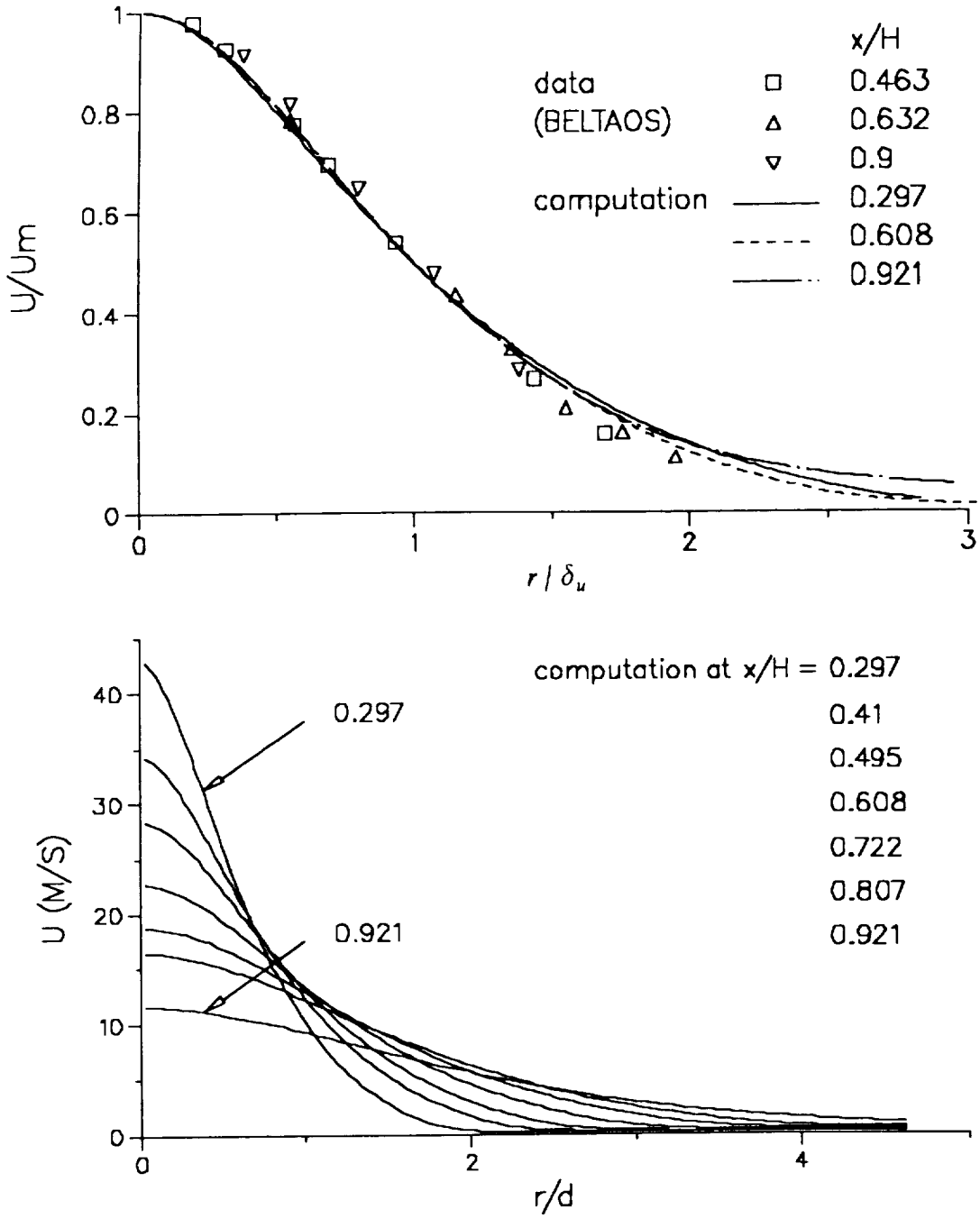

Figure 4.5.3 Round free jet profile for H/d = 21.2 and Re = 80,400.

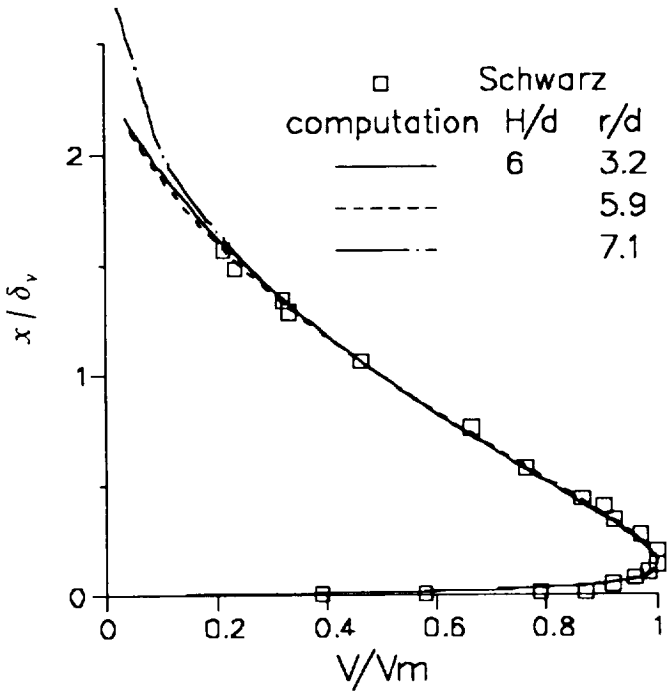

Figure 4.5.4 Radial wall jet profile for $H/d = 6$ and $Re = 23{,}750$.

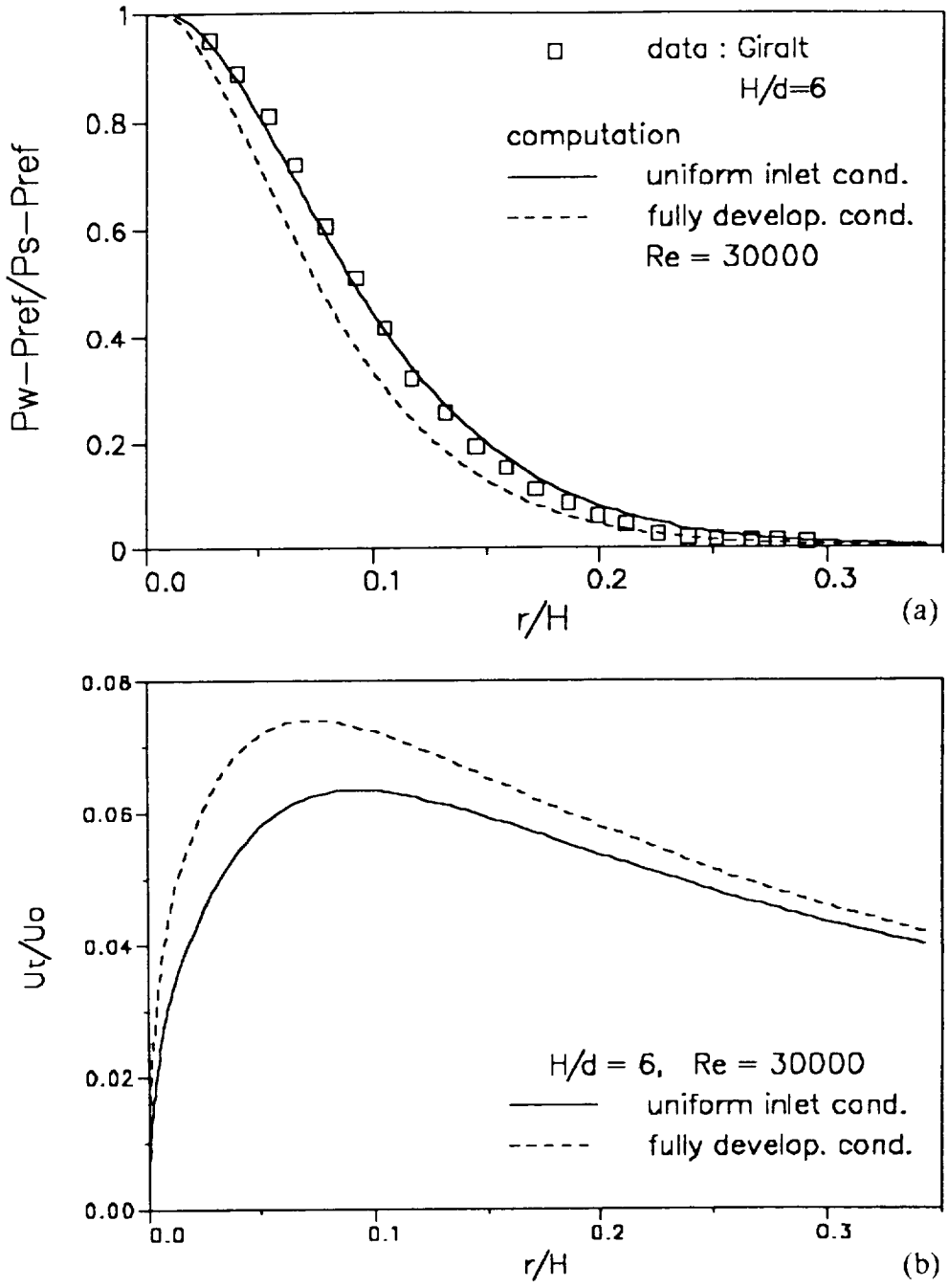

Figure 4.5.5 Comparison for $H/d = 6$ and $Re = 30{,}000$. (a) wall static pressure (b) wall shear stress

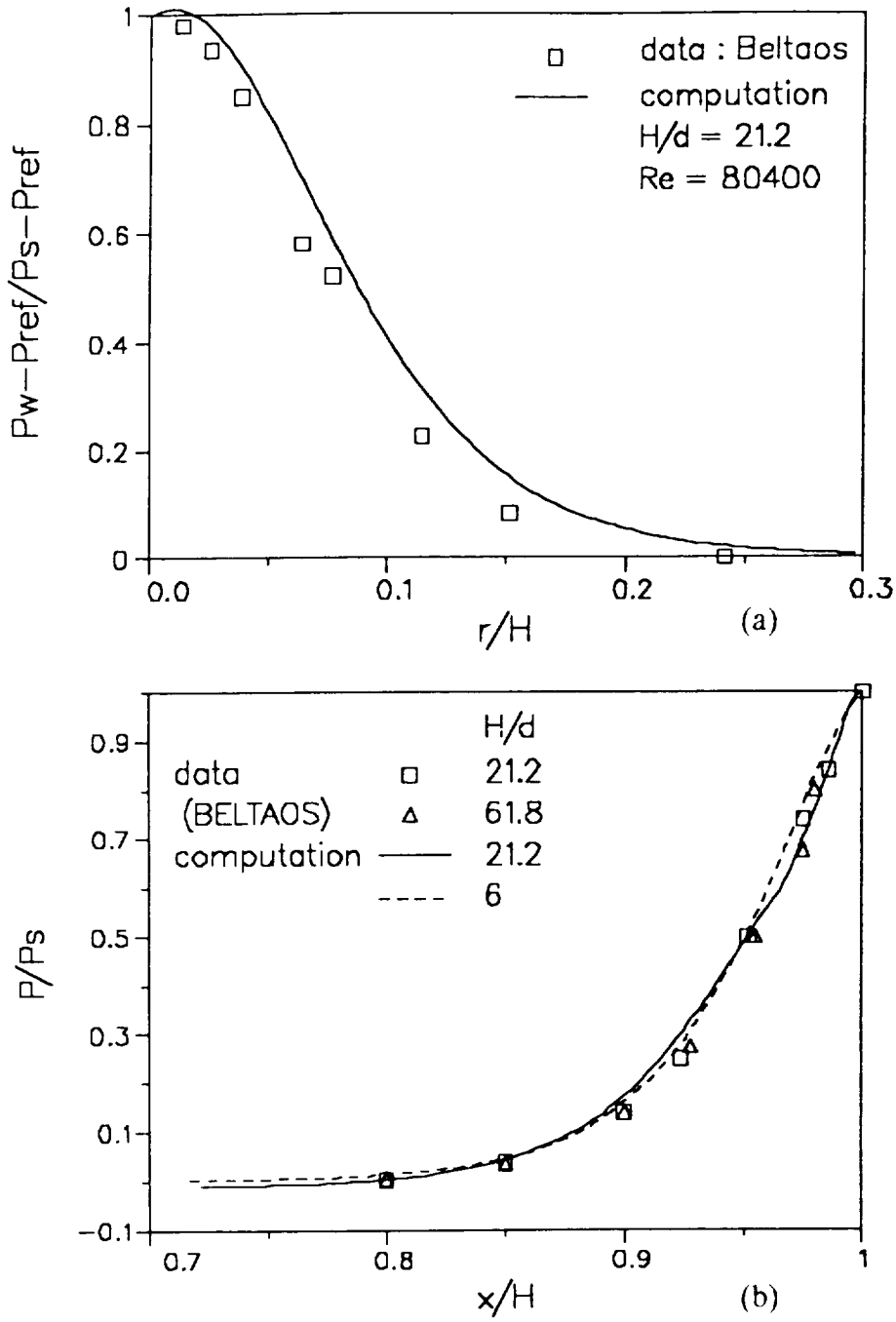

Figure 4.5.6 Comparison for H/d = 21.2 and Re = 80,400. (a) wall static pressure (b) centerline static pressure.

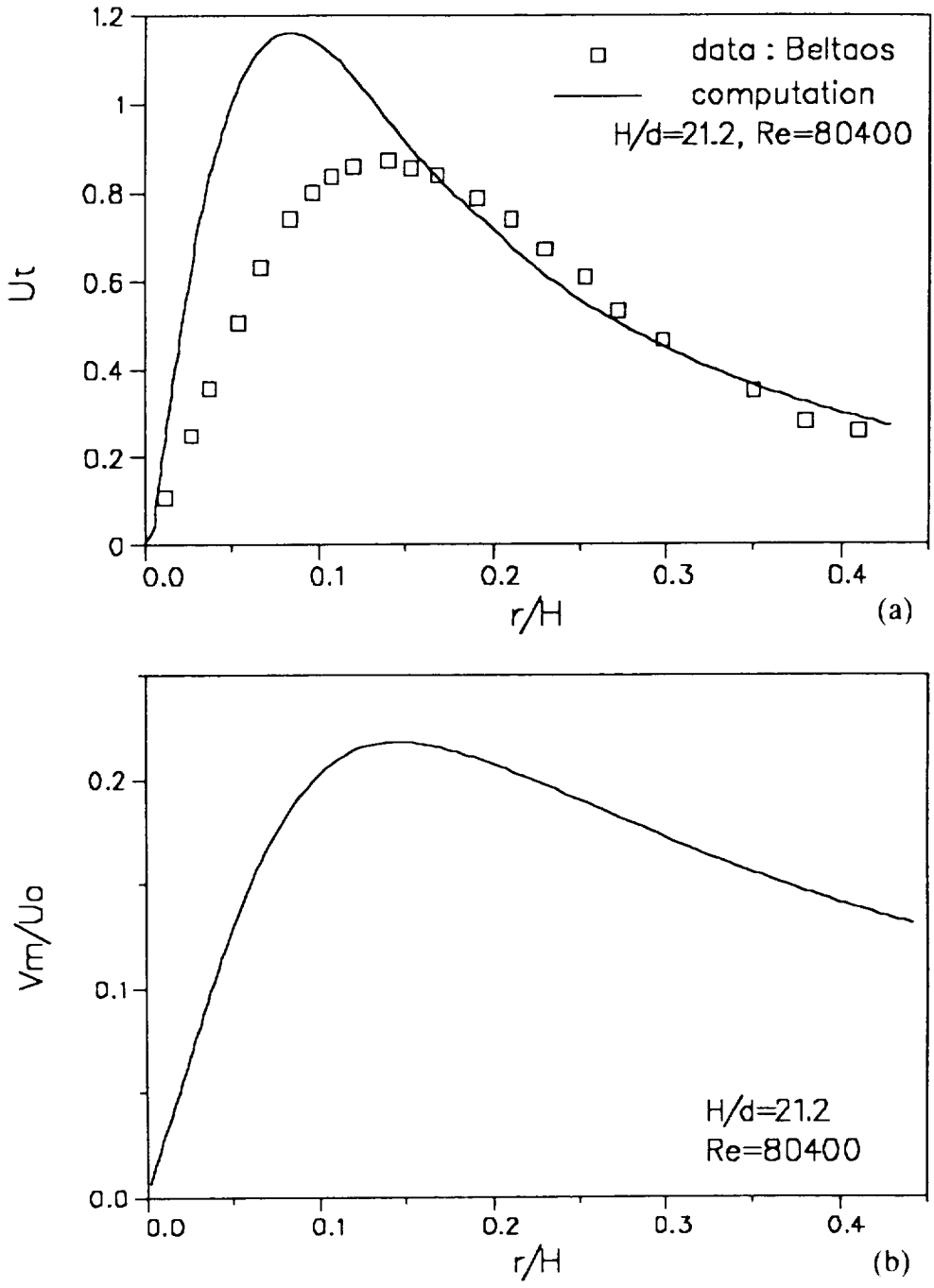

Figure 4.5.7 Predictions for H/d = 21.2 and Re = 80,400. (a) wall shear stress (b) maximum radial velocity.

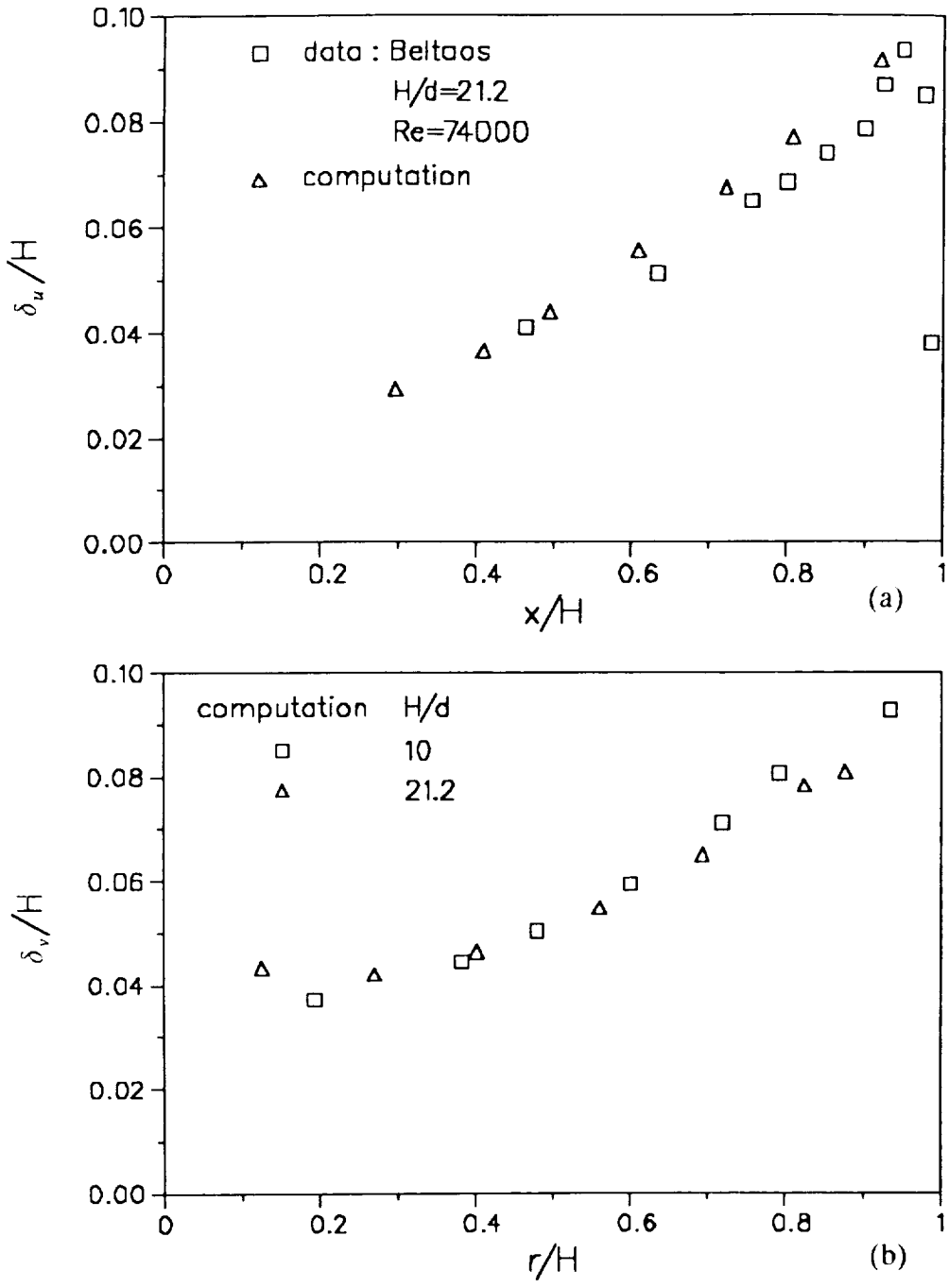

Figure 4.5.8 Predictions of spreading rates for H/d = 21.2 and Re = 74,000, H/d = 10 and Re = 23,750. (a) free jet (b) wall jet

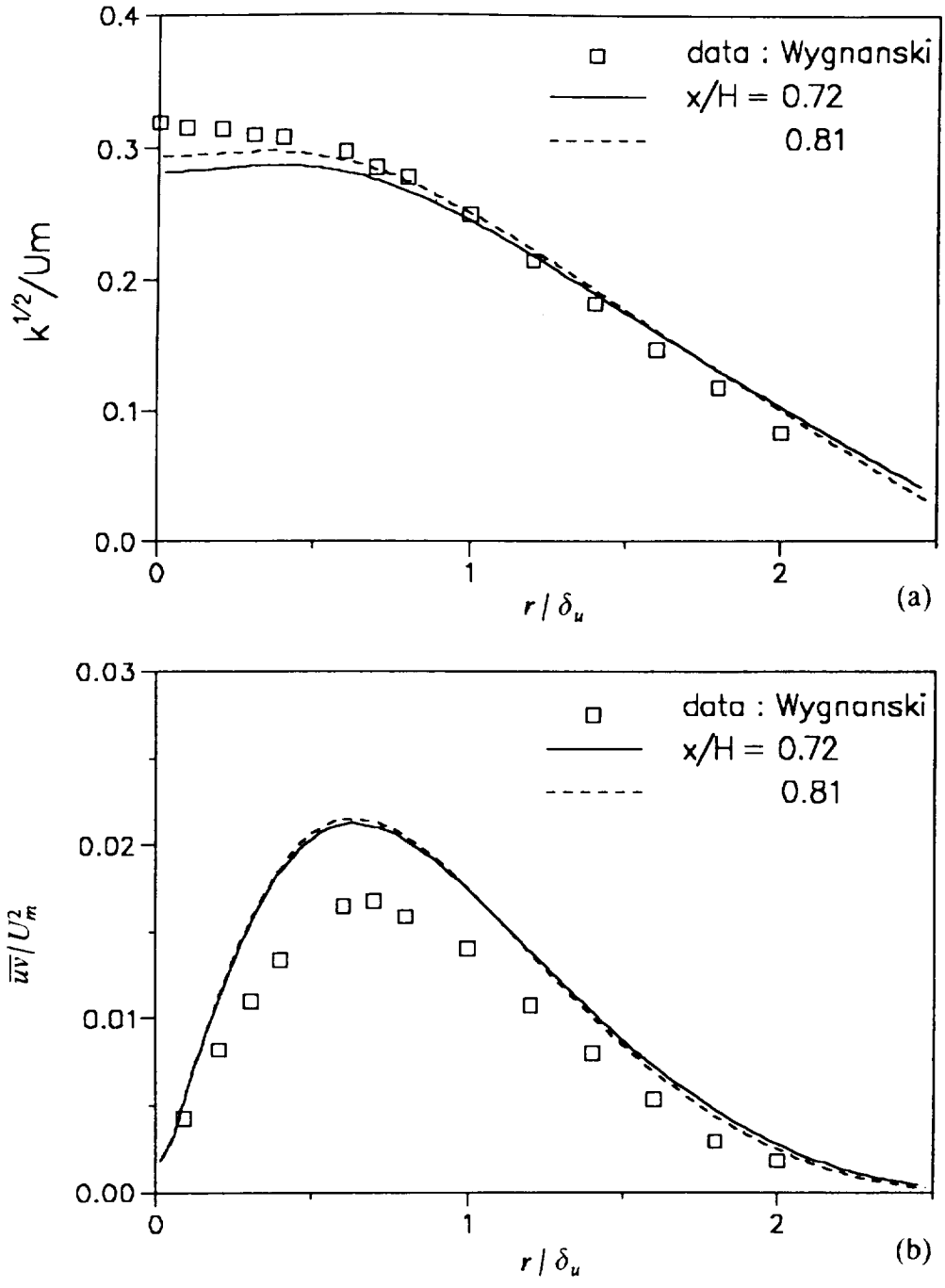

Figure 4.5.9 Prediction of (a) free-jet k profile, (b) free-jet $\overline{uv}$ profile for Re = 74,000.

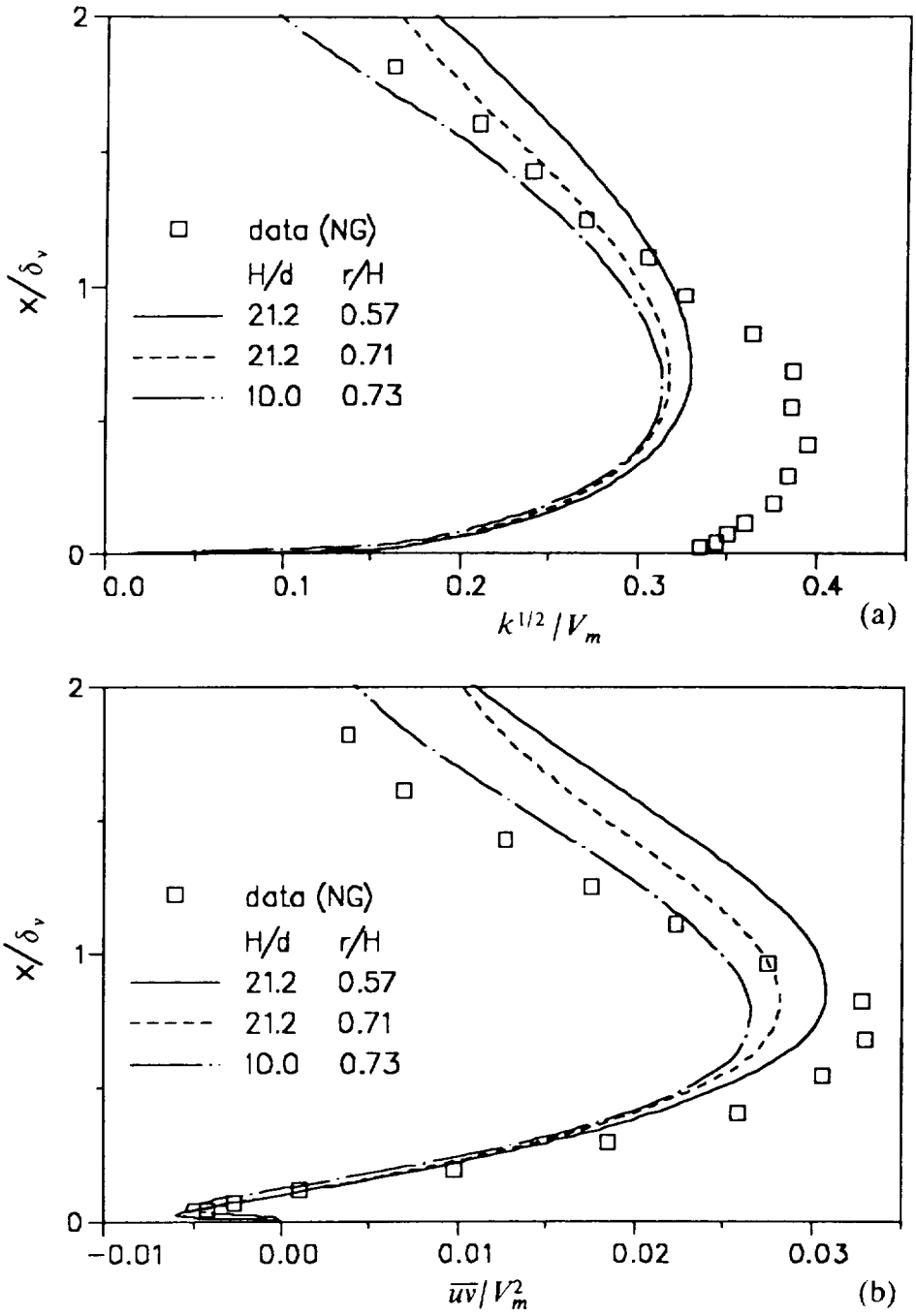

Figure 4.5.10 Prediction for H/d = 21.2 and Re = 74,000, H/d = 10, and Re = 23,750. (a) wall-jet k profile, (b) wall-jet $\overline{uv}$ profile

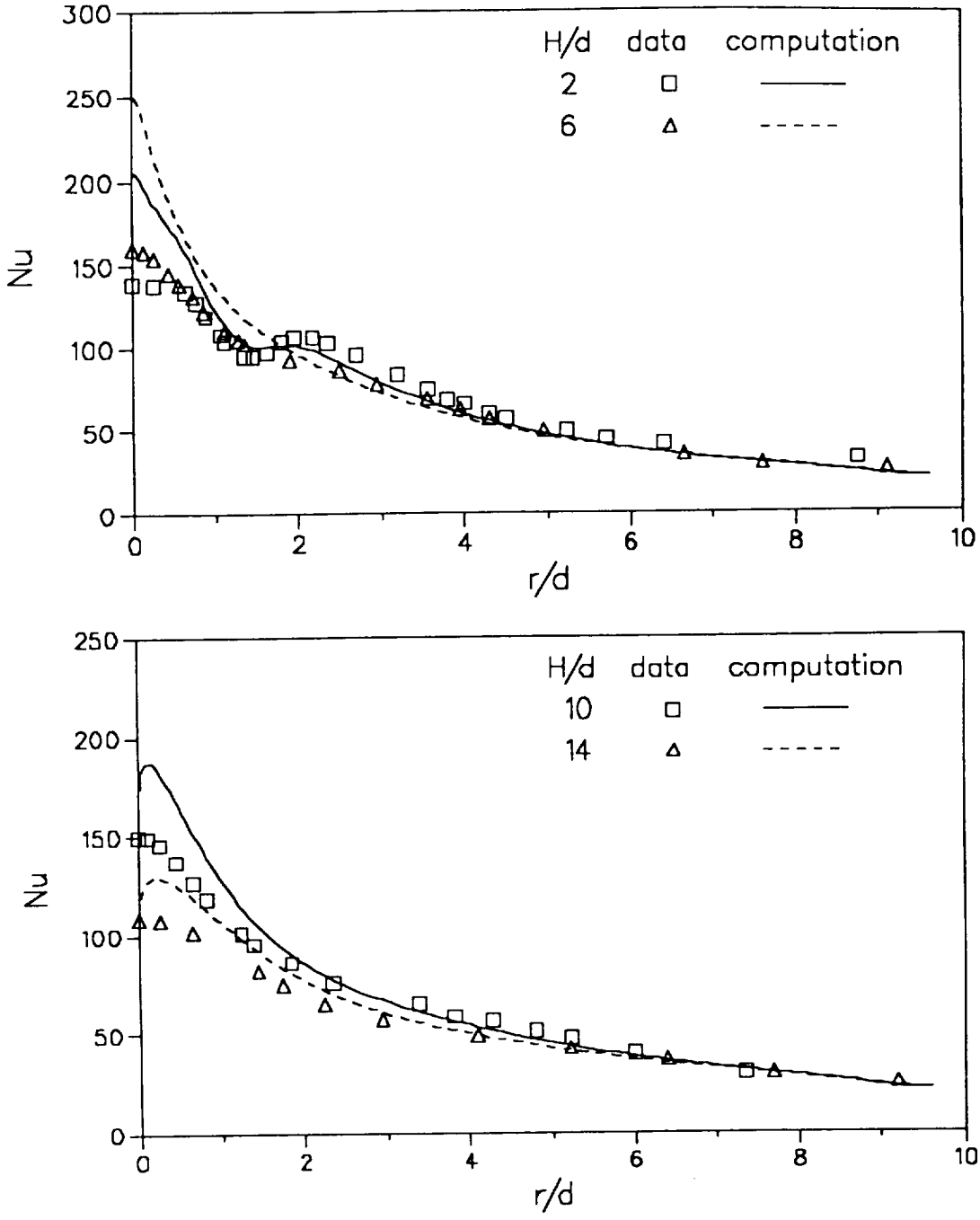

Figure 4.5.11 Comparison of Nusselt number profile for jet impingement cooling with experimental data of Baughn and Shimizu.

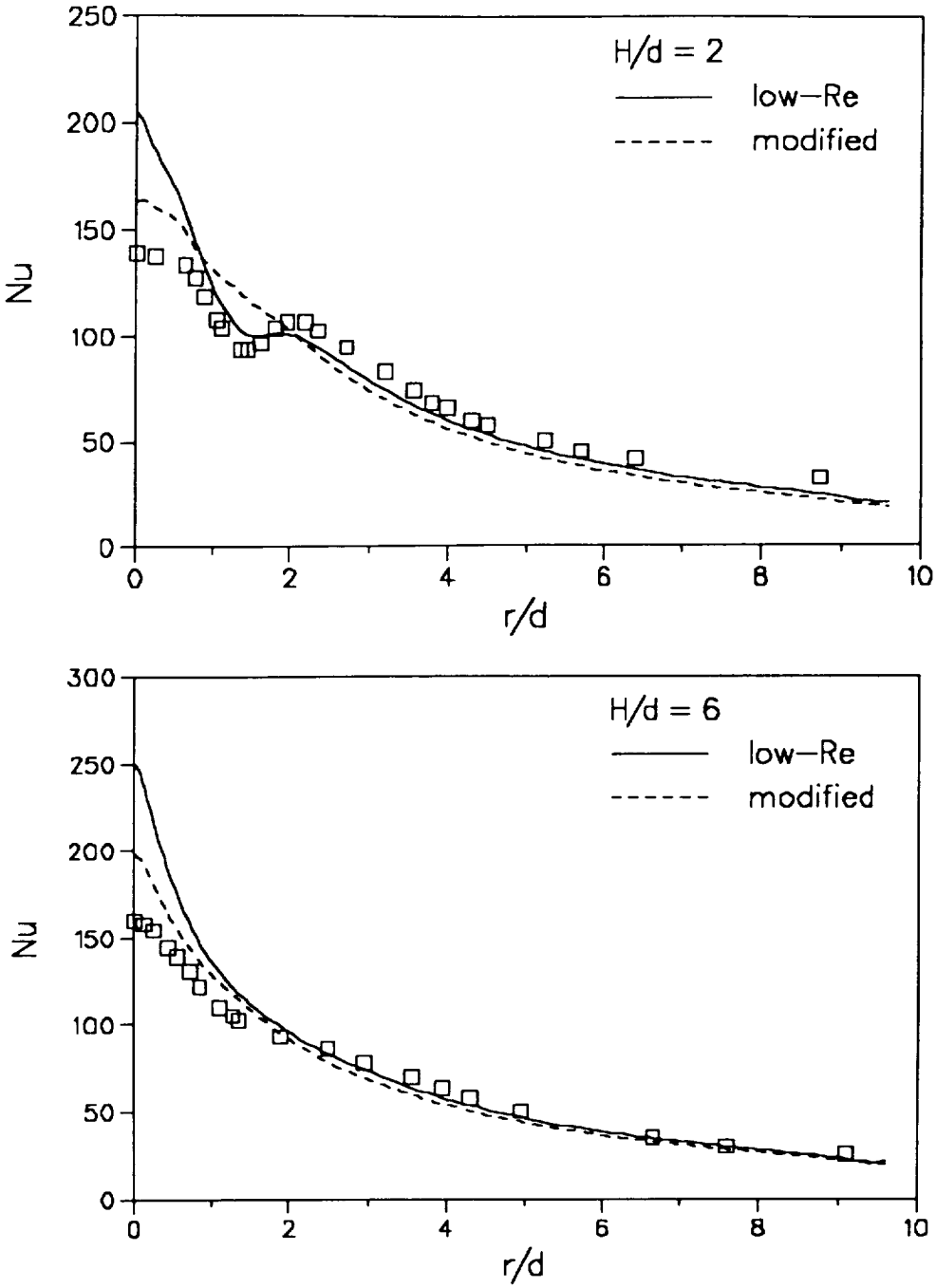

Figure 4.5.12 Comparison of Nusselt number profile with modified damping in ε equation.

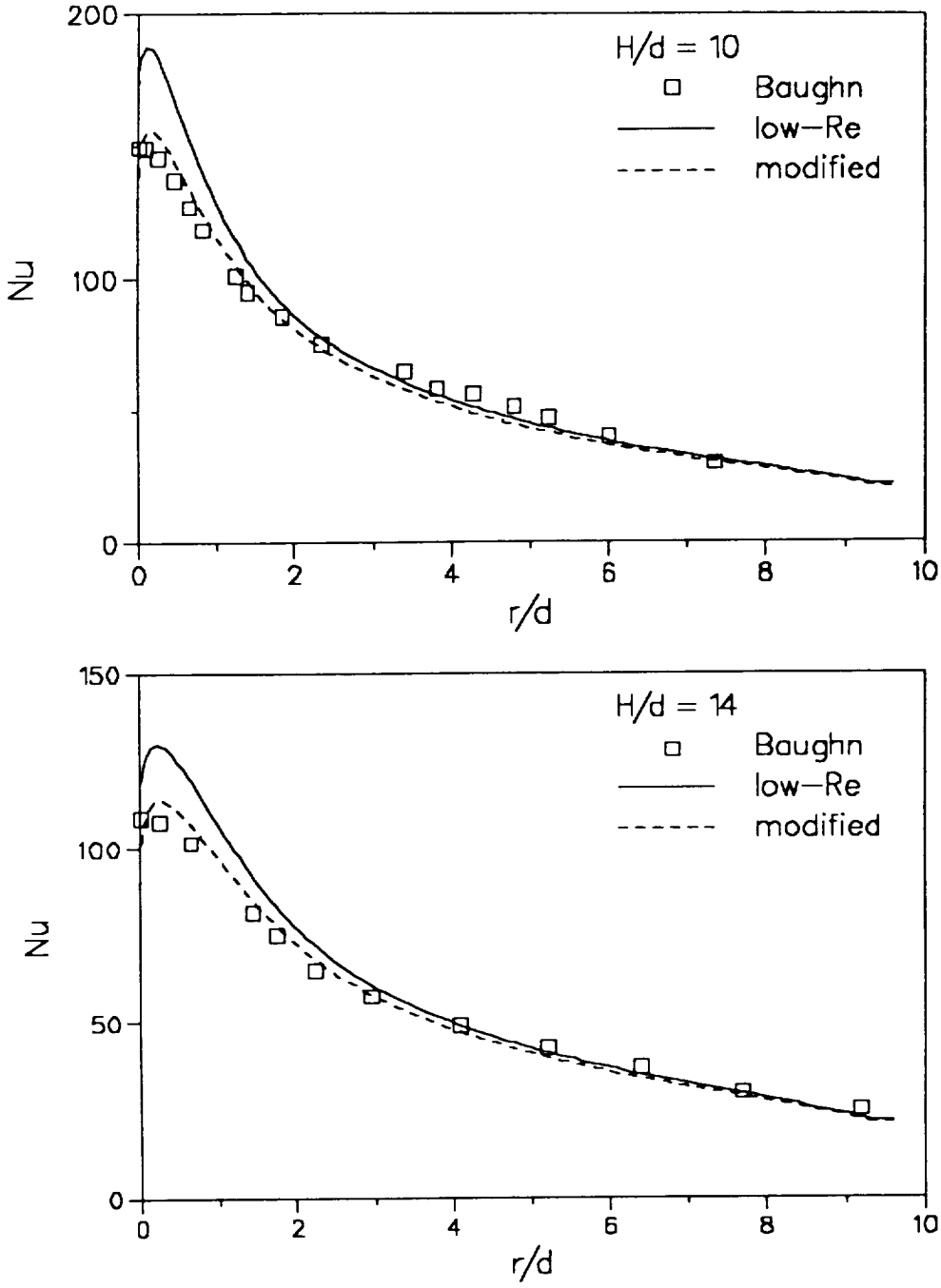

Figure 4.5.13 Comparison of Nusselt number profile with modified damping in ε equation.

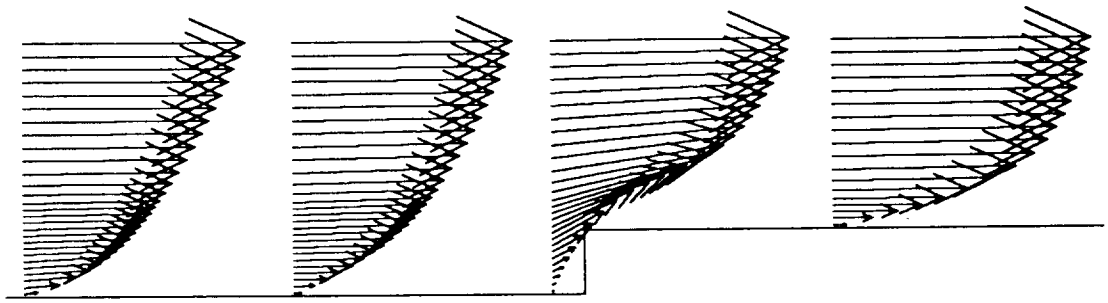

Figure 4.8.1 Velocity field for laminar flow over a forward-facing step. $Re = 550$.

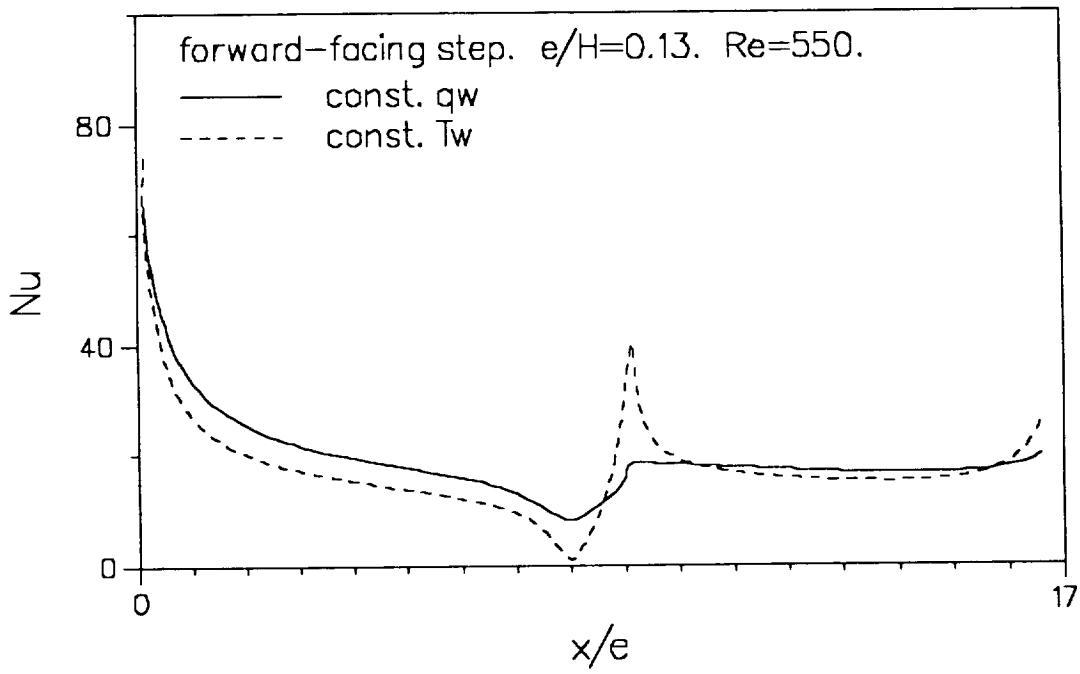

Figure 4.8.2 Nusselt number distribution for constant q_w and T_w boundary condition.

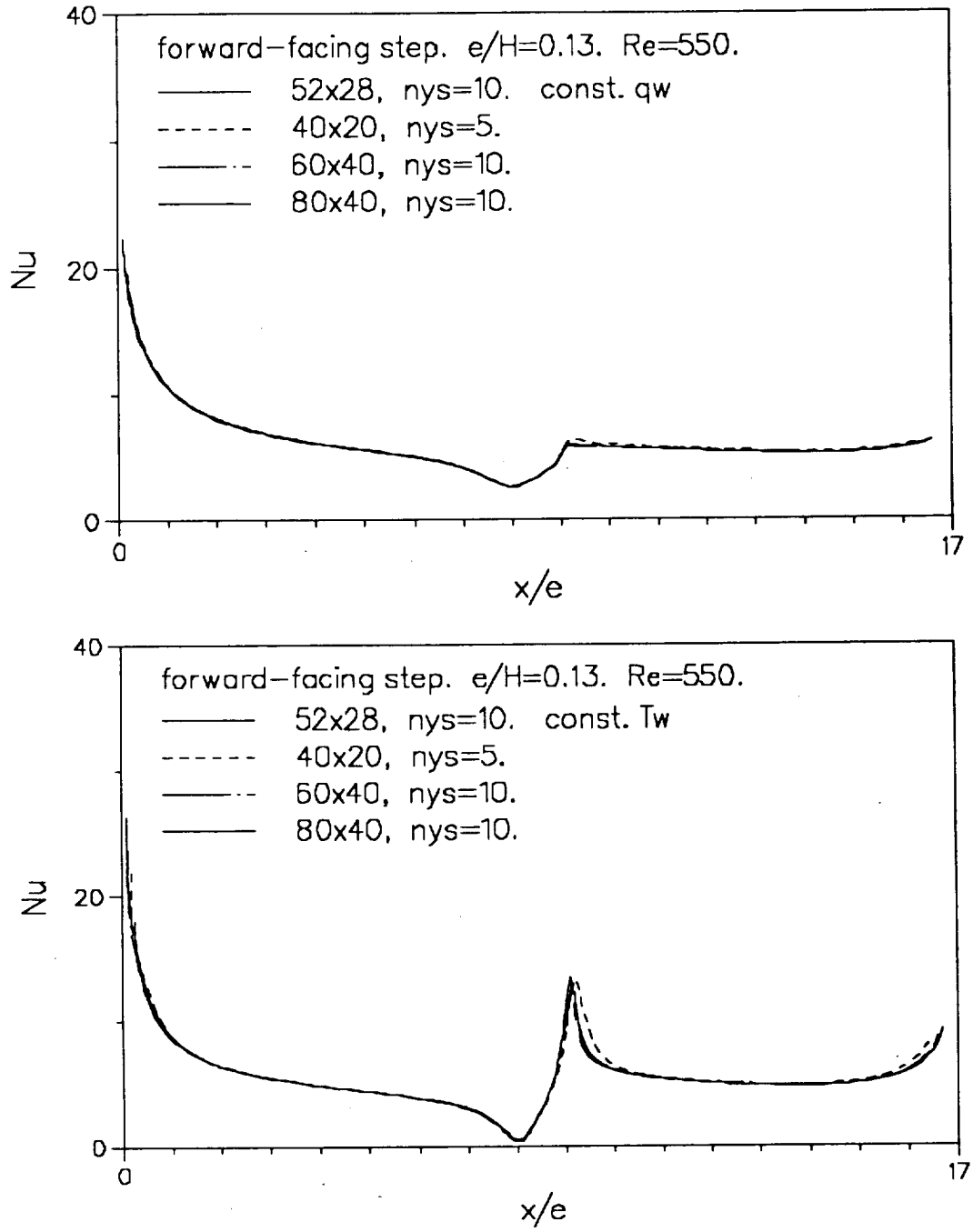

Figure 4.8.3 Grid independency test for laminar flow over a forward-facing step. $Re = 550$.

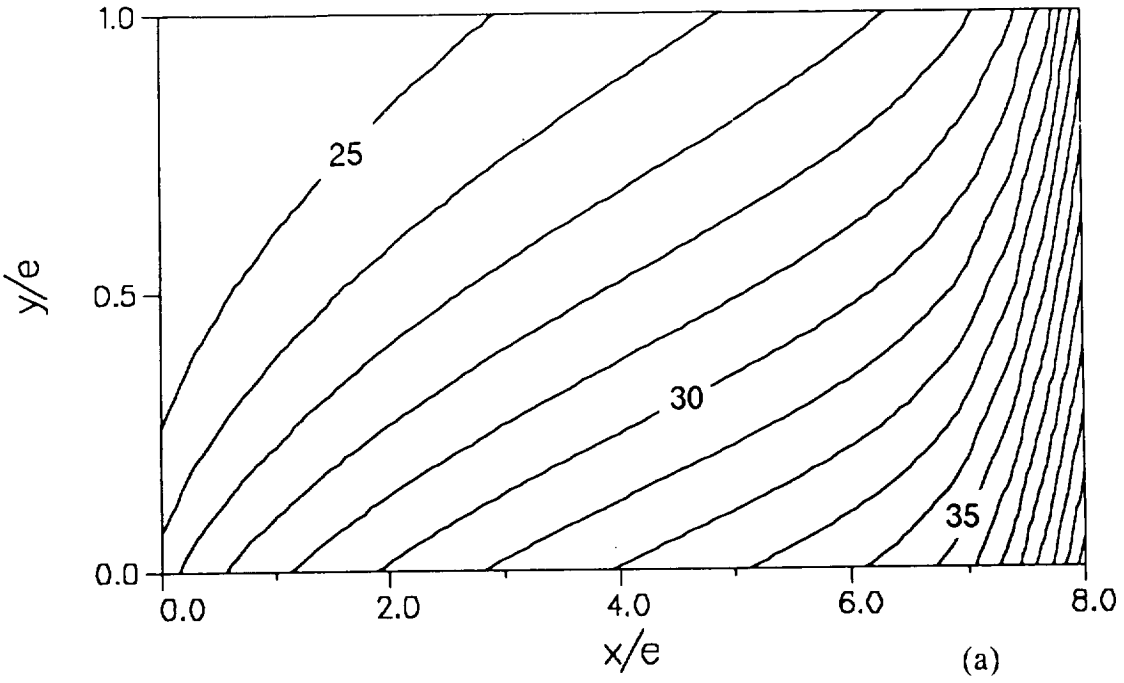

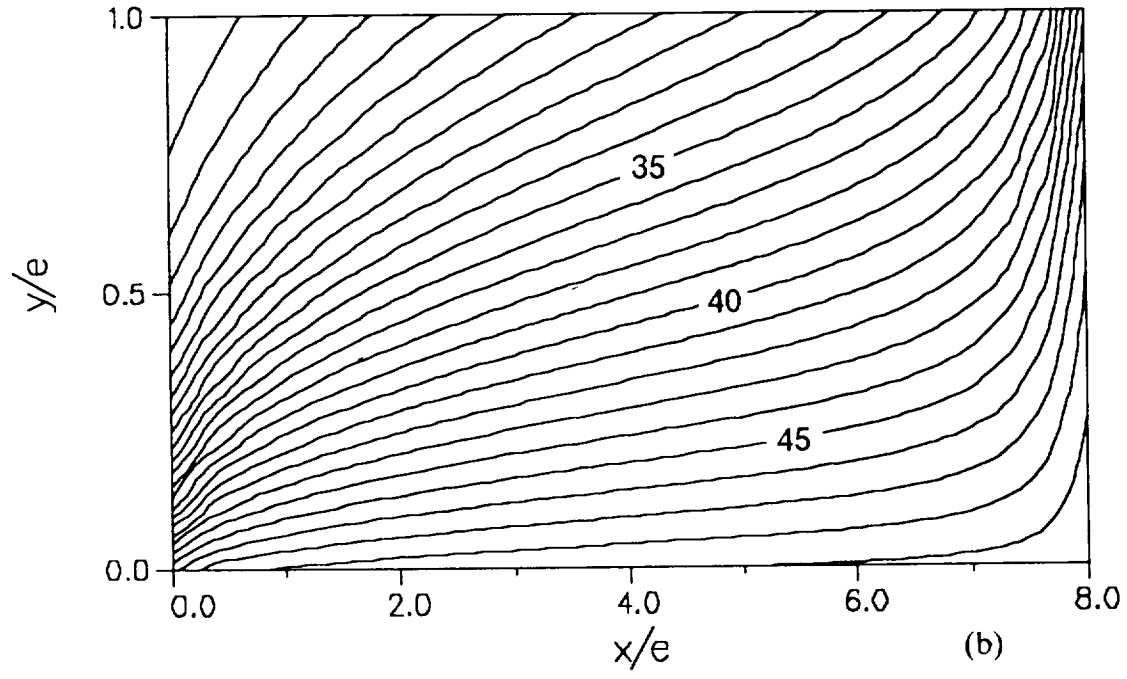

Figure 4.8.4 Isotherms for laminar flow over a forward-facing step. $Re = 550$. (a) const. q_w B.C. (b) const. T_w B.C.

REFERENCES

1. Eaton, J. K. and Johnston, J. P., "A review of research of subsonic turbulent flow reattachment", AIAA J. vol 19, no 9, pp 1093-1100, Sep. 1981

2. Launder, B.E.and Spalding, D.E., " The numerical computation of turbulent flows", Comp. Methods Appl. Mech. Eng., vol 3, pp 269-289, 1974

3. Chieng, C. C. and Launder, B. E., "On the calculation of turbulent heat transport fownstream from an abrupt pipe expansion", Numerical Heat Transfer, vol 3, pp 189-207, 1980

4. Johnson, R. W. and Launder, B. E., Discussion of " On the calculation of turbulent heat transport downstream from an abrupt pipe expansion", Numerical Heat Transfer, vol 5, pp 493-496, 1982

5. Zemanick, P. P. and Dougall, R. S., "Local heat transfer downstream of an abrupt circular channel expansion", J of Heat Transfer, vol 92 , pp 53-60, 1970

6. Amano, R. S., "Development of a turbulence near-wall model and its application to separated and reattached flows", Numerical Heat Transfer, vol 7, pp59-75, 1984

7. Amano, R. S., Jensen, M. K., and Goel, P., "Turbulent heat transport downstream from an abrupt pipe expansion", ASME paper H-17, March 1983

8. Launder, B. E., "Numerical computation of convective heat transfer in complex turbulent flows: time to abandon wall functions?", Int.J Heat Mass Transfer, vol 27, no 9, pp 1485-1491, 1984

9. Baughn, J. W., Hoffman, M. A., Takahashi, R. K., and Launder, B.E., " Local heat transfer downstream of abrupt expansion in a circular channel with constant wall heat flux", J of Heat Transfer, vol 106, pp 789-796, Nov. 1984

10. Launder, B.E., "On the computation of convective heat transfer in complex turbulent flows", J of Heat Transfer, vol.110, pp.1112-1128, Nov. 1988

11. Yap, C., "Turbulent heat and momentum transfer in recirculating and impinging flows", Ph.D. Thesis, Faculty of Technology, University of Manchester, United Kingdom, 1987

12. Kim, J., Kline, S.J., Johnston, J.P., "Investigation of a reattaching turbulent shear layer:flow over a backward-facing step", J. of Fluid Engineering, vol.102, pp.302-308, 1980

13. Durst, F. and Tropea, C., "Turbulent backward-facing step flows in two-dimensional ducts and channels", Proc. 3rd Symp. on Turbulent shear flows, U.C.Davis, pp.18.1-18.6, Sep. 9-11, 1982

14. Driver, D.M. and Seegmiller, H.L., "Features of a reattaching turbulent shear layer subject to an adverse pressure gradient", AIAA-82-1029, AIAA/ASME 3rd Joint Thermophysics, Fluids, Plasma and Heat-Transfer Conference, St. Louis, June 7-11, 1982

15. Seban, R.A., "Heat transfer to the turbulent separated flows of air downstream of a step in the surface of a plate", J. of Heat Transfer, pp.259-264, May 1964

16. Filetti, E.G. and Kays, W.M., "Heat transfer in separated, reattached, and redevelopment regions behind a double step at entrance to a flat duct", J. of Heat Transfer, p.163, May 1967

17. Seki, N., Fudusako, S., and Hirata, T., "Turbulent fluctuations and heat transfer for separated flow associated with a double step at entrance to an enlarged flat duct", J. of Heat Transfer, p.588, Nov. 1976

18. Seki, N., Fudusako, S., and Hirata, T., "Effect of stall length on heat transfer in reattached region behind a double step at entrance to an enlarged flat duct", Int. J. of Heat and Mass Transfer, vol.19, pp.700-702, 1976

19. Vogel, J.C. and Eaton, J.K., "Combined heat transfer and fluid dynamics measurements downstream of a backward-facing step", Journal of Heat Transfer, v107, pp 922-929, 1985

20. Sindir, M., "Effects of expansion ratio on the calculation of parallel -walled backward-facing step flows: comparison of four models of turbulence", paper 83-FE-10, ASME Winter Annual Meeting, Boston. 1983

21. Gooray, A.M., Watkins, C.B., and Aung, W., "Turbulent heat transfer computations for rearward-facing steps and sudden pipe expansions", J. of Heat Transfer, vol.107, pp.70-76, 1985

22. Scherer, V. and Wittig, S., "The influence of the recirculation region: a comparasion of the convective heat transfer downstream of a backward-facing step and behind a jet in a cross flows", ASME paper 89-GT-59, Gas Turbine and Aeroengine Congress and Exposition, June 4-8, 1989, Toronto, Ontario, Canada, 1989

23. Ciofalo, M. and Collins, M.W., "$k-\varepsilon$ predictions of heat transfer in turbulent recirculating flows using an improved wall treatment", Num Heat Transfer, Part B, vol 15, pp21-47, 1989

24. Nikuradse, J., NACA TM 1292 (1950) (also VDI-Forschungsheft 361, 1933)

25. Dipprey, D. F. and Sabersky, R. H., "Heat and momentum transfer in smooth and rough tubes at various Prandtl numbers", Int J of Heat Mass Transfer, vol 6, pp 329-353, 1963

26. Webb, R. L., Eckert, E. R. G. and Goldstein, R. J., "Heat transfer and friction in tubes with repeated-rib roughness", Int J of Heat Mass Transfer, vol 14, pp 601-617, 1971

27. Han, J. C., Glicksman, L. R., and Rohsenow, W. M., "An investigation of heat transfer and friction for rib-roughened surfaces", Int J of Heat Mass Transfer, vol 21, pp 1143-1156, 1978

28. Dalle Donne, M. and Meyer, L., "Turbulent convective heat transfer from rough surfaces with two-dimensional rectangular ribs", Int J of Heat Mass Transfer, vol 20, pp 583-620, 1977

29. Lewis, M. J., "An elementary analysis for predicting the momentum and heat transfer characteristics of a hydraulically rough surface", J of Heat Transfer, vol 97, pp 249-254, May 1975

30. Lee, B. K., Cho, N. H., and Choi, Y. D., "Analysis of periodically fully developed turbulent flow and heat transfer by k- ε equation model in artificially roughened annulus", Int J of Heat Mass Transfer, vol 31, no 9, pp 1797-1806, 1988

31. Patankar, S. V., Liu, C. H., and Sparrow, E. M., "Fully developed flow and heat transfer in ducts having streamwise-preiodic variations of cross-sectional area", J of Heat Transfer, vol 99, pp 180-186, May 1977

32. Leschziner, M.A. and Rodi, W., "Calculation of annular and twin parallel jet using various discretization schemes and turbulence- model variations", J of Fluid Engineering, vol 103, pp352-360, June 1981

33. Petukhov, B.S. "Heat transfer and friction in turbulent pipe flow with variable physical properties", Advances in Heat Transfer, vol 6, pp504-564, 1970

34. Sleicher, C.A. and Rouse M.A., "A convenient correlation for heat transfer to constant and variable property fluids in turbulent pipe flow", Int. J of Heat Mass Transfer, vol 18, pp677-683, 1975

35. McEligot, D.B., Magee, P.M., and Leppert, G., "Effect of large temperature gradient on convective heat transfer: The downstream region", J of Heat Transfer, vol 1, pp67-76, 1965

36. Lelchuk, V.L. and Dyadyakin, B.V., "Heat transfer from a wall to a turbulent current of air inside a tube and the hydraulic resistance at large temperature differentials", Problems of Heat Transfer, AEC-tr-4511, p114, 1962

37. Perkins, H.C. and Worsoe-Schmidt, P., "Turbulent heat and momentum transfer for gases in circular tube at wall to bulk temperature ratios to seven", Int J. of Heat Mass Transfer, vol 8, pp 1011-1031, 1965

38. Vilemas J.V. and Simonis, V.M., "Heat Transfer and friction of rough ducts carrying gas flow with variable physical properties" Int. J of Heat Mass Transfer, vol 28, pp59-68, 1985

39. Wassel, A.T. and Mills, A.F., "Calculation of variable property turbulent friction and heat transfer in rough pipes", J of Heat Transfer, vol 101, pp469-474, 1979

40. Poreh, M., Tsuei, Y.G., Cermak, J.E., "Investigation of a turbulent radial wall jet", ASME Journal of Applied Mechanics, vol.34, pp457-463

41. Beltaos, S. and Rajaratnam, M., "Plane turbulent impinging jets", Journal of Hydraulic Research, no.1, pp29-39, 1973

42. Beltaos, S. and Rajaratnam, M. Journal of Hydraulics Division, pp1313-1328, Oct. 1974

43. Giralt, F., Chia, C., and Trass, O., "Characterization of the impingement region in an axisymmetric turbulent jet", Ind. Eng. Chem. Fundam., v16, no.1, pp 21-28, 1977

44. Wygnanski and Fiedler, "Some measurements in the self preserving jet", Journal of Fluid Mechaincs, vol.38, pp577-612, 1969

45. Gardon, R. and Akfirat, J.C., " The role of turbulence in determining the heat-transfer characteristics of impinging jets", Int. J. of Heat and Mass Transfer, vol.8, pp1261-1272, 1965

46. Goldstein, R.J. and Behbahani A.I., "Impingement of a circular jet with and without cross flow", Int J. of Heat and Mass Transfer, vol 25, pp1377-1382, 1982

47. Hrycak, P., "Heat transfer from round impinging jets to a flat plate", Int. J. of Heat Mass Transfer, vol.26, no.12, pp1857-1865, 1983.

48. Baughn, J.W. and Shimizu, S., "Heat transfer measurements from a surface with uniform heat flux and an impinging jet", J. of Heat Transfer, vol 111, pp1096-1098, Nov. 1989

49. Wolfshtein, M., "Some solutions of the plane turbulent impinging jet", J of Basic Engineering, pp 915-922, Dec. 1970

50. Amano, R.S. and Brandt, H., "Numerical study of turbulent axisymmetric jets impinging on a flat plate and flowing into an axisymmetric cavity", J. of Fluid Engineering, vol 106, pp 410-417, 1984

51. Chuang, S.H., "Numerical simulation of an impinging jet on a flat plate", Int. J. for Numerical Methods in Fluids, vol.9, pp1413-1426, 1989.

52. Hwang, C.J. and Liu, J.L., "Numerical study of two-dimensional impinging jet flow fields", AIAA Journal, vol.27. no.7, pp841-842, 1989.

53. Agarwal, R.K. and Bower, W.W., "Navier Stokes computations of turbulent compressible two-dimensional impinging jet flow fields", AIAA Journal, vol.20, no.5, pp577-584, 1982.

54. Malin, "Modelling the effects of lateral divergence on radially spreading turbulent jets", Computers and Fluids, vol.17, no.3, pp453-465, 1989

55. Spalding, D.B., "The prediction of two-dimensional steady, turbulent elliptic flows", Int. Sem. on Heat and Mass Transfer in Flows with Separated Regions", Herceg Novi, Yugoslavia, 1969

56. Hwang, J.C. and Tsou, F.K., "Numerical solutions for flow and heat transfer of a plane turbulent oblique impinging jet" in Numerical properties and methodologies in heat transfer, edited by T.M.Shih, Hemisphere Publishing Co., 1981

57. Rodi, W. and Scheuerer, G., "Calculation of heat transfer to convection-cooled gas turbine blades", J of Engng for Gas Turbines and power, vol 107, pp 620-627, July 1985

58. Lam, C. K. G., Bremhorst, K. A., "Modified form of the $k-\varepsilon$ model for predicting wall turbulence", J of Fluids Eng., vol 103, pp 456-460, 1981

59. Looney, M.K. and Walsh, J.J., "Mean-flow and turbulent characteristics of free and impinging jet flows", Journal of Fluid Mechanics, vol.147, pp397-429, 1984.

60. Amano, R.S. and Sugiyama, S., "An investigation of turbulent heat transfer of an axisymmetric jet impinging on a flat plate", Bulletin of JSME, vol.28, no.235, pp74-79, 1985.

61. Polat, S., Mujumdar, A.S., van Heiningen, A.R.P., and Douglas, W.J.M., "Effect of near-wall modelling on prediction of impingement heat transfer", Drying Technology, 8(4), pp705-730, 1990.

62. Polat, S., Mujumdar, A.S., van Heiningen, A.R.P., and Douglas, W.J.M., "Numerical model for turbulent jet impinging on a surface with through-flow", Journal of Thermophysics, vol.5, no.2, pp172-180, 1991.

63. Hrycak, P, "Heat transfer from a row of impinging jets to concave cylindrical surfaces", Int. J of Heat Mass Transfer, vol 24, pp 407-419, 1980

64. Metzger, D. E., Yamashita, T, and Jenkins, C. W., "Impingement cooling of concave surfaces with lines of circular air jets", J of Engng Power, vol 91, pp 149-158, 1969

65. Chupp, R. E., Helms, H. E., McFadden, P. W., and Brown, T. R., " Evaluation of internal heat transfer coefficients for impingement-cooled turbined airfoils", J Aircraft, vol 6, pp 203-208, 1969

66. Jusionis, V. J., "Heaat transfer from impinging gas jets on an enclosed concave sruface", J Aircraft, vol 7, pp 87-88, 1970

67. Livingood, J. N. B., and Gauntner, J. W., "Average heat-transfer characteristics of a row of circular air jets impinging on a concave surface", NASA TM X-2657, 1972

68. Livingood, J. N. B., and Gauntner, J. W., "Local heat-transfer characteristics of a row of circular air jets impinging on a concave semicylindrical surface", NASA TN D-7127, 1973

69. Livingood, J. N. B., and Gauntner, J. W., "Heat transfer characteristics of a single circular jet impinging on a concave hemispherical shell", NASA TM X-2895, 1973

70. Schlichting, H., Boundary-layer theory, 7th ed. McGraw-Hill, NY, 1979

71. Hinze, J. O., Turbulence, 2nd ed. McGraw-Hill

72. Jones, W. P. and Launder, B. E., "The calculation of low-Reynolds number phenomena with a two-equation model of turbulence", Int. J of Heat Mass Transfer, vol 16, pp 1119-1130, 1972

73. Hanjalic, K., "Two dimensional asymetrical turbulent flow in ducts" Ph.D. thesis, University of London, 1970

74. Launder, B. E. and Sharma B. I., "Application of the energy-dissipation model of turbulence to the calculation of flow near a spinning disc", Lettters in Heat Mass Transfer, vol 1, pp 131-138, 1974

75. Jayatilleke, C. L. V., "The influence of Prandtl number and surface roughness on the resistance of the laminar sublayer to momentum and heat transfer", Progress in heat and mass transfer. vol 1, Pergamon Press

76. Launder, B. E., and Spalding, D. B., "Lectures in mathematical models of turbulence", Academic Press, 1972

77. Viegas, J.R., and Rubesin, M.W., "Wall-function boundary conditions in the solution of the Navier-Stokes equations for complex compressible flows", AIAA 16th Fluid and Plasma Dynamics Conf. 1983, Denvers, Mass. , AIAA paper 83-1694

78. Chien, K.Y., "Predictions of channel and boundary-layer flows with a low-Reynolds number turbulence model", AIAA J, vol 20, pp33-38, 1982

79. Wilcox, D.C. and Rubesin, M.W., "Progress in turbulence modeling for complex flow fields including effects of compressibility", NASA TP-1517, 1980

80. Viegas, J.R., Rubesin, M.W., and Horstmann, C.C., " On the use of wall functions for two-dimensional separated flows", AIAA Paper 85-0180, June 1985.

81. Rodi, W., "A new algrbraic relation for calculating the Reynolds stresses", ZAMM, vol.56, pp.219-221, 1976

82. Daly, B.J. and Harlow, F.H., "Transport equations in turbulence", Physics of Fluids, vol.13, pp2634-2649, 1970

83. Rotta, J.C., "Statistical theory of non-homogenuous turbulence", F. Physik, Ed.192, pp547-572, 1957

84. Launder, B.E., Reece, G.C., and Rodi, W., " Progress in the development of a Reynodls-stress turbulence closure", J. of Fluid Mechanics, vol.68, pp537-566, 1975

85. Shir, C.C., "A preliminary numerical study of atmospheric turbulent flows in the idealized planetary boundary layer", J. Atoms. Science,' vol.30, p1327, 1973

86. Gibson, M.M. and Launder, B.E., "Gound effects of pressure fluctuations in the atmospheric boundary layer", J. of Fluid Mechanics, vol.86, pp491-511, 1978

87. Launder, B.E., "A generalized algebraic stress transport hypothesis" , AIAA Journal, vol.20, no.3, pp436-437, 1982

88. Rosten, H. I. and Spalding, D. B., The PHOENICS biginner's guides, CHAM report no. TR 100, CHAM Limited, Bakery House, 40 High Street, Wimbledon SW19 5AU England

89. Spalding, D.B., "A novel finite difference formulation for differential expressions involving both first and second derivatives" , Int. J. Numerical Methods Eng., vol.4, p551, 1972

90. de Vahl Davis, G. and Mallinson, G.D., "False duffusion in numerical fluid mechanics, U. of New South Wales, School of Mech. and Ind. Eng. Rept. 1972/FMT/1

91. Leonard, B.P., "A stable and accurate convective modelling procedure based on quadratic upstream interpolation", Computer Methods in Applied Mechanics and Engineering, vol.19, pp59-98, 1979

92. PHOENICS Instruction Course, CHAM Limited, Bakery House, 40 High Street, Wimbledon SW19 5AU England

93. Patankar, S.V. and Spalding,D.B., "A calculation procedure for heat, mass, and momentum transfer in three-dimensional parabolic flows", Int. J of Heat Mass Transfer, vol 15, pp1787-1806

94. Markatos, N.C. and Pericleous, K.A., "Laminar and turbulent natural convection in a enclosed cavity", Int. J. of Heat and Mass Transfer, vol.27, no.5, pp755-772, 1984

95. Mills, A. F., "Average Nusselt numbers for external flows", J of Heat Transfer, vol 101, pp 734-735, Nov. 1979

96. McEligot, D.M., Smith, S.B., and Bankston, C.A., "Quasi-developed turbulent pipe flow with heat transfer", J of Heat Transfer, pp 641-650, Nov. 1970

97. Baek, Y., "Flow of supercritical hydrogen in rectangular ducts", U.C.L.A., Ph.D. thesis, 1991

98. Liou, T.M. and Hwang, J.J., "Turbulent heat transfer augmentation and friction in periodic fully developed channel flows", J. of Heat Transfer, vol.114, pp56-64, 1992

99. Schwarz, W.H. and Cosart, W.P., "The two-dimensional turbulent wall-jet", Journal of Fluid Mechanics, vol.10, pp481-495, Nov. 1961

100. Ng, K.H., "Predictions of turbulent-boundary-layer developments using a two-equation model of turbulence", Ph.D. thesis, University of London, 1971

101. Savage, D.W. and Myers, J.E., "The effect of artificial surface roughness on heat and momentum transfer", A.I.Ch.E. Journal, pp 694-702, Sep. 1963